CYTOPROTECTIVE STRATEGIES THAT SELECTIVELY RECOGNIZE AND SUPPRESS PROTEIN AGGREGATION IN THE CELL

Daniel W. Summers

A dissertation submitted to the faculty of the University of North Carolina at Chapel Hill in partial fulfillment of the requirements for the degree of Doctor of Philosophy in the Department of Cell and Developmental Biology

Chapel Hill
2011

Readers:

Douglas Cyr PhD

Patrick Brennwald PhD

Con Beckers PhD

Nikolay Dokholyan PhD

Cam Patterson MD

ABSTRACT

Daniel W Summers
Cytoprotective Strategies that Selectively Recognize and Suppress Protein Aggregation in the Cell
(Under the direction of Douglas Cyr PhD)

Protein misfolding and aggregation are constant threats to cellular homeostasis. The cell must cope with a diverse range of non-native protein conformers and efficiently triage misfolded proteins between pathways for refolding or degradation. In addition, cellular pathways sequester non-native proteins via the microtubule cytoskeleton to distinct subcellular compartments when degradation pathways are saturated. Deficiencies in protein homeostasis occur in a wide variety of human maladies. For example, several disorders including Alzheimer's disease and Huntington's disease are associated with the accumulation of beta-sheet rich, amyloid-like inclusions. Though molecular chaperones are known regulators of amyloid assembly and neurotoxicity, how molecular chaperones selectively bind beta-sheet rich protein conformers and regulate amyloid fibril assembly is largely unknown. Herein, I describe a novel function for the Type I Hsp40 molecular chaperone Ydj1 in regulating aggregation and toxicity of a glutamine/asparagine-rich prion fragment from the yeast protein Rnq1. In the absence of Ydj1, overexpression of this prion fragment was toxic to yeast and resulted in the accumulation of amyloid-like aggregates. Ydj1 binding and suppression of toxicity required its zinc finger-like domain and farnesyl moiety. As a result, Ydj1 utilizes unique chaperone modules to suppress aggregation of an amyloid-like prion and protect cells from the toxic buildup of protein aggregates. Ydj1 also participates in the degradation of misfolded proteins via the ubiquitin-proteasome system. I found that Ydj1 is required to hold polyubiquitinated forms of a misfolded, cytosolic protein in a soluble state. Investigating the degradation of this misfolded protein further, I found that interfering with specific steps in the degradation pathway partitioned this misfolded protein to distinct outcomes including aggregation. Surprisingly, altering the microtubule cytoskeleton drove

this misfolded protein to form insoluble aggregates in the cytosol that could not be trafficked to the proteasome. Disrupting microtubule dynamics selectively stabilized some misfolded proteins, while other misfolded proteins are degraded in a microtubule-independent pathway. These observations uncover a novel connection between chaperone-mediated protein quality control and the microtubule cytoskeleton. Furthermore, misfolded proteins are managed in the cytosol by sophisticated quality control networks that utilize adaptable molecular chaperones such as Ydj1 to suppress aberrant protein aggregation.

ACKNOWLEDGEMENTS

I would like to thank my mentor Dr. Douglas Cyr for his guidance and support during my graduate career. I also like to thank members of the Cyr laboratory for their assistance and friendship over the past six years.

I would like to thank members of my dissertation committee, Dr. Patrick Brennwald, Dr. Nikolay Dokholyan, Dr. Con Beckers, and Dr. Cam Patterson for their thoughtful suggestions and support. A fruitful collaboration with Dr. Nikolay Dokholyan and his student Pradeep Kota also contributed new and interesting insight on my project. I have also received advice from my department chair Dr. Vytas Bankaitis and many other faculty and students in the Department of Cell and Developmental Biology. Collectively, these interactions have encouraged my scientific development and any success or achievement in my career is a result of this stellar training environment.

TABLE OF CONTENTS

LIST OF FIGURES

LIST OF ABBREVIATIONS

Hsp	Heat shock protein
Gln	glutamine
Asn	asparagine;
G/F	glycine/phenylaline;
G/M	glycine/methionine
ZFLR	zinc finger-like region;
G/M-rich	glycine/methionine-rich;
PrD	prion domain,
UPS	ubiquitin-proteasome system,
PQC	protein quality control,
SDS	sodium dodecyl sulfate
ATP	adenosine triphosphate
ADP	adenosine diphosphate
ZFLR	zinc finger-like region
CTD	C-terminal domain
DD	dimerization domain
aa	amino acid
kDa	kilodalton
mm	millimolar
μM	micromolar
GPD	glyceraldehyde 3-phosphate dehydrogenase
ADH	alcohol dehydrogenase
CEN	centromeric

2μ	episomal
OD	ocular density
M	molar
GFP	green fluorescent protein
mRFP	monomeric red fluorescent protein
YFP	yellow fluorescent protein
ThT	thioflavin T
DTT	dithiothreitol
PMSF	phenylmethanesulfonyl fluoride
NaCl	sodium chloride
EDTA	ethylenediaminetetraacetic acid
$CuSO_4$	copper sulfate
SDS-PAGE	SDS-polyacrylamide gel electrophoresis
hr	hour
min	minute
PVDF	polyvinylidene fluoride
SDD-AGE	semi-denaturing agarose gel electrophoresis
HCl	hydrogen chloride
TAE	Tris-Acetate EDTA

Chapter One

Polypeptide transfer from Hsp40 to Hsp70 molecular chaperones

Reproduced from *Trends in Biochemical Sciences* 2009 Vol. 34 230-233

1.1 Abstract

Hsp40 co-chaperones assist in cellular protein folding and degradation through the binding and delivery of non-native proteins to Hsp70. The mechanism for substrate transfer from Hsp40s to Hsp70 is unknown. Two recent studies provide new details that shed light on novel mechanisms for substrate recognition by Hsp40s and a common mechanism for polypeptide transfer to Hsp70.

1.2 Hsp70s and protein folding

Heat shock protein 70 family members generally referred to as Hsp70 interact with different combinations of Hsp40s and other folding and degradatory co-chaperones to facilitate multiple processes required for protein homeostasis (1,2). Defects in protein homeostasis can trigger aberrant protein aggregation, a hallmark of a broad class of diseases known collectively as "Conformational Disorders". Hsp70 molecular chaperones protect cells against the accumulation of proteotoxic species by maintaining a delicate balance between protein synthesis, folding, and degradation (3). Yet the mechanism(s) by which functionally distinct Hsp40s (also known as J-proteins) bind and deliver a diverse array of proteins to the polypeptide-binding site of Hsp70 remains a major unanswered question.

Polypeptide binding and release by Hsp70 is coordinated via an array of co-chaperones that tightly regulate the Hsp70 ATP hydrolytic cycle (Fig. 1.1) (4-6). This process is initiated when a non-native polypeptide is bound by an Hsp40 co-chaperone (1). This large and structurally diverse family is defined by a highly conserved region called a J-domain that interacts with the Hsp70 nucleotide-binding domain (NBD) and stimulates intrinsic Hsp70 ATPase activity (1,7,8). Hydrolysis of ATP to ADP in the Hsp70 NBD induces a conformational change in the Hsp70 substrate-binding domain (SBD) thus increasing Hsp70's affinity for the substrate (9,10). In most cases, polypeptides are released from Hsp70 when ADP is exchanged for ATP; this reaction is facilitated by structurally diverse nucleotide exchange factors (NEFs) (11,12). Once released, the polypeptide can fold to the native conformation, or remain misfolded and reenter the cycle for subsequent rounds of refolding. However, in some instances Hsp70-bound clients are recognized by the E3 ubiquitin ligase CHIP (carboxyl terminus of Hsc70-interacting protein) and targeted for degradation by the ubiquitin-proteasome system (13). Interestingly, Hsp70 and Hsp40 proteins have recently been identified as partners with additional E3 ubiquitin ligases (14). Thus, the fate of non-native polypeptides is determined via association of Hsp70 with co-factors that facilitate protein folding or degradation via the ubiquitin-proteasome system.

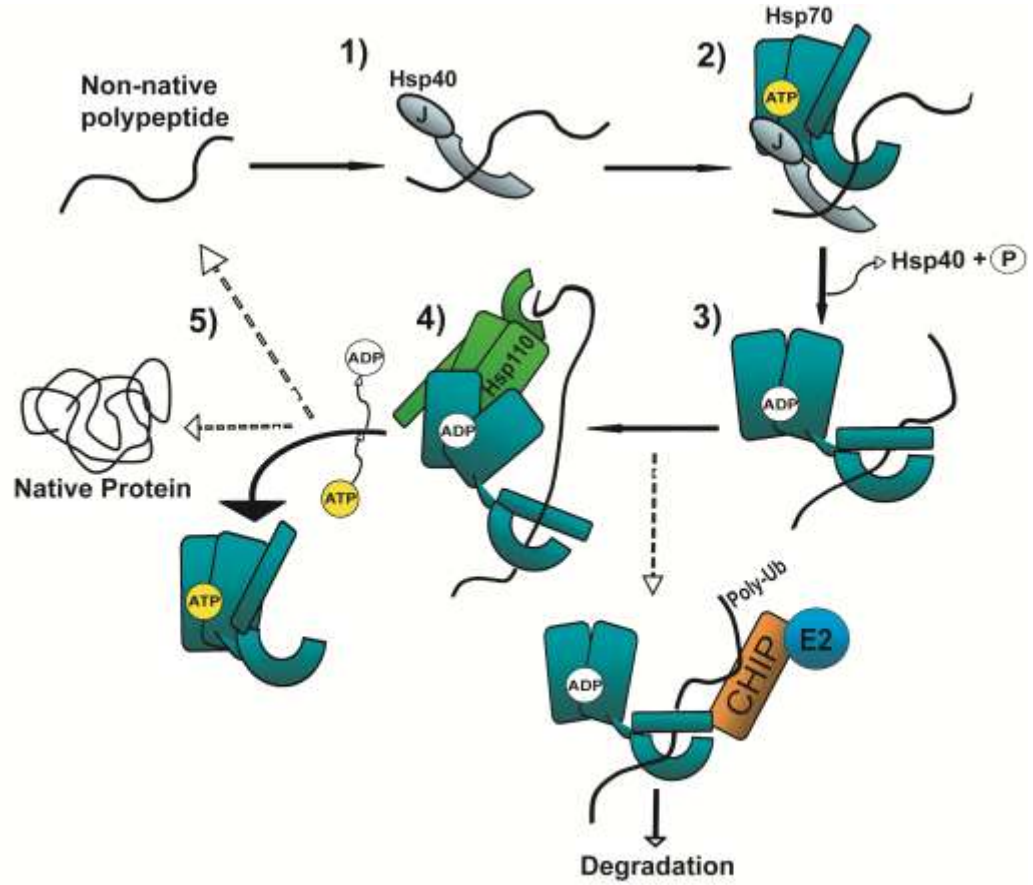

Figure 1.1. Hsp70 polypeptide binding and release is regulated through cycles of ATP hydrolysis and exchange. Protein misfolding is managed in part through action of Hsp70 molecular chaperones in coordination with various cellular cofactors. Initially, a non-native polypeptide is bound by an Hsp40 co-chaperone (light blue). 2) The Hsp40 J-domain then binds Hsp70 (teal) in an ATP-bound state. 3) J-domain-stimulated ATP hydrolysis in the nucleotide-binding domain induces a conformational shift in the Hsp70 substrate-binding domain, increasing affinity for the non-native polypeptide which is released from the Hsp40. Additional cofactors such as the E3 ubiquitin ligase CHIP (orange) with a ubiquitin-conjugating E2 (blue) can bind Hsp70 and the non-native polypeptide, targeting the substrate for degradation by the ubiquitin-proteasome system. 4) Nucleotide exchange factors (NEFs) such as the Hsp110s (green) replace the ADP with ATP, releasing the polypeptide from Hsp70. 5) If the polypeptide remains in a non-native conformation, the cycle can be repeated until folding is complete.

1.3 Hsp40s: diverse Hsp70 binding partners

Through direct binding to non-native substrates, Hsp40s serve as conduits that funnel non-native clients to Hsp70. Despite sharing a conserved J-domain, the Hsp40 family is extensive and members possess unique domains that bind diverse clients and target Hsp70 to distinct cellular machineries. Hsp40s are categorized based on homology to the founding member in *Escherichia coli*, DnaJ (7,8). Type I Hsp40s possess a J-domain, a glycine- and phenylalanine-rich (G/F-rich) region and cysteine-rich, zinc finger-like region (ZFLR). Type II Hsp40s contain the J-domain and G/F-rich region whereas Type III Hsp40s retain only the J-domain. Action of the Hsp40 J-domain alone is sufficient to enable Hsp70 perform its essential cellular functions (15). However, the specialized Hsp40 polypeptide binding domain discussed above impart significant influence over Hsp40 quaternary structure and play critical roles in directing Hsp70 to carry out a variety of specialized functions (16),17.

Importantly, evolutionary diversification of the Hsp40 family has expanded the repertoire of the Hsp40 co-chaperone class (Fig 1.2). Recent studies suggest this structural diversification has generated an array of co-chaperones with unique polypeptide-binding domains that all interact with Hsp70 via the J-domain. This specialization is exemplified by new studies on the function of 3 different ER-localized Hsp40s (17-19). For example, the Hsp40s P58 and ERdj3 specifically bind misfolded substrates in the ER lumen (18,19). However, P58 is unique because this Hsp40 contains nine tetratricopeptide repeats that appear to participate in recognition and binding of misfolded proteins. Thus, P58 and ERdj3 may discriminate between distinct nonnative substrates within the ER. By contrast, the Type III Hsp40 ERdj5 is associated with a supramolecular complex that targets misfolded ER lumenal proteins for degradation via the ER associated degradation pathways (ERAD). ERdj5 contains three cysteine-rich thioredoxin domains could be involved in substrate recognition and facilitate retrotranslocation by cleaving disulfide bonds in non-native proteins within the ER lumen. Thus, highly specialized ER-localized Hsp40s have evolved different mechanisms for substrate binding to meet the protein quality control requirements of this cellular sub-compartment.

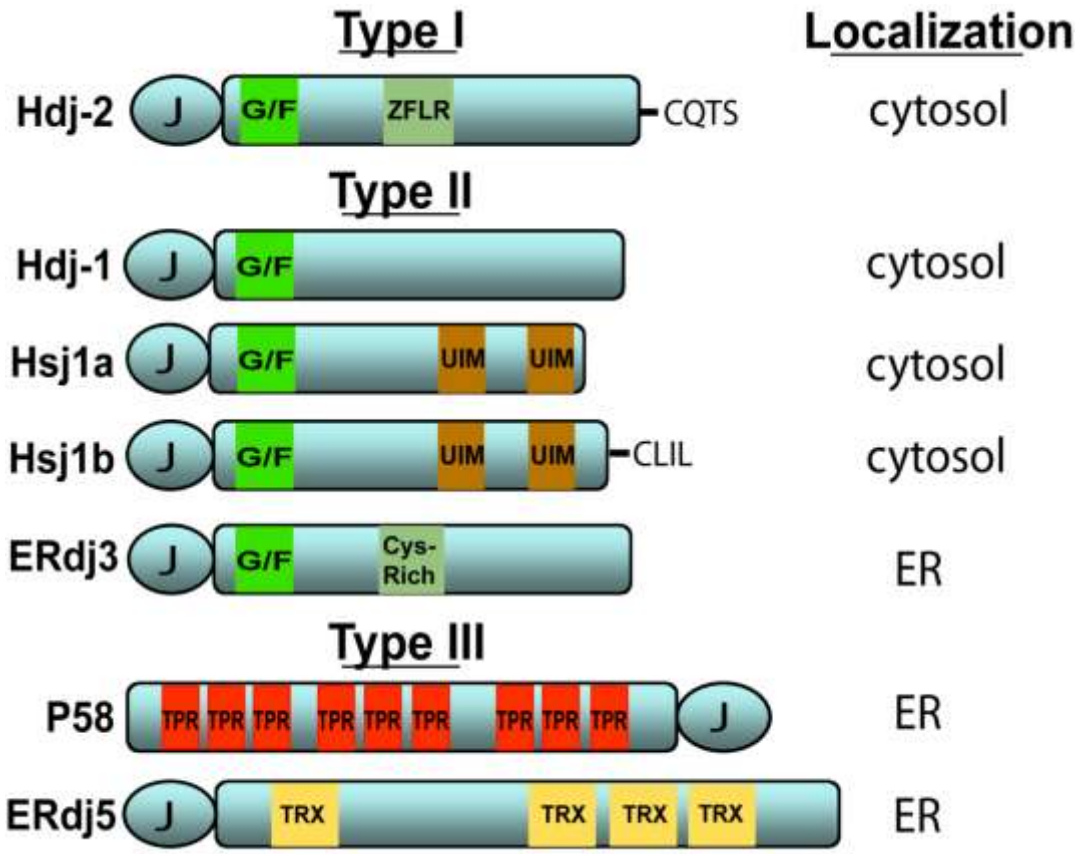

Figure 1.2. Domain structures of several human Hsp40s. Type I Hsp40s such as Hdj-2 (also called DnaJA1) possess a J-domain, G/F-rich region (green) and a ZFLR (blue). Hdj-2 is distinct from many Hsp40s as it is farnesylated at a C-terminal CAAX motif. Type II Hsp40s, such as Hdj-1 (also called DnaJB1), lack the ZFLR. HSJ1a and HSJ1b (also called DnaJB2) are neuron-specific Type II Hsp40 isoforms. Both isoforms possess two ubiquitin interaction motifs (UIMs:brown); however Hsj1b also contains a CAAX motif that is geranylgeranylated. ER-localized Hsp40s have also evolved specialized domains. For example, ERdj3 (also called DnaJB11) contains a cysteine-rich motif (gray) in the C-terminus (21). P58 (also called DnaJC3) contains nine tetratricopeptide repeats (TPR:red) that might bind non-native polypeptides while ERdj5 contains three thioredoxin (TRX;yellow) domains which are responsible for disulfide reductase activity. The length of each Hsp40 represents its relative size. The intracellular location of each Hsp40 is noted.

A unique feature of cytosolic Hsp40s is the modification of Type I and Type II family members by prenylation (1,7,8). For example, the yeast Type I Hsp40 Ydj1p and its human homolog Hdj-2 are farnesylated at a C-terminal CAAX motif (20). Whereas this lipid modification helps localize a pool of Hsp40 to the cytosolic surface of the ER membrane, one recent study suggests that farnesylation is required for Type I Hsp40s to bind specific substrates (21). In addition, the neuron-specific Type II Hsp40 HSJ1b is geranylgeranylated and localized to the ER surface. Similar to Type I Hsp40s, binding between HSJ1b and its client protein rhodopsin relies on this lipid modification (22). Thus, lipid modification not only affects localization, but might also stabilize Hsp40–polypeptide complexes.

1.4 Polypeptide transfer and release from Hsp70

Once Hsp40s bind non-native polypeptides, bound clients must be transferred to Hsp70 for subsequent processing. To begin to address how this occurs, given the extensive structural diversity within the Hsp40s, Petrova *et al* (18) and Jin *et al* (19) recently examined how two different ER-localized Hsp40s release substrates upon interaction with the Hsp70 BiP. In these studies, the Hsp40s P58 and ERdj3 specifically bound misfolded or denatured substrates. Efficient substrate release from either Hsp40 relied upon interaction between BiP and the J-domain, specifically when BiP was ATP-bound. Mutational analysis of BiP revealed that substrate release was functionally coupled to BiP's ATPase activity suggesting that a J-domain–BiP complex was not sufficient to dissociate the substrate. How does Hsp70 binding and ATP hydrolysis provoke Hsp40 to release its substrate? One hypothesis is that binding to Hsp70 induces an allosteric shift in the Hsp40 that reduces substrate affinity in the polypeptide-binding domain. However, Petrova *et al* (16) found that the location of the J-domain within the Hsp40 was inconsequential to BiP-induced substrate release. Furthermore, the extensive variation present in the Hsp40 family argues against a unified allosteric mechanism. However, J-domain–Hsp70 binding might bring the substrate in close proximity to the Hsp70 SBD. Following ATP hydrolysis, the increase in substrate affinity by Hsp70 could then out-compete the Hsp40 for binding.

This new model explains how divergent Hsp40s can uniformly release substrates for transfer to Hsp70 through interactions between the conserved J-domain and the Hsp70 NBD. However, some Hsp40s interact with regions within the Hsp70 SBD (23), suggesting that specific Hsp40s have evolved individualized mechanisms for cooperating with Hsp70. Ydj1p, in particular, requires its ZFLR for substrate transfer and chaperone-dependent refolding (24). The Ydj1p ZFLR (located immediately adjacent to the J-domain) might help orient substrates in a more amenable position for transfer to the Hsp70 SBD (16). Therefore, distinct Hsp40 modules might confer not only unique binding preferences, but also specialized interactions with Hsp70 that impart significant regulatory oversight in this relationship.

Polypeptide release from Hsp70 is mediated by exchange of ADP for ATP. The NEFs that regulate this step are also highly diverse; they do not share a common domain responsible for this activity. Several recent structures suggest that individual NEFs might function by twisting the lobes of the Hsp70 ATPase domain in a manner that decreases affinity for ADP (12). Interestingly, the NEF Sse1p and its human homologs are non-canonical Hsp70s that possesses polypeptide-binding activity and might interact with Hsp70-bound clients (25). Thus, sequential interactions between non-native polypeptides with Hsp40, Hsp70 and other Hsp70 co-chaperones appear to play critical roles in cellular folding and degradation pathways.

1.5 Concluding Remarks

Hsp40 co-chaperones have emerged as complex and essential players in regulating protein homeostasis. This diverse family utilizes a variety of mechanisms to bind and funnel clients to Hsp70. Yet, recent studies suggest a uniform mechanism for substrate release and transfer from Hsp40 to Hsp70 (18,19). Future studies are needed to dissect how specialized Hsp40s selectively recognize different protein conformers and specify Hsp70s cellular functions. In addition, we need to understand how interactions between Hsp70-bound protein clients and folding and degradatory co-chaperones mediate protein triage events (13,25). Further knowledge of this process will lend critical insight into the underlying causes and potential treatments for the expansive list of Protein Conformational Disorders.

1.6 References

1. Cyr, D. M., Langer, T., and Douglas, M. G. (1994) *Trends Biochem Sci* **19**, 176-181

2. Balch, W. E., Morimoto, R. I., Dillin, A., and Kelly, J. W. (2008) *Science* **319**, 916-919

3. Cyr, D. M., Hohfeld, J., and Patterson, C. (2002) *Trends Biochem Sci* **27**, 368-375

4. Langer, T., Lu, C., Echols, H., Flanagan, J., Hayer, M. K., and Hartl, F. U. (1992) *Nature* **356**, 683-689

5. Cyr, D. M., Lu, X., and Douglas, M. G. (1992) *J Biol Chem* **267**, 20927-20931

6. Liberek, K., Galitski, T. P., Zylicz, M., and Georgopoulos, C. (1992) *Proc Natl Acad Sci U S A* **89**, 3516-3520

7. Walsh, P., Bursac, D., Law, Y. C., Cyr, D., and Lithgow, T. (2004) *EMBO Rep* **5**, 567-571

8. Qiu, X. B., Shao, Y. M., Miao, S., and Wang, L. (2006) *Cell Mol Life Sci* **63**, 2560-2570

9. Vogel, M., Bukau, B., and Mayer, M. P. (2006) *Mol Cell* **21**, 359-367

10. Liu, Q., and Hendrickson, W. A. (2007) *Cell* **131**, 106-120

11. Szabo, A., Langer, T., Schroder, H., Flanagan, J., Bukau, B., and Hartl, F. U. (1994) *Proc Natl Acad Sci U S A* **91**, 10345-10349

12. Cyr, D. M. (2008) *Cell* **133**, 945-947

13. Rosser, M. F., Washburn, E., Muchowski, P. J., Patterson, C., and Cyr, D. M. (2007) *J Biol Chem* **282**, 22267-22277

14. Han, S., Liu, Y., and Chang, A. (2007) *J Biol Chem* **282**, 26140-26149

15. Sahi, C., and Craig, E. A. (2007) *Proc Natl Acad Sci U S A* **104**, 7163-7168

16. Ramos, C. H., Oliveira, C. L., Fan, C. Y., Torriani, I. L., and Cyr, D. M. (2008) *J Mol Biol* **383**, 155-166

17. Ushioda, R., Hoseki, J., Araki, K., Jansen, G., Thomas, D. Y., and Nagata, K. (2008) *Science* **321**, 569-572

18. Petrova, K., Oyadomari, S., Hendershot, L. M., and Ron, D. (2008) *Embo J* **27**, 2862-2872

19. Jin, Y., Awad, W., Petrova, K., and Hendershot, L. M. (2008) *Embo J* **27**, 2873-2882

20. Caplan, A. J., Tsai, J., Casey, P. J., and Douglas, M. G. (1992) *J Biol Chem* **267**, 18890-18895

21. Flom, G. A., Lemieszek, M., Fortunato, E. A., and Johnson, J. L. (2008) *Mol Biol Cell* **19**, 5249-5258

22. Chapple, J. P., and Cheetham, M. E. (2003) *J Biol Chem* **278**, 19087-19094

23. Freeman, B. C., Myers, M. P., Schumacher, R., and Morimoto, R. I. (1995) *Embo J* **14**, 2281-2292

24. Fan, C. Y., Ren, H. Y., Lee, P., Caplan, A. J., and Cyr, D. M. (2005) *J Biol Chem* **280**, 695-702

25. Polier, S., Dragovic, Z., Hartl, F. U., and Bracher, A. (2008) *Cell* **133**, 1068-1079

Chapter Two

Prion Propagation by Hsp40 Molecular Chaperones

Reproduced from *Prion* Vol 3 59-64 2009

2.1 Abstract

Molecular chaperones regulate essential steps in the propagation of yeast prions. Yeast prions possess domains enriched in glutamines and asparagines that act as templates to drive the assembly of native proteins into beta-sheet-rich, amyloid-like fibrils. Several recent studies highlight a significant and complex function for Hsp40 co-chaperones in propagation of prion elements in yeast. Hsp40 co-chaperones bind non-native polypeptides and transfer these clients to Hsp70s for refolding or degradation. How Hsp40 co-chaperones bind amyloid-like prion conformers that are enriched in hydrophilic residues such as glutamines and asparagines is a significant question in the field. Interestingly, selective recognition of amyloid-like conformers by distinct Hsp40s appears to confer opposing actions on prion assembly. For example, the Type I Hsp40 Ydj1 and Type II Hsp40 Sis1 bind different regions within the prion protein Rnq1 and function respectively to inhibit or promote [RNQ^{+}] prion assembly. Thus, substrate selectivity enables distinct Hsp40s to act at unique steps in prion propagation.

2.2 Molecular chaperones and yeast prions

Proteins adopt a diverse and dynamic array of structural conformations. Prions are unique in that these proteins induce conversion of the soluble, native structure into the prion conformer with a high propensity to self-assemble into beta-sheet-rich, amyloid-like fibrils.(1) Extensive investigation of prion biogenesis in the budding yeast *Saccharomyces cerevisiae* has uncovered some of the basic mechanisms underlying prion assembly into amyloid-like fibrils and inheritance of the prion state. One intriguing development in this story was the intimate role for heat shock protein (HSP) molecular chaperones in these pathways.(2,3) Indeed, numerous yeast prions are dependent upon molecular chaperones for efficient maintenance and propagation of prion structures.(4,5) On the other hand, overexpression of some molecular chaperones "cure" yeast of the heritable prion suggesting molecular chaperones antagonize prion assembly.(4,6,7) How such opposing activities efficiently coordinate prion assembly into amyloid-like fibrils and propagation of the prion state inside the cell is an outstanding question in the field. Study of this process is significant because amyloid-like fibrils accumulate in numerous conformational disorders.(8,9) However, the connection between amyloid assembly and neuronal cell death is still controversial as several recent studies implicate the assembly of amyloid-like fibrils as benign or even protective.(10-12) In addition, prions found in *S. cerevisiae* possess domains enriched in glutamines (Gln) and asparagines (Asn)(13), resembling proteins with expanded polyglutamine repeats (such as human huntingtin and several ataxins) that are very susceptible to aggregation.(14,15) Many molecular chaperones are functionally conserved from yeast to humans, and as such, studying how molecular chaperones modulate prion propagation yields substantial mechanistic insight on the regulation of amyloid assembly in conformational disorders.

Several classes of molecular chaperone are implicated in prion propagation. For example, the AAA+ protein remodeling factor Hsp104 is required for propagation of several prions in yeast.(4,16,17) Hsp104 is proposed to shear prion polymers to generate "seeds" that drive conversion of native protein into the prion conformation.(18-21) Hsp70 molecular chaperones also regulate prion propagation although the particular function depends on the Hsp70 class and specific yeast prion. For

example, mutations in the Hsp70 Ssa1 destabilize [*PSI*$^{+}$] prion propagation while overexpression of Hsp70s from the Ssa family can stabilize the [*PSI*$^{+}$] state.(22-24) Interestingly, overexpression of Ssa1 has been shown to cure yeast of the prion [*URE3*].(6,7) In contrast, Hsp70s of the Ssb family appear to antagonize [*PSI*$^{+}$] prion propagation.(24-26) As a result, protein flux through Hsp70 refolding pathways is a crucial step in prion biogenesis. Hsp70 chaperone activity is tightly coordinated by Hsp40 co-chaperones (also known as J-proteins). Additionally, Hsp40 and Hsp70 chaperones cooperate with Hsp104 to refold aggregated proteins.(27) Several recent studies underscore a complex, yet fundamental role for Hsp40 co-chaperones in prion assembly and propagation.(5,12,28-31) In this review we first describe the Hsp40 co-chaperone family and basic mechanisms underlying Hsp40:substrate recognition. Then, general roles for Hsp40s in propagation of the yeast prions [*PSI*$^{+}$] and [*URE3*], and [*RNQ*$^{+}$]/[*PIN*$^{+}$] are discussed. Recent studies investigating the function of Hsp40s on assembly of the [*RNQ*$^{+}$] prion are emphasized to highlight novel mechanisms in which Hsp40s bind Gln/Asn-rich prion proteins and modulate the accumulation of toxic or benign prion conformers. We propose that the distinct binding preferences of individual Hsp40s determine specific Hsp40 actions in prion assembly and propagation.

2.3 Protein Quality Control by Hsp40 Molecular Chaperones

Hsp40 co-chaperones are essential partners in Hsp70 function.(32) Hsp40s share a highly conserved region called a J-domain that stimulates the intrinsic ATPase activity of its partner Hsp70.(33) ATP hydrolysis causes a series of conformational changes that increase the affinity of client:Hsp70 interactions.(34,35) Client release from Hsp70 is induced when ADP is replaced with ATP by a Hsp70 nucleotide exchange factor.(36) The Hsp40 J-domain alone appears sufficient to maintain basic cellular processes required for physiological growth.(37) However, based upon homology to the J-domain from the founder Hsp40 in *Escherichia coli* (DnaJ), there are twenty-two Hsp40s in budding yeast and forty-one Hsp40s in humans.(32,38) Given the evolutionary expansion of the Hsp40 family, how these various Hsp40s specify Hsp70 function is an important unanswered question.

Importantly, Hsp40s utilize a variety of specialized domains outside of the J-domain to bind misfolded polypeptides and transfer these non-native clients to Hsp70 for refolding or degradation.(39,40) Thus, Hsp40s select substrates for Hsp70 chaperone action and serve as the first line of defense in protein conformational disorders by recognizing non-native protein conformers. Hsp40s are classified based on the presence of several core domains found in DnaJ. Type I Hsp40s possess a J-domain, glycine/phenylaline(G/F)-rich region, and a zinc finger-like region (ZFLR)(Fig. 2.1). Type II Hsp40s possess the J-domain and G/F-rich region while Type III Hsp40s retain only the J-domain. The core Hsp40 domains described above influence Hsp40 quaternary structure and substrate selectivity (Fig. 2.1B).(41,42) Specialized Hsp40s have further acquired unique domains and modifications that likewise influence substrate preferences as well as regulation of Hsp70 refolding activity.(43-45) For example, the yeast Type I Hsp40 Ydj1 possesses a hydrophobic depression in its C-terminal domain that binds hydrophobic peptides(46) as well as a CaaX motif that is modified by farnesylation.(47) Interestingly, the Ydj1 ZFLR, hydrophobic polypeptide-binding pocket, and farnesyl modification all have been shown to participate in substrate binding.(29,46,48) yet specific features are either necessary or dispensable for binding to individual substrates. Thus,

Hsp40s can utilize various domain combinations to bind a wide range of non-native clients. The yeast Type II Hsp40 Sis1 also possesses a hydrophobic polypeptide-binding pocket(49) yet does not contain a ZFLR nor a CaaX motif. However, Sis1 does contain a G/M-rich region adjacent to the G/F-rich region,(50) both of which appear to influence essential cellular functions of this Hsp40.(51) While Ydj1 and Sis1 exhibit some overlapping physiological function,(52,53) these Hsp40s also display distinct substrate preferences(41) and as discussed below, exert very different activities on propagation of prions in yeast.

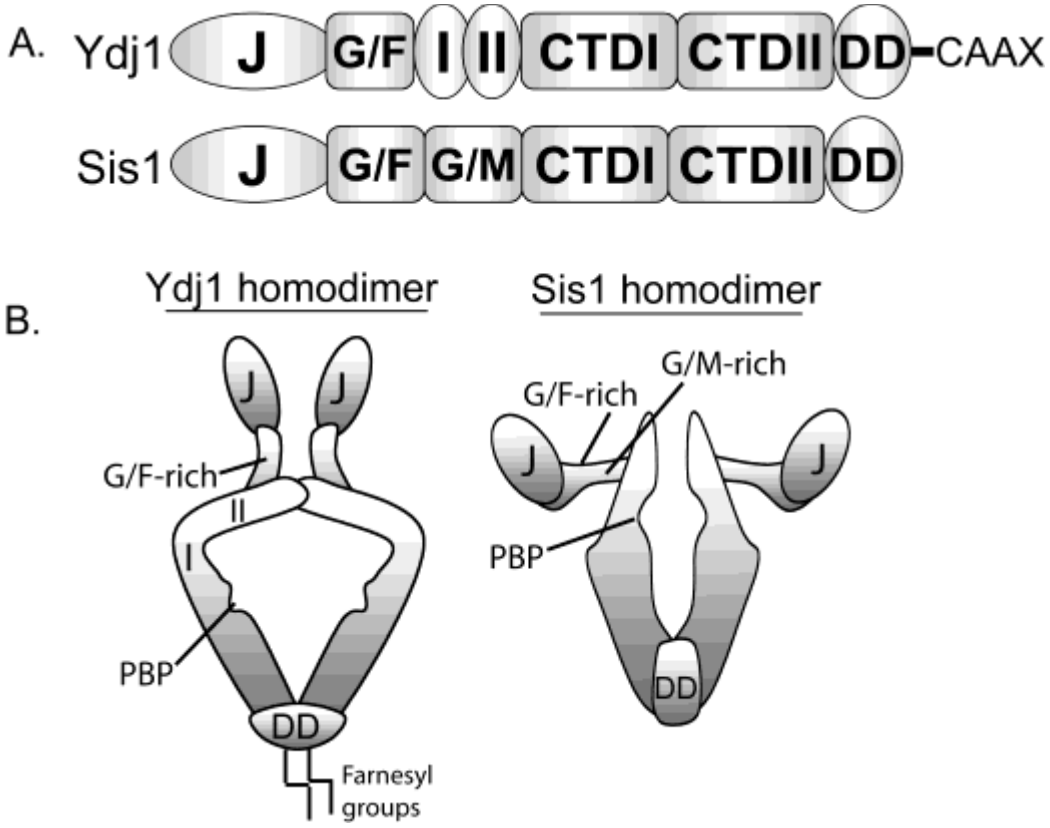

Figure 2.1 Domain structures of the Type I Hsp40 Ydj1 and Type II Hsp40 Sis1 (A). Both Hsp40s possess N-terminal J-domains and adjacent G/F-rich regions. Ydj1 also contains a zinc finger-like region with two zinc-binding domains (denoted as I and II). Sis1 contains a G/M-rich region in addition to the G/F-rich region. C-terminal domains (CTD) in these Hsp40s share limited homology although both possess hydrophobic polypeptide-binding pockets (PBP) and dimerization domains (DD). Furthermore, Ydj1 is farnesylated at a C-terminal CaaX motif. (B) Quaternary structures of Ydj1 and Sis1 homodimers (for details see Ref. 42). The polypeptide-binding pockets of each Hsp40 are noted by a small grove in the C-terminus. While the J-domains are highly conserved between Ydj1 and Sis1, the orientations of these domains with respect to the polypeptide-binding pocket are very different.

2.4 Hsp40 activity in propagation of [*PSI*$^+$] and [URE3] prions

Studies of the yeast prions [*PSI*$^+$] and [*URE3*] have identified complex roles for Hsp40 co-chaperones in prion propagation and assembly into amyloid-like fibrils. The inheritable element [*PSI*$^+$] is formed by the yeast translation termination factor Sup35.(18,54) Both Ydj1 and Sis1 physically associate with large Sup35 aggregates,(55) though propagation of the [*PSI*$^+$] prion is specifically dependent upon Sis1.(5,30) On the other hand, overexpression of Ydj1 in conjunction with its cognate Hsp70 destabilizes "weak" [*PSI*$^+$] variants.(6) Also noteworthy, overexpression of Apj1 (another Type I Hsp40 in yeast) cures cells of specific [*PSI*$^+$] variants.(56) Apj1 shares strong homology with Ydj1 yet its cellular functions are still unclear. Recent studies on Sup35 fibril assembly in vitro have demonstrated a direct role for Hsp40 molecular chaperones in regulating the assembly of amyloid-like fibrils.(31,57) Interestingly, select Hsp40:Hsp70 pairs exert different actions on Sup35 assembly as well as the prion remodeling activity of Hsp104.(58) Therefore, distinct chaperone complexes might selectively regulate prion assembly and propagation to alternate outcomes.

Hsp40s also regulate propagation of the yeast prion [*URE3*]. The [*URE3*] prion is formed by Ure2, a modulator of nitrogen catabolism in yeast.(59) Similar to [*PSI*$^+$], propagation of the [*URE3*] prion requires Sis1(5) while overexpression of the Ydj1 cures yeast of [*URE3*].(16) Furthermore, Ydj1 inhibits the in vitro assembly of Ure2 into amyloid-like fibrils.(60,61) In recent studies though, overexpression of J-domains from other yeast Hsp40s was shown to be sufficient to cure yeast of the [*URE3*] trait.(5,62) These data indicate that modulating cycles of Hsp70 activity in the cell perturb [*URE3*] prion biogenesis and inheritance. This effect seems specific for the [*URE3*] prion,(5) suggesting this yeast prion is particularly sensitive to aberrations in prion flux through Hsp70 refolding pathways. Altogether, Sis1 and Ydj1 drive [*PSI*$^+$] and [*URE3*] propagation to completely different outcomes whereby Sis1 promotes the efficient propagation of prion elements yet Ydj1 antagonizes this pathway. However, studies on [*PSI*$^+$] and [*URE3*] propagation have not revealed the molecular mechanisms underlying these divergent chaperone actions.

2.5 Selective recognition of the [*RNQ*$^+$] prion by opposing Hsp40 activities

Studies of the yeast prion [*RNQ*$^+$] have recently revealed novel mechanisms by which Hsp40 co-chaperones bind amyloid-like prion conformers and perhaps regulate prion propagation pathways to distinct endpoints. The yeast prion [*RNQ*$^+$]/[*PIN*$^+$] is formed by the yeast protein Rnq1 (rich in asparagines and glutamines) (Fig. 2.2A).(63,64) The [*RNQ*$^+$] state facilitates the conversion of other prions in yeast(64,65) as well as seeding toxic conformers of an expanded glutamine form of human huntingtin.(66) Rnq1 possesses a C-terminal Gln/Asn-rich prion domain that is sufficient to assemble into amyloid-like fibrils in vitro(67,68) and induce prion formation when fused in place of the Gln/Asn-rich N-terminal domain of Sup35.(63) The N-terminal non-prion domain of Rnq1 appears to regulate [*RNQ*$^+$] prion propagation though the function of this domain is still unclear.(69) Not long after [*RNQ*$^+$] was first described, propagation of [*RNQ*$^+$] prions was shown to be dependent upon Sis1.(70) Deletion of other Hsp40s in yeast has no effect on the [*RNQ*$^+$] state suggesting this dependency is specific for Sis1.(5) In contrast to Sis1, overexpression of Ydj1 cures yeast of some [*RNQ*$^+$] prion variants.(71) Thus, similar to other yeast prions discussed above, Sis1 promotes [*RNQ*$^+$] propagation while Ydj1 can inhibit [*RNQ*$^+$] assembly perhaps reflecting distinct fundamental functions for these two Hsp40 co-chaperones in the prion assembly pathway (Fig. 2.2B).

What might account for the opposing functions of Sis1 and Ydj1 on [*RNQ*$^+$] prion propagation? Recent studies demonstrated that Sis1 and Ydj1 bind to different regions within the Rnq1 protein. For example, Sis1 binds a short, hydrophobic motif in the non-prion domain(12) while Ydj1 binds numerous motifs in the Gln/Asn-rich prion domain of Rnq1 (Fig. 2.2A).(29) Interestingly, interaction between Rnq1 and either Hsp40 is dependent upon the [*RNQ*$^+$] prion conformation.(29,70) Conformational conversion of native Rnq1 into the [*RNQ*$^+$] prion state might expose the Sis1-binding site in the non-prion domain. This provides a mechanism by which Sis1 action in [*RNQ*$^+$] propagation is regulated through conformation-specific recognition by an Hsp40 co-chaperone. Binding between

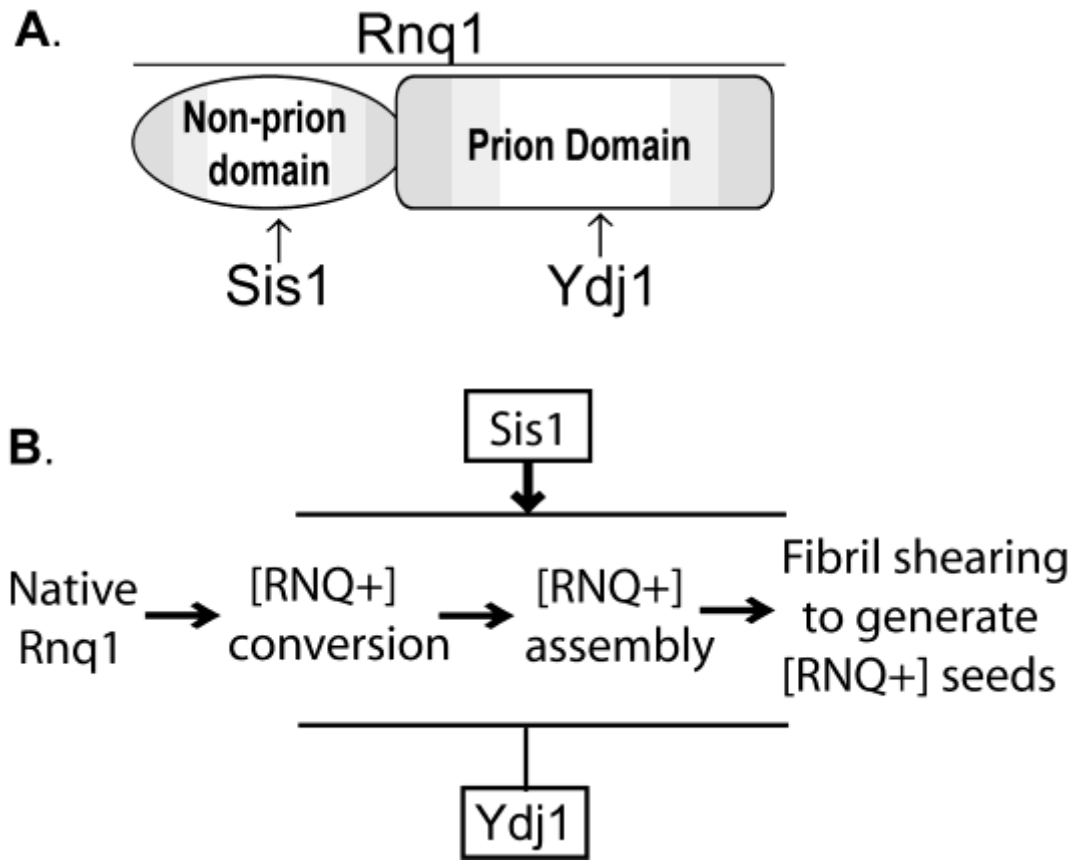

Figure 2.2. Domain structure of Rnq1 from *S. cerevisiae* (A). Rnq1 contains a N-terminal non-prion domain (aa1-152) and a C-terminal, Gln/Asn-rich prion domain (aa153-405). Sis1 binds a short, hydrophobic motif in the non-prion domain while Ydj1 binds numerous motifs in prion domain. (B) Model for Hsp40 action in [*RNQ*$^+$] prion assembly pathway. Native Rnq1 is converted to the [*RNQ*$^+$] prion state and assembles into large, [*RNQ*$^+$] prion aggregates that are sheared to generate heritable [*RNQ*$^+$] prion seeds. Sis1 might facilitate shearing to maintain a pool of [*RNQ*$^+$] prion seeds thereby propagating the [*RNQ*$^+$] prion state. In addition Sis1 might promote the elongation of [*RNQ*$^+$] prion particles. In contrast, Ydj1 might antagonize [*RNQ*$^+$] prion assembly through binding an early [*RNQ*$^+$] prion conformer thus hindering [*RNQ*$^+$] assembly or by accelerating the disassembly of large, [*RNQ*$^+$] prions such that Rnq1 is eventually converted to its native state.

Ydj1 and the Gln/Asn-rich prion domain of Rnq1 is quite surprising because peptide array studies suggest Type I Hsp40s such as Ydj1 prefer substrates enriched in hydrophobic residues.(41,72,73) Furthermore, select binding to the Rnq1 prion domain in the [*RNQ*$^{+}$] prion state implies that Ydj1 recognizes the Gln/Asn-rich motifs in a conformation-specific manner. Altogether, two Hsp40s in the cell bind [*RNQ*$^{+}$] prions yet target different regions in the Rnq1 protein. The outcome of such binding preferences might (at a rudimentary level) account for the disparate chaperone activities on [*RNQ*$^{+}$] prion propagation.

What features in Ydj1 and Sis1 direct these Hsp40 chaperones to bind distinct domains within Rnq1? Interestingly, binding between Ydj1 and the Rnq1 prion domain is dependent upon the Ydj1 ZFLR and farnesylation at its C-terminal CaaX motif.(29) The Ydj1 ZFLR is adjacent to two anti-parallel beta-strands that might bind the beta-rich Rnq1 prion domain through a beta-strand donor mechanism.(74,75) How lipid modification of an Hsp40 co-chaperone contributes to substrate interaction is unclear, although farnesylation of Ydj1 has been implicated in binding to the kinase Ste11.(48) Thus, farnesylation appears required for binding to numerous chaperone substrates including yeast prions. In contrast, Sis1-dependent maintenance of the [*RNQ*$^{+}$] prion state requires unique extensions in the G/F-rich region of Sis1.(76) These observations collectively suggest that Hsp40 co-chaperones rely on specialized modules to bind distinct domains in Rnq1 and regulate different aspects of [*RNQ*$^{+}$] prion propagation.

Given such discrete binding preferences, how might Sis1 and Ydj1 exert their opposing activities on [*RNQ*$^{+}$] prion propagation? Importantly, Sis1 binds to Rnq1 in a near 1:1 stoichoimetric complex while binding between Ydj1 and Rnq1 (or its Gln/Asn-rich prion domain) appears substoichiometric.(29,76) Sis1 might coat [*RNQ*$^{+}$] prion assemblies via binding the Rnq1 non-prion domain, direct Hsp70/Hsp104 molecular chaperones to [*RNQ*$^{+}$] fibrils, and facilitate shearing to generate heritable [*RNQ*$^{+}$] prion seeds.(28,30) In addition, Sis1 might facilitate addition of new Rnq1 subunits into an elongating [*RNQ*$^{+}$] fibril because overexpression of Sis1 increases the pool of

amyloid-like [*RNQ*$^{+}$] assemblies while overexpression of Hsp70 and Hsp104 does not result in such an increase.(12)

In contrast to Sis1, Ydj1 might cap the exposed ends of [*RNQ*$^{+}$] prion assemblies and thereby inhibit fibril elongation by sterically hindering contacts between exposed Gln/Asn-rich motifs in the [*RNQ*$^{+}$] prion conformer. In addition, Ydj1 might bind a [*RNQ*$^{+}$] prion assembly intermediate and cooperate with Hsp70 to refold the Rnq1 protein into its native conformation or partition this protein conformer into an alternative off-pathway assembly that is subsequently remodeled by another chaperone complex.(77) The net result of either mechanism would be solubilization of assembled Rnq1 and loss of the [*RNQ*$^{+}$] prion trait. Importantly, Sis1 activity must normally out-compete Ydj1 to promote efficient [*RNQ*$^{+}$] propagation. This might occur because Sis1-binding to Rnq1 is stoichiometric(76) and Ydj1-binding motifs in the Rnq1 prion domain are buried within most [*RNQ*$^{+}$] assemblies. Furthermore, some but not all [*RNQ*$^{+}$] prion variants are sensitive to Ydj1 overexpression(71) suggesting that Ydj1 may differentially recognize Rnq1 prion domain surfaces exposed in specific [*RNQ*$^{+}$] prion variants.

These studies provide novel insight on the selectivity of Hsp40 interaction with amyloid-like substrates, yet several significant questions still remain. For example, if Sis1 and Ydj1 bind distinct domains in Rnq1 do these co-chaperones bind simultaneously to the same Rnq1 protein or do Sis1 and Ydj1 act on discrete [*RNQ*$^{+}$] intermediates/assemblies? Future studies will be required to dissect this question conclusively, yet the answer will likely reveal significant insight on the basic mechanisms of chaperone recognition of amyloid-like protein species in conformational disorders.

2.6 Hsp40s protect cells from toxic prion conformers

The study of Hsp40 action in [*RNQ*$^{+}$] assembly has further revealed that Sis1 and Ydj1 protect the cell from the accumulation of cytotoxic protein conformers. Overexpression of Rnq1 is toxic to yeast in the presence of pre-existing [*RNQ*$^{+}$] prion.(12) Importantly, overexpression of Sis1 suppresses cytotoxicity caused by excess Rnq1, an effect that correlates with enhanced [*RNQ*$^{+}$] prion assembly into SDS-insoluble aggregates and a decrease in the pool of SDS-soluble, Rnq1 protein species. Furthermore, mutating the Sis1-binding site in the Rnq1 non-prion domain decreases the efficiency of [*RNQ*$^{+}$] prion assembly and exacerbates toxicity.(12) Thus, chaperone-mediated [*RNQ*$^{+}$] assembly appears protective although the specific nature of the cytotoxic protein conformer is still unclear.

In contrast to full length Rnq1, overexpression of the Rnq1 prion domain alone is not toxic to yeast.(12) However, overexpression of this prion fragment becomes toxic in the absence of Ydj1.(29) Unlike full-length Rnq1, whose toxicity correlated with the appearance of a low molecular weight, soluble protein species, the toxicity by the Rnq1 prion domain in a *ydj1*-null background correlated with an increase in the pool of large, SDS-insoluble assemblies.(29) Thus, Ydj1 might be required for the cell to tolerate excessive levels of large, amyloid-like species, although this point requires further investigation. Altogether, the above observations suggest a model in which Sis1 and Ydj1 coordinate the flux of Rnq1 proteins through the [*RNQ*$^{+}$] prion assembly pathway in order to maintain the accumulation of soluble versus amyloid-like particles within a tolerable threshold for the cell. Interestingly, Sis1 and Ydj1 were previously shown to have opposing effects on aggregation and toxicity of an expanded polyglutamine model in yeast.(78) Altogether, Hsp40 co-chaperones selectively bind non-native protein species to either maintain protein solubility or drive aggregation.(79) Even though amyloid assembly can be protective it is important to consider that excessive amyloid burden might also result in cell death.(80) Susceptibility to various amyloid-like protein conformers is likely dependent upon the global expression pattern of environmental factors that buffer proteotoxicity.(81)

2.7 Concluding Remarks and Future Directions

Hsp40 molecular chaperones have recently emerged as critical regulators of prion propagation in yeast. Interestingly, individual Hsp40s modulate discrete steps in the prion assembly pathway and in the case of Ydj1 and Sis1, execute opposing activities on propagation of several yeast prions. Such disparate activities might originate from the unique binding preferences exhibited the Hsp40 co-chaperone family, including recognition of Gln/Asn-rich regions responsible for assembly into beta-rich amyloid-like fibrils. Sis1 and Ydj1 possess unique structural domains that might account for such differential binding preferences.(41) For example, Ydj1 utilizes its ZFLR and a farnesyl moiety to bind the prion domain of Rnq1.(29) These features are conserved in various human Hsp40s and might contribute to the recognition of expanded polyglutamine conformers in various human diseases.(82-84) Studies of Hsp40 action in [RNQ^{+}] assembly have also demonstrated that Sis1-mediated acceleration of [RNQ^{+}] prion assembly is cytoprotective.(12) Such a role for an Hsp40 chaperone in cytoprotection is consistent with other recent observations that facilitated protein aggregation protects against cell death mediated by Abeta(1-42)(85,86) and the expanded polyglutamine huntingtin(77,87,88) altogether suggesting that multiple protein quality control pathways might exist to cope with the accumulation of toxic protein conformers. Thus, dissecting how Hsp40s selectively recognize toxic protein species and recruit other chaperone complexes (such as Hsp70 and Hsp104) will yield significant insight on how aggregation pathways are regulated in human conformational disorders.

2.3 References

1. Tuite, M. F., and Cox, B. S. (2003) *Nat Rev Mol Cell Biol* **4**, 878-890

2. Jones, G. W., and Tuite, M. F. (2005) *Bioessays* **27**, 823-832

3. Rikhvanov, E. G., Romanova, N. V., and Chernoff, Y. O. (2007) *Prion* **1**, 217-222

4. Chernoff, Y. O., Lindquist, S. L., Ono, B., Inge-Vechtomov, S. G., and Liebman, S. W. (1995) *Science* **268**, 880-884

5. Higurashi, T., Hines, J. K., Sahi, C., Aron, R., and Craig, E. A. (2008) *Proc Natl Acad Sci U S A* **105**, 16596-16601

6. Kushnirov, V. V., Kryndushkin, D. S., Boguta, M., Smirnov, V. N., and Ter-Avanesyan, M. D. (2000) *Curr Biol* **10**, 1443-1446

7. Schwimmer, C., and Masison, D. C. (2002) *Mol Cell Biol* **22**, 3590-3598

8. Carrell, R. W., and Lomas, D. A. (1997) *Lancet* **350**, 134-138

9. Sipe, J. D., and Cohen, A. S. (2000) *J Struct Biol* **130**, 88-98

10. Chiti, F., and Dobson, C. M. (2006) *Annu Rev Biochem* **75**, 333-366

11. Kayed, R., Head, E., Thompson, J. L., McIntire, T. M., Milton, S. C., Cotman, C. W., and Glabe, C. G. (2003) *Science* **300**, 486-489

12. Douglas, P. M., Treusch, S., Ren, H. Y., Halfmann, R., Duennwald, M. L., Lindquist, S., and Cyr, D. M. (2008) *Proc Natl Acad Sci U S A*

13. Ross, E. D., Minton, A., and Wickner, R. B. (2005) *Nat Cell Biol* **7**, 1039-1044

14. Williams, A. J., and Paulson, H. L. (2008) *Trends Neurosci* **31**, 521-528

15. Orr, H. T., and Zoghbi, H. Y. (2007) *Annu Rev Neurosci* **30**, 575-621

16. Moriyama, H., Edskes, H. K., and Wickner, R. B. (2000) *Mol Cell Biol* **20**, 8916-8922

17. Derkatch, I. L., Bradley, M. E., Zhou, P., Chernoff, Y. O., and Liebman, S. W. (1997) *Genetics* **147**, 507-519

18. Paushkin, S. V., Kushnirov, V. V., Smirnov, V. N., and Ter-Avanesyan, M. D. (1996) *Embo J* **15**, 3127-3134

19. Kryndushkin, D. S., Alexandrov, I. M., Ter-Avanesyan, M. D., and Kushnirov, V. V. (2003) *J Biol Chem* **278**, 49636-49643

20. Shorter, J., and Lindquist, S. (2004) *Science* **304**, 1793-1797

21. Wegrzyn, R. D., Bapat, K., Newnam, G. P., Zink, A. D., and Chernoff, Y. O. (2001) *Mol Cell Biol* **21**, 4656-4669

22. Newnam, G. P., Wegrzyn, R. D., Lindquist, S. L., and Chernoff, Y. O. (1999) *Mol Cell Biol* **19**, 1325-1333

23. Jung, G., Jones, G., Wegrzyn, R. D., and Masison, D. C. (2000) *Genetics* **156**, 559-570

24. Allen, K. D., Wegrzyn, R. D., Chernova, T. A., Muller, S., Newnam, G. P., Winslett, P. A., Wittich, K. B., Wilkinson, K. D., and Chernoff, Y. O. (2005) *Genetics* **169**, 1227-1242

25. Chernoff, Y. O., Newnam, G. P., Kumar, J., Allen, K., and Zink, A. D. (1999) *Mol Cell Biol* **19**, 8103-8112

26. Chacinska, A., Szczesniak, B., Kochneva-Pervukhova, N. V., Kushnirov, V. V., Ter-Avanesyan, M. D., and Boguta, M. (2001) *Curr Genet* **39**, 62-67

27. Glover, J. R., and Lindquist, S. (1998) *Cell* **94**, 73-82

28. Aron, R., Higurashi, T., Sahi, C., and Craig, E. A. (2007) *Embo J* **26**, 3794-3803

29. Summers, D. W., Douglas, P. M., Ren, H. Y., and Cyr, D. M. (2009) *J Biol Chem* **284**, 3628-3639

30. Tipton, K. A., Verges, K. J., and Weissman, J. S. (2008) *Mol Cell* **32**, 584-591

31. Shorter, J., and Lindquist, S. (2008) *Embo J* **27**, 2712-2724

32. Walsh, P., Bursac, D., Law, Y. C., Cyr, D., and Lithgow, T. (2004) *EMBO Rep* **5**, 567-571

33. Szabo, A., Langer, T., Schroder, H., Flanagan, J., Bukau, B., and Hartl, F. U. (1994) *Proc Natl Acad Sci U S A* **91**, 10345-10349

34. Langer, T., Lu, C., Echols, H., Flanagan, J., Hayer, M. K., and Hartl, F. U. (1992) *Nature* **356**, 683-689

35. Cyr, D. M., Lu, X., and Douglas, M. G. (1992) *J Biol Chem* **267**, 20927-20931

36. Cyr, D. M. (2008) *Cell* **133**, 945-947

37. Sahi, C., and Craig, E. A. (2007) *Proc Natl Acad Sci U S A* **104**, 7163-7168

38. Qiu, X. B., Shao, Y. M., Miao, S., and Wang, L. (2006) *Cell Mol Life Sci* **63**, 2560-2570

39. Lu, Z., and Cyr, D. M. (1998) *J Biol Chem* **273**, 5970-5978

40. Fan, C. Y., Ren, H. Y., Lee, P., Caplan, A. J., and Cyr, D. M. (2005) *J Biol Chem* **280**, 695-702

41. Fan, C. Y., Lee, S., Ren, H. Y., and Cyr, D. M. (2004) *Mol Biol Cell* **15**, 761-773

42. Ramos, C. H., Oliveira, C. L., Fan, C. Y., Torriani, I. L., and Cyr, D. M. (2008) *J Mol Biol* **383**, 155-166

43. Holstein, S. E., Ungewickell, H., and Ungewickell, E. (1996) *J Cell Biol* **135**, 925-937

44. Yan, W., Schilke, B., Pfund, C., Walter, W., Kim, S., and Craig, E. A. (1998) *Embo J* **17**, 4809-4817

45. Lu, Z., and Cyr, D. M. (1998) *J Biol Chem* **273**, 27824-27830

46. Li, J., Qian, X., and Sha, B. (2003) *Structure* **11**, 1475-1483

47. Caplan, A. J., Tsai, J., Casey, P. J., and Douglas, M. G. (1992) *J Biol Chem* **267**, 18890-18895

48. Flom, G. A., Lemieszek, M., Fortunato, E. A., and Johnson, J. L. (2008) *Mol Biol Cell* **19**, 5249-5258

49. Sha, B., Lee, S., and Cyr, D. M. (2000) *Structure* **8**, 799-807

50. Luke, M. M., Sutton, A., and Arndt, K. T. (1991) *J Cell Biol* **114**, 623-638

51. Yan, W., and Craig, E. A. (1999) *Mol Cell Biol* **19**, 7751-7758

52. Caplan, A. J., and Douglas, M. G. (1991) *J Cell Biol* **114**, 609-621

53. Johnson, J. L., and Craig, E. A. (2001) *J Cell Biol* **152**, 851-856

54. Glover, J. R., Kowal, A. S., Schirmer, E. C., Patino, M. M., Liu, J. J., and Lindquist, S. (1997) *Cell* **89**, 811-819

55. Bagriantsev, S. N., Gracheva, E. O., Richmond, J. E., and Liebman, S. W. (2008) *Mol Biol Cell*

56. Kryndushkin, D. S., Smirnov, V. N., Ter-Avanesyan, M. D., and Kushnirov, V. V. (2002) *J Biol Chem* **277**, 23702-23708

57. Krzewska, J., and Melki, R. (2006) *Embo J* **25**, 822-833

58. Sweeny, E. A., and Shorter, J. (2008) *Prion* **2**, 1-6

59. Coschigano, P. W., and Magasanik, B. (1991) *Mol Cell Biol* **11**, 822-832

60. Lian, H. Y., Zhang, H., Zhang, Z. R., Loovers, H. M., Jones, G. W., Rowling, P. J., Itzhaki, L. S., Zhou, J. M., and Perrett, S. (2007) *J Biol Chem*

61. Savistchenko, J., Krzewska, J., Fay, N., and Melki, R. (2008) *J Biol Chem*

62. Sharma, D., Stanley, R. F., and Masison, D. C. (2009) *Genetics* **181**, 129-137

63. Sondheimer, N., and Lindquist, S. (2000) *Mol Cell* **5**, 163-172

64. Derkatch, I. L., Bradley, M. E., Hong, J. Y., and Liebman, S. W. (2001) *Cell* **106**, 171-182

65. Derkatch, I. L., Uptain, S. M., Outeiro, T. F., Krishnan, R., Lindquist, S. L., and Liebman, S. W. (2004) *Proc Natl Acad Sci U S A* **101**, 12934-12939

66. Meriin, A. B., Zhang, X., He, X., Newnam, G. P., Chernoff, Y. O., and Sherman, M. Y. (2002) *J Cell Biol* **157**, 997-1004

67. Vitrenko, Y. A., Gracheva, E. O., Richmond, J. E., and Liebman, S. W. (2007) *J Biol Chem* **282**, 1779-1787

68. Wickner, R. B., Dyda, F., and Tycko, R. (2008) *Proc Natl Acad Sci U S A* **105**, 2403-2408

69. Kurahashi, H., Ishiwata, M., Shibata, S., and Nakamura, Y. (2008) *Mol Cell Biol* **28**, 3313-3323

70. Sondheimer, N., Lopez, N., Craig, E. A., and Lindquist, S. (2001) *Embo J* **20**, 2435-2442

71. Bradley, M. E., Edskes, H. K., Hong, J. Y., Wickner, R. B., and Liebman, S. W. (2002) *Proc Natl Acad Sci U S A* **99 Suppl 4**, 16392-16399

72. Li, J., and Sha, B. (2004) *Biol Proced Online* **6**, 204-208

73. Rudiger, S., Schneider-Mergener, J., and Bukau, B. (2001) *Embo J* **20**, 1042-1050

74. Sauer, F. G., Futterer, K., Pinkner, J. S., Dodson, K. W., Hultgren, S. J., and Waksman, G. (1999) *Science* **285**, 1058-1061

75. Choudhury, D., Thompson, A., Stojanoff, V., Langermann, S., Pinkner, J., Hultgren, S. J., and Knight, S. D. (1999) *Science* **285**, 1061-1066

76. Lopez, N., Aron, R., and Craig, E. A. (2003) *Mol Biol Cell* **14**, 1172-1181

77. Behrends, C., Langer, C. A., Boteva, R., Bottcher, U. M., Stemp, M. J., Schaffar, G., Rao, B. V., Giese, A., Kretzschmar, H., Siegers, K., and Hartl, F. U. (2006) *Mol Cell* **23**, 887-897

78. Gokhale, K. C., Newnam, G. P., Sherman, M. Y., and Chernoff, Y. O. (2005) *J Biol Chem* **280**, 22809-22818

79. Douglas, P. M., Summers, D. W., and Cyr, D. M. (2009) *Prion* **3**

80. Fiala, J. C. (2007) *Acta Neuropathol* **114**, 551-571

81. Balch, W. E., Morimoto, R. I., Dillin, A., and Kelly, J. W. (2008) *Science* **319**, 916-919

82. Chai, Y., Koppenhafer, S. L., Bonini, N. M., and Paulson, H. L. (1999) *J Neurosci* **19**, 10338-10347

83. Chan, H. Y., Warrick, J. M., Gray-Board, G. L., Paulson, H. L., and Bonini, N. M. (2000) *Hum Mol Genet* **9**, 2811-2820

84. Cummings, C. J., Mancini, M. A., Antalffy, B., DeFranco, D. B., Orr, H. T., and Zoghbi, H. Y. (1998) *Nat Genet* **19**, 148-154

85. Cohen, E., Bieschke, J., Perciavalle, R. M., Kelly, J. W., and Dillin, A. (2006) *Science* **313**, 1604-1610

86. Cheng, I. H., Scearce-Levie, K., Legleiter, J., Palop, J. J., Gerstein, H., Bien-Ly, N., Puolivali, J., Lesne, S., Ashe, K. H., Muchowski, P. J., and Mucke, L. (2007) *J Biol Chem* **282**, 23818-23828

87. Wyttenbach, A., Carmichael, J., Swartz, J., Furlong, R. A., Narain, Y., Rankin, J., and Rubinsztein, D. C. (2000) *Proc Natl Acad Sci U S A* **97**, 2898-2903

88. Wacker, J. L., Zareie, M. H., Fong, H., Sarikaya, M., and Muchowski, P. J. (2004) *Nat Struct Mol Biol* **11**, 1215-1222

Chapter Three

Use of Yeast as a System to Study Amyloid Toxicity

Reproduced from *Methods* Vol 53 2011 226-231

3.1 Abstract

The formation of amyloid-like fibrils is a hallmark of several neurodegenerative diseases. How the assembly of amyloid-like fibrils contributes to cell death is a major unresolved question in the field. The budding yeast *Saccharomyces cerevisiae* is a powerful model organism to study basic mechanisms for how cellular pathways regulate amyloid assembly and proteotoxicity. For example, studies of the amyloidogenic yeast prion [*RNQ+*] have revealed novel roles by which molecular chaperones protect cells from the accumulation of cytotoxic protein species. In budding yeast there are a variety of cellular assays that can be employed to analyze the assembly of amyloid-like aggregates and mechanistically dissect how cellular pathways influence proteotoxicity. In this review, we describe several assays that are routinely used to investigate aggregation and toxicity of the [*RNQ+*] prion in yeast.

3.2. Introduction

An extensive group of neurodegenerative disorders are characterized by the formation of amyloid-like fibrils, including Alzheimer's disease, Huntington's disease, and Creutzfeldt-Jakob disease (1). Amyloid-like fibrils are composed of β-sheet-rich conformers of a non-native protein that are assembled in a unique structure called a cross-β spine (2).This structure confers several unique properties that distinguish amyloid-like fibrils from amorphous, or disordered aggregates including resistance to proteases and insolubility in ionic detergents (3). While the accumulation of amyloid deposits is a diagnostic biomarker of amyloidosis, the connection between the assembly of amyloid-like fibrils and neuronal cell death is currently unclear (4-6). Furthermore, specific neuronal subpopulations are selectively susceptible to misfolding and aggregation of particular disease proteins suggesting there are complex cellular pathways that influence amyloid assembly and proteotoxicity. Our understanding of this process is still rudimentary and many questions remain to be answered.

There are numerous model organisms available to study amyloid-linked diseases. While every model organism has unique benefits and limitations, studies in the budding yeast *Saccharomyces cerevisiae* have provided substantial insight on mechanisms underlying the assembly of amyloid-like fibrils and proteotoxicity (7). Several proteins in *S. cerevisiae* known collectively as yeast prions can exist in a beta-rich conformation that possesses a high propensity to assemble into amyloid-like fibrils inside the cell (8). Molecular chaperones shear these amyloid-like assemblies to generate a steady pool of prion seeds that convert the native form of the protein into the beta-rich prion conformation and propagate the prion state (9). While studies on yeast prion biogenesis have centered on the yeast prions [*PSI+*] and [*URE3*], the prion [*RNQ+*]/[*PIN+*] has recently emerged as a powerful tool in the study of amyloid-linked toxicity in yeast. The [*RNQ+*] prion is formed by the yeast protein Rnq1 (10,11). Like other proteins that propagate as prions in budding yeast, Rnq1 possesses a domain enriched in glutamine/asparagines residues that is sufficient to assemble into amyloid-like fibrils and propagate as a prion (12-14). Interestingly, the induction of other prions in yeast requires Rnq1 to be in the [*RNQ+*] state. Rnq1 has no other known function in the cell outside

of this role in prion induction although yeast strains isolated in the wild are predominantly in a [*RNQ*+] state (15) suggesting there may be an important, yet undiscovered function for this prion (16). In addition, expression of the expanded-polyglutamine form of huntingtin is selectively toxic to yeast when Rnq1 is the [*RNQ*+] prion conformation (17). Thus, the [*RNQ*+] prion influences aggregation and toxicity of other glutamine-enriched proteins in yeast although the mechanism underlying this relationship is unclear.

Importantly, overexpression of Rnq1 is toxic to yeast specifically in the presence of the [*RNQ*+] prion (18). Toxicity was correlated with the accumulation of a soluble, non-amyloid-like Rnq1 protein species and chaperone-dependent [*RNQ*+] assembly protected cells from Rnq1-induced toxicity. Therefore, aberrations in [*RNQ*+] prion biogenesis can result in the accumulation of proteotoxic species and further investigation into this pathway will likely yield additional discoveries on how amyloid assembly pathways contribute to cell death. This review will describe a variety of assays to analyze Rnq1-induced toxicity and methods for characterizing amyloid-like aggregates in yeast.

3.3 Basic methods for culturing yeast

Methods for culturing and manipulating yeast are well-established and readily available (19). As such, this section will focus primarily on central guidelines for growing yeast cultures to study amyloid assembly and toxicity. All experiments described herein were performed at 30°C although the specific experimental temperature may vary depending upon the optimal growth conditions for the yeast strain background. Plasmids expressing aggregation-prone proteins can easily be transformed into yeast and maintained under selection by utilizing auxotrophic markers (ex. amino acids). Individual colonies are used to inoculate liquid cultures that can be expanded into liter-size volumes as long as cultures are properly aerated and nutrient-rich. The ability to collect large quantities of cells is one of the distinct advantages of using budding yeast over most other model systems. The most important consideration when culturing yeast is to maintain the cells in log-phase growth by consistently diluting cells in fresh media. However, yeast cells will undergo physiological changes similar to aging after repetitive diluting or indefinite time in stationary phase (20). As a result, exogenous plasmids should be freshly transformed to improve reproducibility between experiments.

One additional advantage to working with budding yeast is the availability of diverse promoters (both inducible and constitutive) that provide extensive flexibility in the time and level of protein expression. Inducible promoters are particularly important when studying proteotoxicity because the expression of a toxic protein needs to be tightly controlled during an experiment. One of the more common promoters for this kind of analysis is the *GAL1* promoter (21). As described below, this promoter is often used to examine how high level expression of a disease protein impacts cell viability by spotting assays or growth curves. There are several advantages to using the *GAL1* promoter for this kind of analysis. Expression from this promoter is repressed in the presence of glucose permitting very robust control of protein expression. To facilitate rapid expression from the *GAL1* promoter, yeast cells are initially grown in media containing raffinose as the carbon source because raffinose does not induce or repress expression from the *GAL1* promoter. Addition of galactose to the media rapidly induces protein expression within 30 minutes. One drawback is that

expression from the *GAL1* promoter cannot be titrated by varying the levels of galactose. Furthermore, some yeast strains are unable to unable to metabolize galactose and are thus inviable when galactose is the sole carbon source.

In contrast to the *GAL1* promoter, the *CUP1* promoter can be tightly controlled by varying levels of copper sulfate added to the media. Expressing a toxic protein such as Rnq1 from the CUP1 promoter can inhibit cell growth (22); however, caution should be exercised if levels of copper sulfate cause growth defects independent o f protein expression. This promoter is also used to constitutively express a protein of choice using low levels of copper sulfate (ex. 50μM or lower). Long-term, low level expression of an aggregation-prone protein such as Rnq1 allows the exogenous protein to reach steady state equilibrium with cellular pathways that regulate assembly of amyloid-like aggregates. As such, Rnq1 aggregation can be studied under conditions when this protein is not toxic to yeast and independent of changes in cell physiology that might accompany cytotoxicity. Constitutive, high level expression can also be achieved using promoters from housekeeping enzymes such as glyceraldehyde-3-phosphate dehydrogenase (GPD) or alcohol dehydrogenase (ADH). These promoters are powerful tools to analyze how overexpression of various cellular factors affects amyloid assembly and toxicity.

Expression constructs can also be placed in different plasmid backbones with unique elements that control the plasmid copy number within the cell (19). For example, episomal (2μ) vectors vary from 10-40 copies per cell and thus provide high levels of expression yet also display extensive variation from cell to cell. These plasmids are generally used in growth assays (ex. high copy suppressor screens) where cell to cell variation is not visible in measurements of population growth. Centromeric (CEN) plasmids are maintained at approximately 1-3 plasmids per cell and thus display more consistency in expression from cell to cell, yet also result in lower expression levels. To maintain consistent expression from cell to cell, expression constructs can also be integrated into the yeast genome. Ultimately, the decision to use one plasmid backbone may depend upon the specific protein of choice and the experimental context.

In the context of studying prion biogenesis, budding yeast offer one unique advantage over other model systems. Yeast strains can be "cured" of the prion state. For example, Rnq1 is soluble and does not assemble into amyloid-like aggregates in strains that are cured of the [*RNQ+*] prion state; now designated [*rnq-*]. The cured strain can be compared back to the [*RNQ+*] strain to determine how cellular factors such as molecular chaperones interact with the soluble versus amyloidogenic conformer of the same protein. Yeast strains can be cured of the prion state by two methods. First, if the protein determinant is non-essential such as Rnq1 then deleting the *RNQ1* gene will eventually cure yeast of the [*RNQ+*] prion state as the remaining Rnq1 protein is diluted over successive generations. If the Rnq1 protein is subsequently expressed in this strain from an exogenous plasmid, it will not assemble into amyloid-like aggregates because pre-existing [*RNQ+*] prion seeds are not present in the cell. An alternative and more common method is to treat cells with low doses of guanidine hydrochloride. This compound inhibits a molecular chaperone called Hsp104 that shears prion fibrils to generate new prion seeds and is required to propagate yeast prions (23,24). Two to three passages on solid media containing 3mM guanidine hydrochloride is typically sufficient to cure yeast of the prion state. One drawback to this method is that it is not selective for any specific prion. Both methods permanently cure yeast of the prion state because spontaneous prion induction is a highly unfavorable event (25).

3.4 Growth and viability assays

Spotting Assay

The most basic tool for studying amyloid toxicity in yeast is to monitor cell growth under conditions where an amyloidogenic protein is expressed compared to conditions when this protein either is not expressed or does not assemble into amyloid-like fibrils (ex. a cured prion strain). This method is readily applicable to high through-put screening of genetic factors that influence toxicity. Defects in cell growth can most easily be assessed by spotting yeast cells on solid agar media and comparing growth between strain expressing a toxic protein and a control strain. As shown in Figure 3.1, expressing Rnq1 from the *GAL1* promoter is toxic to yeast in a [*RNQ+*] dependent-manner (18). To perform this assay, single colonies from freshly transformed yeast are used to inoculate a liquid culture and when yeast cells have reach mid-log phase, equal concentrations of cells (~0.5 OD_{600}) are serially diluted onto solid selective media containing 2% galactose as the carbon source and incubated for 2-4 days at 30°C depending upon the strain. As a control, strains are simultaneously spotted on selective media containing glucose to show that changes in growth rates are dependent upon expression of the aggregation-prone protein.

Growth Curve

If differences in growth are too slight to detect by the spotting assay then toxicity can be quantitatively assessed by measuring growth curves in liquid media. The procedure begins as described above, except liquid cultures are induced with galactose at a very low density (OD_{600} 0.01-0.05) and OD_{600} measured approximately every 2 hours until strains reach stationary phase. Compared to the spotting assay, measuring growth curves is more labor intensive however this assay can determine at what point expression of a proteotoxic protein such as Rnq1 affects cell growth. Furthermore, resolving whether a defect in cell growth reflect cell cycle arrest or cell death might lead to a better understanding of the mechanism underlying proteotoxicity in this model system. To determine whether yeast cells have entered cell cycle arrest or cell death, an aliquot is removed from liquid cultures at varying timepoints post-expression and plated on selective media with 2% glucose

to repress the *GAL1* promoter. If cell viability is indeed reduced upon protein expression, then yeast cells will not grow on media with glucose while yeast cells would be expected to reenter the cell cycle when the proteotoxic insult is removed.

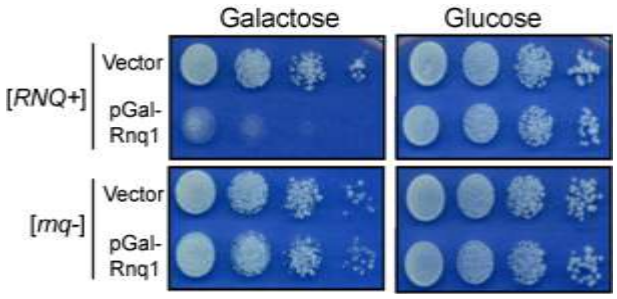

Figure 3.1. **Expression of amyloid-forming proteins is toxic to yeast.** Yeast cells (strain BY4741-[RNQ^{+}] or [*rnq*-]) were transformed with an empty pRS416 vector or pRS416(*GAL1-RNQ1)*. Liquid cultures were inoculated with freshly transformed yeast and incubated for one day at 30°C. Equal quantities of cells in mid-log phase (0.5 OD_{600}) were serially diluted (1:5) onto selective media containing glucose or galactose and incubated for approximately 3 days at 30°C and photographed.

3.5 Morphological analysis of protein aggregation

Fluorescence microscopy

A rapid method to analyze protein aggregation is fluorescently-tagging a protein of interest and visualizing intracellular localization via fluorescence microscopy. For example, Rnq1-GFP forms punctuate structures in [*RNQ+*] cells while is predominantly diffuse in [*rnq-*] cells (Fig. 3.2). If tagged constructs are expressed from inducible promoters, then a time-course can be performed to determine the kinetics of aggregation. To freeze cells at specific timepoints, cells in mid-log phase are treated with 0.1M phosphate buffer (pH6.8) and 3.7% formaldehyde then incubated at 25°C for 30 minutes to 1 hour. Cells are then washed once in phosphate buffer (pH7.4) and resuspended in phosphate buffer (pH 7.4) plus 1.2M sorbitol. Cells can be stored in this solution for several days at 4°C and further processed for immunofluorescent detection of other proteins or stained with commercially available dyes to identify organelles. Alternatively, fluorophore-conjugated proteins can be visualized by live cell imaging to characterize the dynamics of protein aggregation on the order of seconds to minutes.

There are several considerations when assessing protein aggregation by fluorescence microscopy. First, the appearance of foci within the cell does not imply the protein of interest is aggregating, yet may represent localization to a specific subcellular compartment or protein complex. Indeed, recent studies have suggested that misfolded and aggregated proteins are transported to distinct subcellular compartments (26), Thus, subcellular localization of a protein of interest should be compared with a panel of known organelle markers (ex nuclei, vacuole, etc). Furthermore, intracellular foci might be disordered, amorphous aggregates rather than amyloid-like assemblies. Additional analysis using the methods described below need to be performed to determine whether intracellular foci are indeed amyloid-like fibrils.

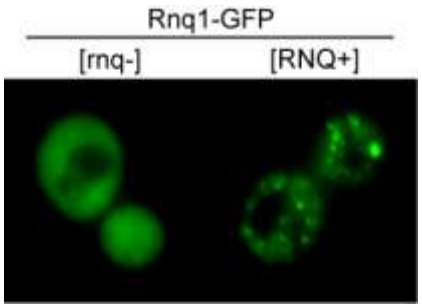

Figure 3. 2. **Visualization of protein aggregates by fluorescence microscopy.** (A)BY4741 cells ([*RNQ*$^{+}$] or [*rnq*-]) in mid-log phase expressing Rnq1-GFP from the *CUP1* promoter were induced with 50uM $CuSO_4$ for 2 hours and live cells visualized with a FITC filter set.

Thioflavin T Staining of Amyloid-like Fibrils in Yeast

One of the classic, defining characteristics of an amyloid-like fibril is recognition by amyloid-indicator dyes such as thioflavin T (27). Similar to amyloid fibrils formed in human diseases, intracellular yeast prion assemblies are also recognized by thioflavin T (18,28,29). To stain intracellular, amyloid-like particles with thioflavin T, an aggregation-prone protein such as Rnq1 is induced for an extended period of time (at least four hours) until it is predominantly assembled into single, distinct foci. Cells are fixed as described above, briefly permeabilized with phosphate buffer (pH 7.5) plus a weak non-ionic detergent such as 0.1% Triton-X, and treated with 0.001% thioflavin T for approximately 10 minutes at room temperature. The cells should be washed at least 3-4 times with phosphate buffer. Thioflavin T has excitation and emission wavelengths of 450nm and 482nm respectively when bound to amyloid-like fibrils and can be visualized in cells under standard FITC filter range. As a control [*RNQ*+] cells transformed with an empty vector can be used to determine the level of background staining and show thioflavin-t positive foci are dependent upon Rnq1 overexpression. If background ThT staining is very high, then reducing the concentration of ThT or increasing the number of washes should alleviate this problem.

3.6. Biochemical analysis of amyloid-like aggregates

The structure of amyloid-like aggregates renders these assemblies insoluble in ionic detergents such as sodium dodecyl sulfate (SDS). There are several assays that exploit this unique property to biochemically distinguish large, SDS-insoluble assemblies from unassembled, SDS-soluble protein species in yeast cell extracts. As mentioned above, maintaining cells in mid-log phase is critical when performing these experiments. Additionally, if the aggregate-prone protein is expressed from an inducible promoter, a time-course experiment should be performed to characterize assembly kinetics. Once the basic dynamics of protein assembly into SDS-resistant aggregates is established, then these assays can be performed under conditions where select cellular factors are overexpressed or deleted to determine how specific cellular pathways influence the assembly of amyloid-like aggregates.

Differential high speed centrifugation

The most simple approach to characterizing the formation of amyloid-like aggregates is to separate SDS-insoluble aggregates by high speed centrifugation. This technique allows direct comparison between soluble and insoluble pools of an amyloid-forming protein. However, this technique is relatively insensitive to slight changes in the size of amyloid-like oligomers or fibrils. As shown in Figure 3.3A, excess Rnq1-YFP partitions predominantly in the SDS-insoluble fraction yet a pool also remains in the SDS-soluble supernatant. In contrast, excess Rnq1-YFP resolves exclusively in the SDS-soluble fraction in [*rnq*-] cells (18).

To analyze solubility of Rnq1, cells expressing Rnq1 are first lysed by glass bead disruption under moderately denaturing conditions (150mM NaCl, Hepes pH7.4, 1mM EDTA, 1mM DTT, 1% Triton-X, 0.2% SDS, 1mM PMSF, protease inhibitor cocktail). Depending upon the amyloidogenic protein, the concentration of SDS can be increased to 2% to increase the stringency of this assay. Cell lysates are first processed by a short centrifugation step (650xg for 3min at 4°C) to remove unbroken cells. After the spin, the supernatant is subsequently spun at 100,000 x g for 30min to 1 hour in 1.5mL Beckman polyallomer centrifuge tubes. The speed and time may vary depending upon the

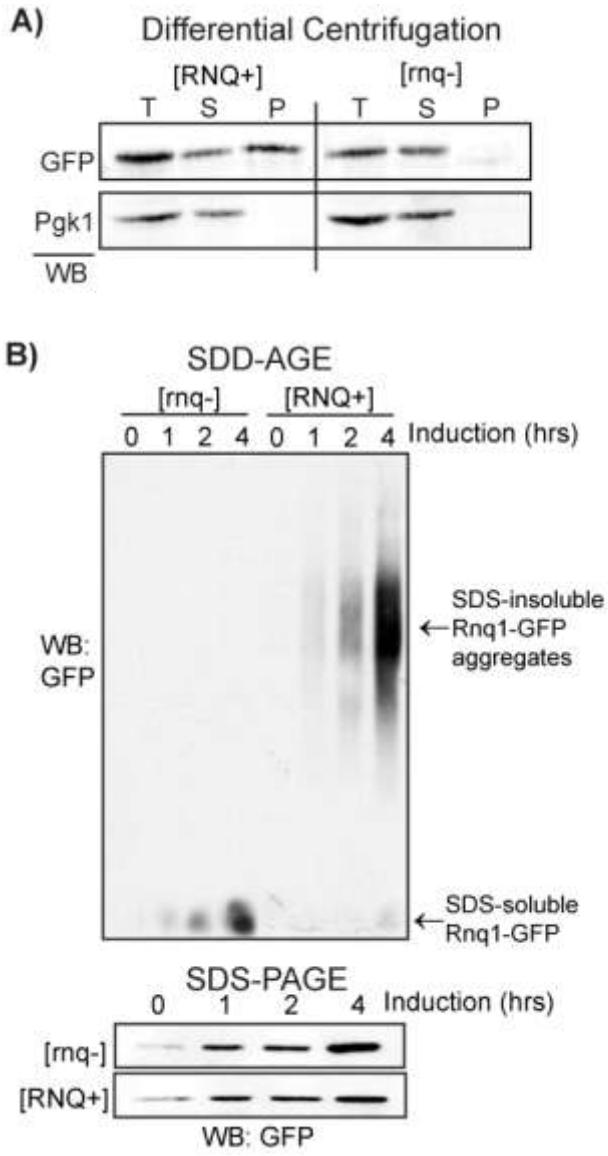

Figure 3.3. Biochemical analysis of SDS-insoluble, amyoid-like aggregates. (A) Separation of SDS-insoluble Rnq1-GFP aggregates by high-speed differential centrifugation. BY4741 cells ([*RNQ*$^{+}$] or [*rnq*-] transformed with pGAL-RNQ1YFP were induced for 2 hours with 2% galactose. Cells were processed as described in the main text and equal volumes of total, supernatant, and pellet fractions were analyzed by SDS-PAGE and western immunoblotting for GFP (Roche) and Pgk1 (Invitrogen). (B) SDD-AGE analysis of Rnq1-GFP SDS-insoluble aggregates. BY4741 cells ([*RNQ*$^{+}$] or [*rnq*-] transformed with pCUP-RNQ1GFP were induced with 50uM $CuSO_4$ and samples were collected at 0hr, 1hr, 2hr, and 4hr post-induction. Cells were processed as described in the main text and the PVDF membrane analyzed by western immunoblotting for GFP. Lysates were also analyzed by SDS-PAGE and western immunobloting for GFP (lower panel).

specific protein but these conditions appear sufficient for a majority of endogenous Rnq1 to resolve in the insoluble pellet in [*RNQ+*] cells. An aliquot from the lysate is saved prior to the spin represent the input (or Total) fraction. After the spin, an aliquot from the supernatant is saved and the pellet is resupended in lysis buffer (in a volume equivalent to the original volume used for the spin). Each fraction (total, supernatant, pellet) is mixed with a equal volume of 2X sample buffer (125mM Tris-HCl pH6.8, 4% SDS, 4mM EDTA, and 20% glycerol, 8% beta-mercaptoethanol) and samples are analyzed by SDS-polyacrylamide gel electrophoresis (SDS-PAGE).

Semi-denaturing detergent agarose gel electrophoresis (SDD-AGE)

SDS-insoluble aggregates can also be separated from SDS-soluble protein species in an agarose gel. In contrast to methods that rely on SDS-PAGE, this method can resolve changes in the size of SDS-insoluble oligomers. For example, Kryndushkin *et al* demonstrated that inhibiting the chaperone Hsp104 results in a transient increase in the size of SDS-insoluble oligomers and subsequent conversion into the SDS-soluble pool (30). This experiment provided crucial evidence that Hsp104 shears prion fibrils to generate new prion seeds in order to propagate the prion state. In Figure 3.3B, Rnq1-GFP was induced from a copper promoter and lysates from various timepoints resolved by SDD-AGE. As Rnq1-GFP accumulates, a SDS-insoluble pool appears first then a SDS-soluble pool appears at the latest time point. However, Rnq1-GFP is entirely soluble in [*rnq-*] cells. Compared to differential high speed centrifugation, this technique is relatively more labor intensive, though it can provide significant insight into the relative ratio of soluble vs insoluble pools as well as changes in the size of SDS-insoluble oligomers. To perform this assay, yeast cells are lysed by glass bead disruption moderately denaturing conditions (150mM NaCl, 50mM Hepes pH 7.4, 1mM EDTA, 1mM DTT, 1% Triton X, 0.2% SDS, 1mM PMSF, yeast protease inhibitor cocktail). Yeast lysates are cleared by centrifugation (650 x g, 3min, 4°C). The supernatant is saved and protein concentrations normalized between samples (higher concentrations are ideal >2.0mg/mL). Normalized lysates are added to an equal volume of 2X SDD-AGE buffer (1XTAE buffer [0.8mM Tris-Acetate,0 .02mM EDTA], 4% SDS, 10% glycerol 8% beta-mercaptoethanol). Lysates are incubated at 37°C for 10

minutes and at least 100µg loaded into a 1.5% agarose gel (made with 1xTAE buffer + 0.1%SDS). Lysates are run at ~70 volts for approximately 2-3 hours. The gel is transferred onto a PVDF membrane at 24 volts for 1.5 hours in standard Tris-based buffer (alternatively you can transfer for 8 hours at 12 volts).The transfer step generates a large amount of heat so the buffer and transfer apparatus should be chilled at 4°C prior to use. The transfer step is inefficient and requires practice and some optimization. The PVDF membrane is analyzed by western immunoblotting for the protein of interest using standard methods.

Filter Trap

A filter trap assay is another common and rapid method for analyzing the formation of large, SDS-insoluble aggregates. Initially, this technique was used to analyze aggregation of the polyglutamine-expanded form of huntingtin from cell and tissue extracts (31). However, this assay can also be applied to the analysis of large, SDS-insoluble aggregates formed by yeast prions (32,33). In contrast to the assays described above only the large, SDS-insoluble pool is observed and cannot be directly compared to the SDS-soluble pool that is lost through the cellulose acetate membrane. However, this technique is applicable to large scale analysis, for example, assessing changes in SDS-insoluble aggregate formation under a variety of environmental conditions or genetic backgrounds.

To perform this assay, yeast lysates are generated as described above for SDD-AGE analysis. After protein concentrations are standardized between samples, lysates are applied to a cellulose acetate membrane (0.2µM pore size -Beckman) that is previously equilibrated with lysis buffer and assembled in a slot blot apparatus. The samples are allowed to flow through the membrane by gravity. While still in the slot blot apparatus, the membrane is washed with lysis buffer containing 2% SDS. Once the membrane is dry, it is subsequently processed by western immunoblotting for the protein of interest. Samples should also be spotted onto a nitrocellulose membrane or analyzed by SDS-PAGE to analyze total protein levels. If there is a high level of background, then the concentration of SDS can be increased or the samples heated at various temperatures prior to application on the membrane. Alternatively, the samples can be titrated onto the membrane to identify the linear range of the signal.

If there is a poor signal, then the amount of SDS can be reduced or the protein induction time increased to accumulate more of the SDS-insoluble aggregate pool.

Size-exclusion chromatography

The assays described above separate amyloid-like particles into a SDS-soluble and SDS-insoluble protein species. However, there are times when more detailed resolution is required to characterize assembly intermediates that are solubilized by the presence of SDS. In addition, protein-protein interactions are typically disrupted by the presence of SDS and lost in these assays. To bypass this complication, amyloid-like assemblies can be resolved by size exclusion chromatography. We have previously used this technique to distinguish the ratio of assembled, high molecular weight pools of Rnq1 from unassembled, low molecular protein species (22,32,33). Resolving yeast cell extracts by size-exclusion chromatography requires a large quantity of yeast (>100 OD_{600}) because cell extracts are diluted over the column volume which can exceed 100mL depending upon the specific column. Cell growth conditions are the same was described above with a particular emphasis on maintaining cells in mid-log phase and proper aeration throughout the experiment especially as the culture volume is expanded to liter-size to collect enough yeast cells for this experiment. Cells are lysed as described above by glass bead disruption in non-denaturing lysis buffer (150mM NaCl, 50mM Hepes pH 7.4, 1mM EDTA, 0.1% Triton X, plus 1mM PMSF and protease inhibitor cocktail). Specific components in this buffer can be modified depending upon the protein-protein interactions that are under investigation. For example, if a specific protein-protein interaction is ATP-dependent, then EDTA should be omitted and ATP included in the buffer. Cell lysates are precleared twice by centrifugation (650 x g, 3min, 4°C) to ensure cell debris is completely removed from the lysate. Inject about 1-5mg cell lysate into size-exclusion column (pre-equilibrated with cold lysis buffer) and collect fractions spanning the void volume to the fractions eluting with the molecular weight of the monomer. The void volume is typically identified by the elution volume of blue dextran and the included volume of the column calibrated by a series of known molecular weight markers. Fractions can be assessed for proteins of interest by SDS-PAGE and western immunoblotting.

If lysates are separated on the appropriate resin then the relative ratio of assembled to unassembled protein can be directly compared. One important consideration is that this approach does not distinguish SDS-insoluble, amyloid-like particles from disordered aggregates or large protein complexes because denaturing buffers are not always compatible with resins in size-exclusion columns. To overcome this restriction, elution fractions can be applied to the assays described above to identify fractions that contain SDS-insoluble aggregates. Furthermore, the elution profile of Rnq1 in a [*RNQ+*] strain can be compared back to the elution profile in a [*rnq-*] strain when these proteins do not assemble into amyloid-like conformers (17,18,32).

In summary, these biochemical assays offer distinct methods for analyzing the assembly of amyloid-like aggregates. Differential centrifugation and filter trap are the least labor techniques yet do not reveal insight on aggregate size and are most insensitive to subtle changes in the levels of SDS-insoluble aggregates. In contrast, SDD-AGE and size exclusion chromatography are more labor intensive and provide more sensitive information on aggregate assembly such as relative oligomer size. Finally, while size exclusion chromatography does not distinguish SDS-soluble from SDS-insoluble aggregates, it is the most sensitive method for separating aggregates based on oligomer size and allows for identification of protein:protein interactions that are lost during solubilization in SDS. A comprehensive approach (using methods from both categories) is ideal when trying to understand how cellular factors such as molecular chaperones influence amyloid assembly pathways and proteotoxicity.

3.7. Final Conclusions

The connection between amyloid fibril formation and neurodegeneration is a significant matter of debate. Despite enormous effort over several decades, our basic understanding of the amyloid assembly pathway is still lacking and the complex interplay between protein quality control networks and protein aggregation remains unclear. Budding yeast has emerged as a powerful model system to investigate mechanistic details underlying how assembly of amyloid-like aggregates contributes to cell death. A wide variety of cellular assays are available to dissect this problem utilizing the power of yeast genetics as well as biochemical manipulation of yeast extracts. While yeast cells cannot recapitulate every feature specific to neurons studies in *S. cerevisiae* can provide a sound foundation of mechanistic understanding to test specific hypothesizes in more complex model organisms.

3.8. References

1. Carrell, R. W., and Lomas, D. A. (1997) *Lancet* **350**, 134-138

2. Nelson, R., Sawaya, M. R., Balbirnie, M., Madsen, A. O., Riekel, C., Grothe, R., and Eisenberg, D. (2005) *Nature* **435**, 773-778

3. Chiti, F., and Dobson, C. M. (2006) *Annu Rev Biochem* **75**, 333-366

4. Haass, C., and Selkoe, D. J. (2007) *Nat Rev Mol Cell Biol* **8**, 101-112

5. Treusch, S., Cyr, D. M., and Lindquist, S. (2009) *Cell Cycle* **8**, 1668-1674

6. Robakis, N. K. (2010) *Neurodegener Dis* **7**, 32-37

7. Khurana, V., and Lindquist, S. (2010) *Nat Rev Neurosci* **11**, 436-449

8. Shorter, J., and Lindquist, S. (2005) *Nat Rev Genet* **6**, 435-450

9. Jones, G. W., and Tuite, M. F. (2005) *Bioessays* **27**, 823-832

10. Sondheimer, N., and Lindquist, S. (2000) *Mol Cell* **5**, 163-172

11. Derkatch, I. L., Bradley, M. E., Hong, J. Y., and Liebman, S. W. (2001) *Cell* **106**, 171-182

12. Wickner, R. B., Dyda, F., and Tycko, R. (2008) *Proc Natl Acad Sci U S A* **105**, 2403-2408

13. Patel, B. K., and Liebman, S. W. (2007) *J Mol Biol* **365**, 773-782

14. Vitrenko, Y. A., Pavon, M. E., Stone, S. I., and Liebman, S. W. (2007) *Curr Genet* **51**, 309-319

15. Resende, C. G., Outeiro, T. F., Sands, L., Lindquist, S., and Tuite, M. F. (2003) *Mol Microbiol* **49**, 1005-1017

16. Halfmann, R., Alberti, S., and Lindquist, S. (2010) *Trends Cell Biol*

17. Meriin, A. B., Zhang, X., He, X., Newnam, G. P., Chernoff, Y. O., and Sherman, M. Y. (2002) *J Cell Biol* **157**, 997-1004

18. Douglas, P. M., Treusch, S., Ren, H. Y., Halfmann, R., Duennwald, M. L., Lindquist, S., and Cyr, D. M. (2008) *Proc Natl Acad Sci U S A*

19. Guthrie, C., and Fink, G. R. (2002) *Guide to yeast genetics and molecular and cell biology. Part B*. Methods in enzymology, Academic Press, San Diego, Calif.

20. Steinkraus, K. A., Kaeberlein, M., and Kennedy, B. K. (2008) *Annu Rev Cell Dev Biol* **24**, 29-54

21. St John, T. P., Scherer, S., McDonell, M. W., and Davis, R. W. (1981) *J Mol Biol* **152**, 317-334

22. Douglas, P. M., Treusch, S., Ren, H. Y., Halfmann, R., Duennwald, M. L., Lindquist, S., and Cyr, D. M. (2008) *Proc Natl Acad Sci U S A* **105**, 7206-7211

23. Jung, G., and Masison, D. C. (2001) *Curr Microbiol* **43**, 7-10

24. Ferreira, P. C., Ness, F., Edwards, S. R., Cox, B. S., and Tuite, M. F. (2001) *Mol Microbiol* **40**, 1357-1369

25. Cox, B. S., Byrne, L. J., and Tuite, M. F. (2007) *Prion* **1**, 170-178

26. Kaganovich, D., Kopito, R., and Frydman, J. (2008) *Nature* **454**, 1088-1095

27. Sipe, J. D., and Cohen, A. S. (2000) *J Struct Biol* **130**, 88-98

28. Kawai-Noma, S., Pack, C. G., Kojidani, T., Asakawa, H., Hiraoka, Y., Kinjo, M., Haraguchi, T., Taguchi, H., and Hirata, A. (2010) *J Cell Biol* **190**, 223-231

29. Kimura, Y., Koitabashi, S., and Fujita, T. (2003) *Cell Struct Funct* **28**, 187-193

30. Kryndushkin, D. S., Alexandrov, I. M., Ter-Avanesyan, M. D., and Kushnirov, V. V. (2003) *J Biol Chem* **278**, 49636-49643

31. Scherzinger, E., Lurz, R., Turmaine, M., Mangiarini, L., Hollenbach, B., Hasenbank, R., Bates, G. P., Davies, S. W., Lehrach, H., and Wanker, E. E. (1997) *Cell* **90**, 549-558

32. Douglas, P. M., Summers, D. W., Ren, H. Y., and Cyr, D. M. (2009) *Mol Biol Cell* **20**, 4162-4173

33. Summers, D. W., Douglas, P. M., Ren, H. Y., and Cyr, D. M. (2009) *J Biol Chem* **284**, 3628-3639

Chapter Four

The type I Hsp40 Ydj1 utilizes a farnesyl moiety and zinc finger-like region to suppress prion toxicity

Reproduced from *J. Biol. Chem*. 2009 *Vol 284* 3628-3639

4.1 Abstract

Type I Hsp40s are molecular chaperones that protect neurons from degeneration by modulating the aggregation state of amyloid-forming proteins. How Type I Hsp40s recognize β-rich, amyloid-like substrates is currently unknown. Thus, we examined the mechanism for binding between the Type I Hsp40 Ydj1 and the yeast prion [RNQ^{+}]. Ydj1 recognized the Gln/Asn-rich prion domain from Rnq1 specifically when it assembled into the amyloid-like [RNQ^{+}] prion state. Upon deletion of *YDJ1*, overexpression of the Rnq1 prion domain killed yeast. Surprisingly, binding and suppression of prion domain toxicity by Ydj1 was dependent upon farnesylation of its C-terminal CAAX box and action of a zinc-finger-like region. In contrast, folding of luciferase was independent of farnesylation, yet required Ydj1's zinc finger-like region and a conserved hydrophobic peptide-binding pocket. Type I Hsp40s contain at least three different domains that that work in concert to bind different protein conformers. The combined action of a farnesyl moiety and zinc finger-like region enable Type I Hsp40s to recognize amyloid-like substrates and prevent formation of cytotoxic protein species.

4.2 Introduction

Protein misfolding and aggregation are common themes in neurodegenerative maladies termed conformational diseases. A subset of these disorders including Alzheimer's disease and the transmissible spongiform encephalopathies (prion diseases) are characterized by the accumulation of a stable, ß-sheet rich fibrils called amyloid (1). Criteria that distinguish amyloid-like fibrils from amorphous aggregates include resistance to SDS-solubilization and binding of the dye thioflavin T (2). The direct connection between amyloid accumulation and neuropathology is still a matter of debate (3-5). Yet, the flux of proteins through amyloid forming pathways correlates well with disease (3-5).

Hsp70 molecular chaperones protect against neurodegeneration associated with conformational disease via suppression of protein aggregation or conversion of toxic species into non-toxic aggregates or amyloid (6,7). Hsp70 has broad substrate selectivity and co-chaperones in the Hsp40/DnaJ family specify Hsp70 targets. Upon delivery of substrate, Hsp40s stimulate Hsp70 ATPase activity through a conserved J-domain and thereby stabilize Hsp70:polypeptide complexes. Nucleotide exchange factors (NEFs) convert Hsp70-ADP to Hsp70-ATP releasing non-native substrate for further rounds of folding or degradation (8,9). Escape of disease-related proteins from the action of Hsp70/Hsp40 and other quality control machinery leads to the accumulation of toxic protein species (10).

Recognition of pathogenic proteins by Hsp40s represents an important line of defense against the accumulation of cytotoxic protein species (4,11). However, the mechanism for substrate recognition by Hsp40s is unclear because the Hsp40 family is large and members have specialized domains that direct them to different subcellular locations or enable binding to select substrates (12,13). Type I Hsp40s possess a centrally located domain, which contains a zinc-finger like region (ZFLR), that appears to control the quaternary structure of Type I Hsp40 homodimers (14). The ZFLR has been implicated in substrate transfer to Hsp70 and the binding

of some Type I Hsp40 substrates (15-17). Type I Hsp40s can independently bind non-native polypeptides and also cooperate with Hsp70 to suppress protein aggregation (18,19). Importantly, human and yeast Type I Hsp40s are highly conserved and functionally interchangeable (12).

Interestingly, Type I Hsp40s such as human DnaJ 2 (HDJ-2) and yeast DnaJ 1 (Ydj1) are unique in that they contain a C-terminal CAAX box that is post-translationally modified by farnesyl (20,21). Farnesylation helps localize a pool of Type I Hsp40s to the cytoplasmic face of the endoplasmic reticulum (ER) and is required for cells to survive heat stress (22). One function of ER-localized Type I Hsp40s is the folding of polytopic membrane proteins (21). However, even though the entire pool of Ydj1 is farnesylated a large portion is found in the cytosol (22). Thus, it is conceivable that the farnesyl moiety of Ydj1/Hdj-2 has additional roles in cytoprotection including regulation of stress response or assistance with polypeptide binding.

Study of Hsp40 action in propagation of the yeast prion [RNQ^+]/[PIN^+] (23,24) provides a tractable model system to answer basic questions about mechanisms for chaperone action in the suppression of proteotoxicity. Overexpression of Rnq1 kills yeast in the presence of [RNQ^+] seeds, yet toxicity is associated with the accumulation of off-pathway, non-amyloid forms of Rnq1 (4). Rnq1 has an N-terminal non-prion domain with no known enzymatic function though it appears to regulate the conversion of native Rnq1 into the [RNQ^+] prion (25). Rnq1 also possesses a C-terminal prion domain (PrD) that is enriched in glutamines (Gln) and asparagines (Asn) and readily assembles into the [RNQ^+] prion state when expressed alone or as a chimera (23,26). Interestingly, the Type II Hsp40 Sis1 is required for [RNQ^+] propagation (27) and suppresses Rnq1 toxicity via increasing the flux of Rnq1 into the [RNQ^+] assembly pathway (4). On the other hand, the Type I Hsp40 Ydj1 can cure yeast of some [RNQ^+] variants (28), but it cannot suppress Rnq1 cytotoxicity (4). While Sis1 binds a hydrophobic motif in the Rnq1 non-prion domain (4) the Ydj1-binding site is unknown (29). Since Ydj1 and Sis1 show distinct substrate selectivity (13) we investigated whether they exert their disparate effects on Rnq1 biogenesis and toxicity via binding different Rnq1 domains.

We found that purified Ydj1 recognizes Gln/Asn-rich peptides in the PrD of Rnq1. In *in vivo* studies, Ydj1 specifically recognized the amyloid-like [*RNQ*$^{+}$] form of the Gln/Asn-rich Rnq1 PrD. Furthermore, deletion of *YDJ1* sensitized yeast to excess levels of the PrD. Interestingly, Ydj1 binding and suppression of toxicity was dependent upon both the Type I Hsp40 ZFLR and farnesylation. On the other hand, the ZFLR and peptide-binding pocket cooperated in the folding of luciferase, while farnesylation of Ydj1 was dispensable in this activity. Thus, Type I Hsp40s utilize specialized domains to recognize non-native proteins that exist in different conformational states. Demonstration of the domain requirements for Ydj1 binding to the amyloid-like conformer of the Rnq1 helps explain how human Type I Hsp40s fight conformational disease.

4.3 Results

The Rnq1 PrD forms benign intracellular aggregates. Overexpression of Rnq1 is toxic to yeast when endogenous Rnq1 is assembled in its [*RNQ*$^{+}$] conformation (4). Cell death is thought to occur due to inefficient conversion of overexpressed Rnq1 into amyloid-like [*RNQ*$^{+}$] prions and the accumulation of a templated toxic species. Furthermore, defects in Sis1-binding exacerbate Rnq1 toxicity by decreasing the efficiency of [*RNQ*$^{+}$] assembly. The nature of the toxic Rnq1 species is not clear and how defects in chaperone binding lead to its accumulation are unknown. Thus, we investigated whether removal of the entire non-prion domain and elimination of the Sis1 binding site would enhance Rnq1 proteotoxicity. However, while overexpression of Rnq1 was toxic to [*RNQ*$^{+}$] cells, overexpression of the PrD was not (Fig. 4.1A & B). Overexpression of Rnq1 or PrD did not alter cell growth in the absence of prion seeds ([*rnq*-] background). Thus, the presence of the non-prion domain on Rnq1 somehow leads to the accumulation of a toxic Rnq1 species.To gain insight into the nature of the toxic Rnq1 species we characterized intermediates on the pathway for conversion of native Rnq1 and PrD into amyloid-like [*RNQ*$^{+}$] prion. Rnq1-GFP and PrD-GFP each formed intracellular aggregates in a [*RNQ*$^{+}$] background that were morphologically indistinguishable by fluorescence microscopy (Fig. 4.1C). Rnq1 was not observed to coalesce in a [*rnq*-] background though a small population of cells (<5%) expressing PrD-GFP contained non-toxic aggregates. In a [*RNQ*$^{+}$] background, Rnq1-GFP partitioned predominantly in the Triton-insoluble pellet of yeast extracts, though a significant population was present in the Triton-soluble supernatant (Fig. 4.1D). In contrast, PrD-GFP fractionated exclusively in the Triton-insoluble pellet in a [*RNQ*$^{+}$] background. In a [*rnq*-] state, Rnq1-GFP was predominantly soluble while PrD-GFP was present in both Triton-soluble and insoluble appear toxic.

Next, the size of Rnq1-GFP and PrD-GFP assembly intermediates was examined by gel filtration chromatography (Fig. 4.1E). In [*RNQ*$^{+}$] cells, Rnq1-GFP eluted in two distinct high molecular pools; one near the void volume (Vo) and the other in a broad peak that was larger than

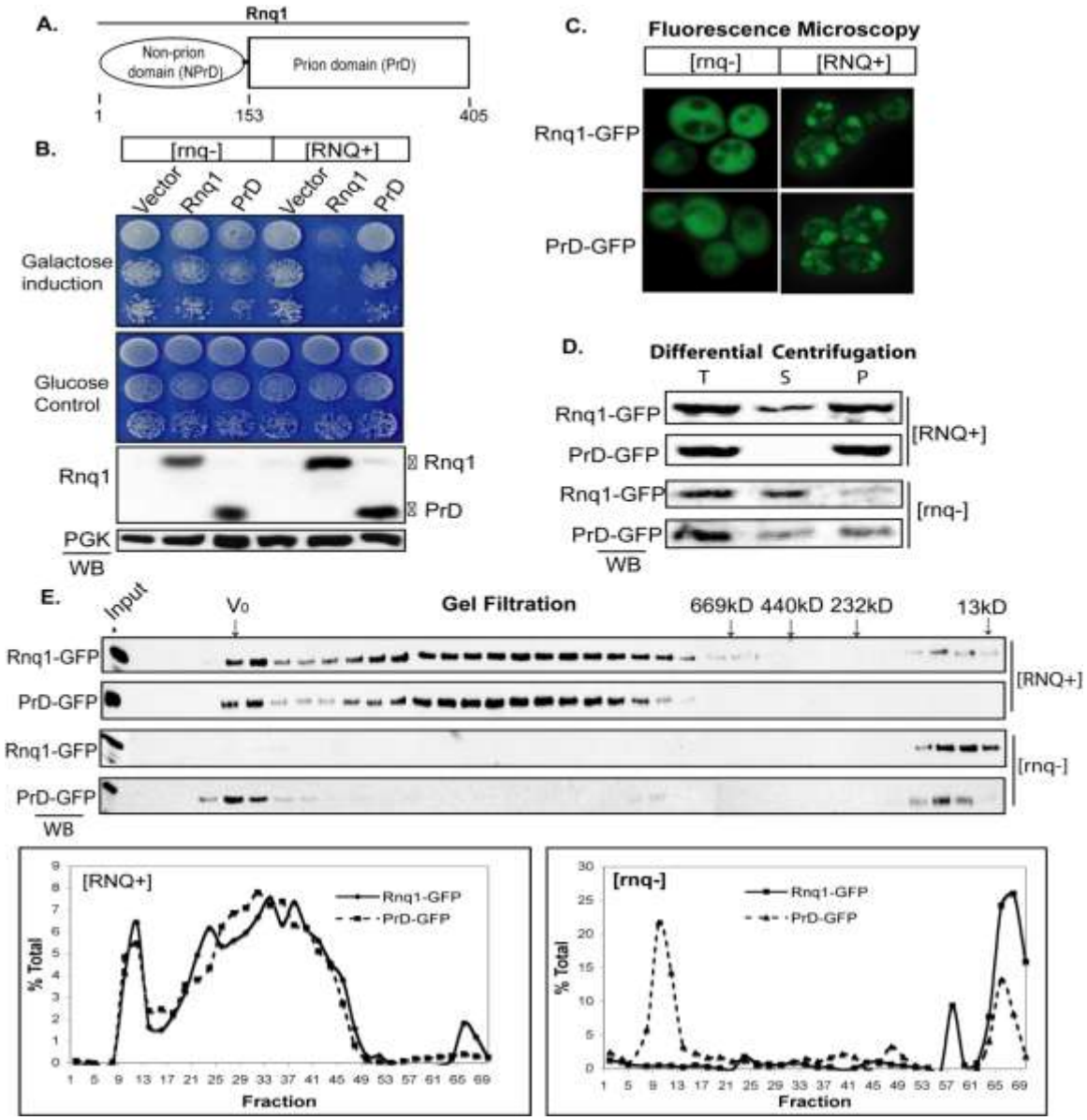

Figure 4.1 The Rnq1 PrD assembles into benign [RNQ$^+$] prion. (**A**) Domain boundaries of Rnq1 from *S. cerevisiae*. (**B**) Wild type yeast in a [*RNQ*$^+$] or [*rnq*$^-$] background harboring galactose-inducible forms of Rnq1, PrD, or an empty vector were serially diluted onto media containing galactose or glucose. Western blots below show protein levels. (**C**) Fluorescence microscopy of representative cells expressing Rnq1-GFP or PrD-GFP in a [*RNQ*$^+$] or [*rnq*$^-$] background. **(D)** Differential centrifugation of Rnq1-GFP and PrD-GFP in a [*RNQ*$^+$] or [*rnq*$^-$] background. Briefly, cell lysates were generated under non-denaturing conditions (50mM Hepes pH 7.4, 150mM NaCl, 0.1% Triton X-100, 1mM EDTA) and separated by high-speed centrifugation (100,000xg). Total input (T), supernatant (S), and pellet (P) fractions were resolved by SDS-PAGE. **(E)** Yeast lysates generated as above under non-denaturing conditions were resolved on a Sephacryl S-500HR gel filtration column. Every other fraction was examined by SDS-PAGE. Below is quantification of fractions normalized to total signal from [*RNQ*$^+$] lysates (left graph) or [*rnq*-] lysates (right graph).

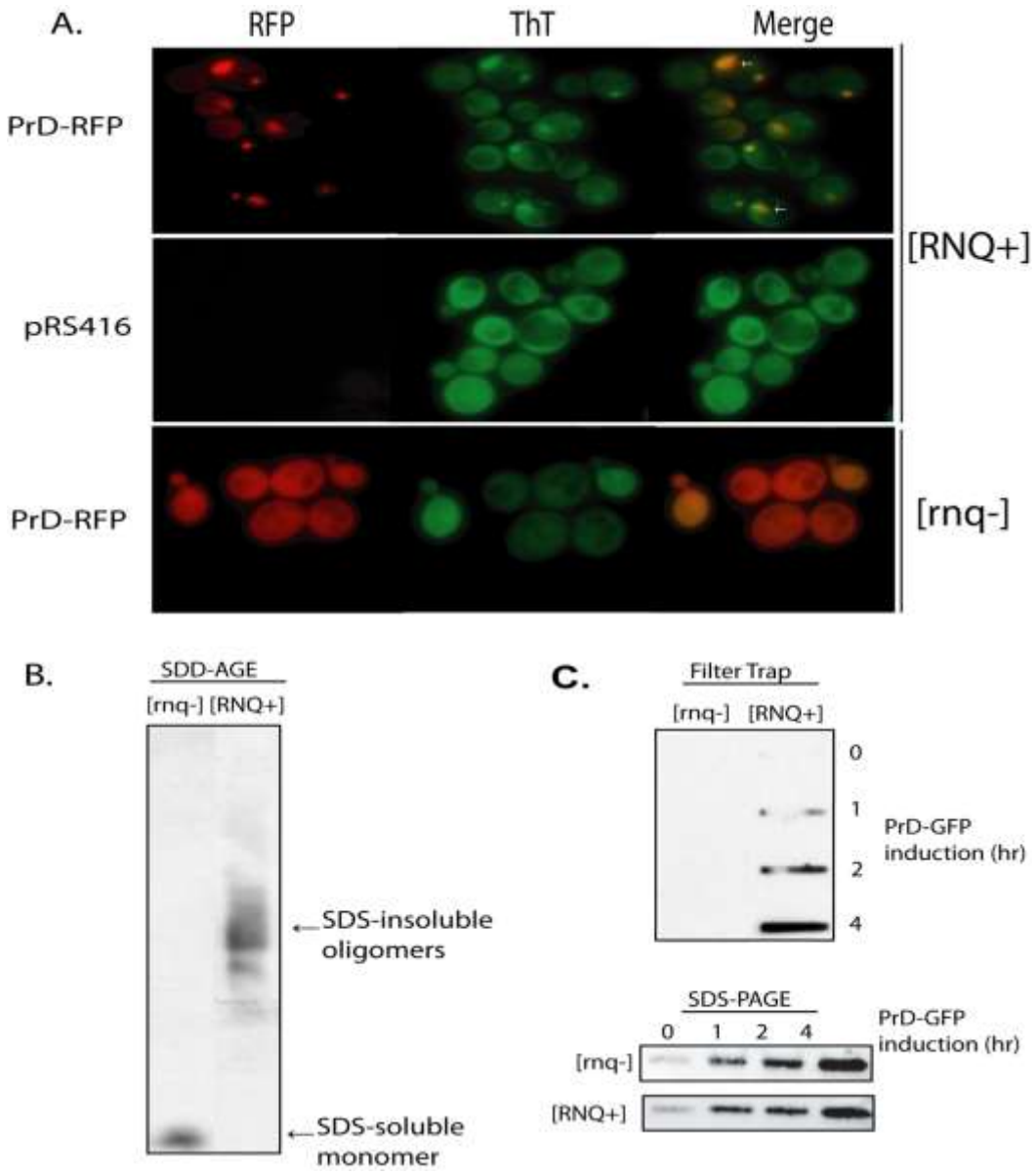

Figure 4.2 The Rnq1 PrD forms SDS-insoluble, amyloid-like [RNQ$^+$] prion. **(A)** In wildtype cells, PrD-RFP was expressed overnight from a copper inducible promoter in [*RNQ*$^+$] and [*rnq*$^-$] cells. Cells were fixed and permeabilized then treated with the amyloid indicator dye Thioflavin t. Arrows indicate PrD-RFP aggregates that co-localized with thioflavin T positive puncta. Thioflavin T staining was diffuse in [*rnq*$^-$] background. As a control, [*RNQ*$^+$] cells harboring an empty vector were treated simultaneously to demonstrate Thioflavin t positive puncta were dependent upon PrD-RFP expression and did not represent amyloid-like aggregates from other yeast prions. **(B)** PrD-GFP was expressed in wild type cells in a [*RNQ*$^+$] and [*rnq*$^-$] background and cell lysates subjected to SDD-AGE analysis. PrD-GFP formed SDS-insoluble only observed in [*RNQ*$^+$] cells. **(C)** PrD-GFP assembly into SDS-insoluble aggregates was also assessed by filter trap. Cell lysates were analyzed during a time course for retention on a cellulose acetate membrane under denaturing conditions. PrD-GFP only formed SDS-insoluble aggregates in [*RNQ*$^+$] cells.

thyroglobulin (669kDa), but still in the included volume. In addition, a pool of Rnq1-GFP eluted similar to a monomeric form. PrD-GFP also formed two high molecular weight pools, yet in contrast to Rnq1; no low molecular weight species was detected. The material in the void volume was predominantly SDS-soluble while Rnq1/PrD-GFP species in the broad included peak were insoluble in SDS (data not shown). In a [*rnq*-] background, Rnq1-GFP resided exclusively in the low molecular weight pool while PrD-GFP eluted in the void volume as well as a low molecular weight pool (Fig. 4.1E).

These observations suggest deletion of the non-prion domain predisposes the PrD to spontaneous aggregation in either a [RNQ^+] or [*rnq*-] background. However, PrD aggregates in a [*rnq*-] background are not amyloid-like because the PrD only forms thioflavin T-positive, SDS-resistant aggregates in a [RNQ^+] background (Fig. 4.2). Thus, the presence of the non-prion domain predisposes a small portion of Rnq1 to accumulate in a soluble pool, which could result from inefficient assembly or increased shearing of [RNQ^+] prions into [RNQ^+] seeds by Hsp104 (27). Observations that PrD overexpression is not toxic and it's assembly into amyloid-like prions is not accompanied by the accumulation of a soluble PrD pool supports the notion that accumulation of soluble Rnq1 in a [RNQ^+] background leads to death (4).

Ydj1 binds the Gln/Asn-rich PrD in its [RNQ$^+$] conformation. Deletion of the Rnq1 non-prion domain and the Sis1-binding motif (4), renders the PrD prone to form benign aggregates in [RNQ^+] and [*rnq*-] cells. The combined ability of the cell to package the PrD into amyloid-like assemblies as well as SDS-sensitive aggregates may account for the benign consequences of PrD overexpression. Chaperones facilitate the formation of benign, non-amyloid aggregates of $A\beta_{1-42}$ (30). Therefore, we speculated that an Hsp40 other than Sis1 may recognize the Gln/Asn-rich PrD and prevent the formation of a toxic PrD species by facilitating the conversion of soluble, unassembled PrD species into benign SDS-sensitive aggregates.

The Type I Hsp40 Ydj1 binds Rnq1 (29), so it may modulate PrD assembly. To identify the Ydj1 binding site in Rnq1, we screened a Rnq1 peptide array with purified Ydj1 (Fig. 4.3A & B).

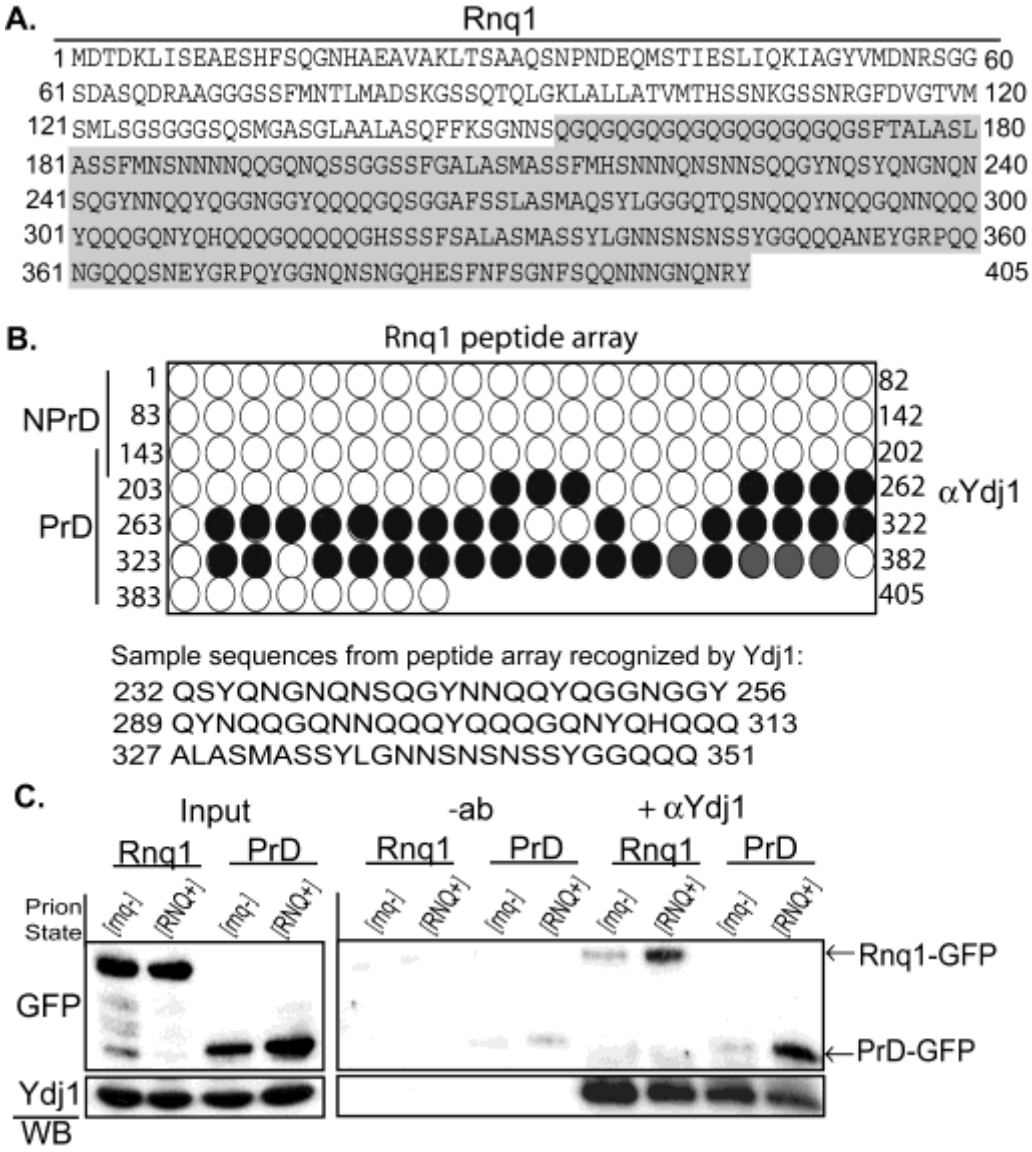

Figure 4.3 Ydj1 interacts with the PrD of Rnq1. (A) Rnq1 amino acid sequence from *S. cerevisiae*. Residues in the PrD of Rnq1 are highlighted. **(B)** A 25 amino acid peptide array from Rnq1 was screened with purified Ydj1. Peptides bound by Ydj1 are highlighted. The intensity of the highlight designates relative binding as assessed by immunoblotting for Ydj1. Three sample peptides from the PrD that were recognized by Ydj1 are listed below. **(C)** Rnq1-GFP or PrD-GFP were expressed in wild type yeast in a [*RNQ*$^{+}$] or [*rnq*$^{-}$] background and cell lysates generated under non-denaturing conditions. Ydj1 was co-immunoprecipitated and bound Rnq1-GFP or PrD-GFP was assessed by western immunoblotting for GFP (right panel). The same lysates were incubated in the absence of αYdj1 antisera to show background binding to Protein G beads (-ab). Expression levels from whole cell lysates represent 10% input (left panel).

Each peptide in the array was 25 amino acids in length and shared 22 amino acids with the adjacent peptide such that small binding motifs could be identified. Ydj1 bound numerous peptides from the PrD, but no peptides from the non-prion domain (Fig. 2.3B). Ydj1 bound peptides that were typically composed of Gln/Asn-rich motifs interrupted by aliphatic or aromatic residues (Fig. 4.3B). These hydrophobic residues may facilitate binding with the Ydj1 hydrophobic peptide-binding pocket (31). Consistent with this possibility, Ydj1 did not bind a glutamine/glycine repeat at the beginning of the PrD. However, numerous hydrophobic residues are present in the non-prion domain and the terminal 50 amino acids of Rnq1 that were not bound by Ydj1. As such, the arrangement of Gln and Asn amino acids along with hydrophobic residues appears critical for Ydj1 to specifically recognize PrD peptides.

Ydj1 binds proteins with polyglutamine repeats in a manner that is dependent upon the expansion length and regulates their assembly into higher order aggregates (32,33). Thus, Ydj1 may be able to recognize substrates enriched in b-structure. To address whether conversion of Rnq1 or the PrD into a b-rich conformation is required for Ydj1 binding, we assessed Ydj1's interaction with the native or amyloid-like prion forms of Rnq1 and the PrD. Ydj1 co-immunoprecipitated Rnq1-GFP and PrD-GFP from [RNQ^{+}] lysates, yet not from [*rnq*-] lysates suggesting Ydj1 prefers the [RNQ^{+}] prion conformation of these proteins (Fig. 4.3C). In addition, Ydj1 did not co-immunoprecipitate the non-prion domain alone and the PrD was a poor substrate for Sis1 in [RNQ^{+}] lysates (Fig. 4.4). The PrD from Rnq1 assembles into thioflavin T-positive, amyloid-like fibrils (34,35). Therefore Ydj1, but not Sis1, recognizes the PrD of Rnq1 in its β-sheet rich, amyloid-like conformation.

Overexpressing the PrD is toxic to yeast in the absence of *YDJ1*. If Ydj1 binds the PrD in its amyloid-like conformation, then Ydj1 may act analogous to Sis1 in suppressing Rnq1 toxicity by facilitating assembly of the PrD into a benign conformation. To test this hypothesis, the PrD was overexpressed in a *Δydj1* strain that contains pre-existing [RNQ^{+}] prions. Indeed, PrD

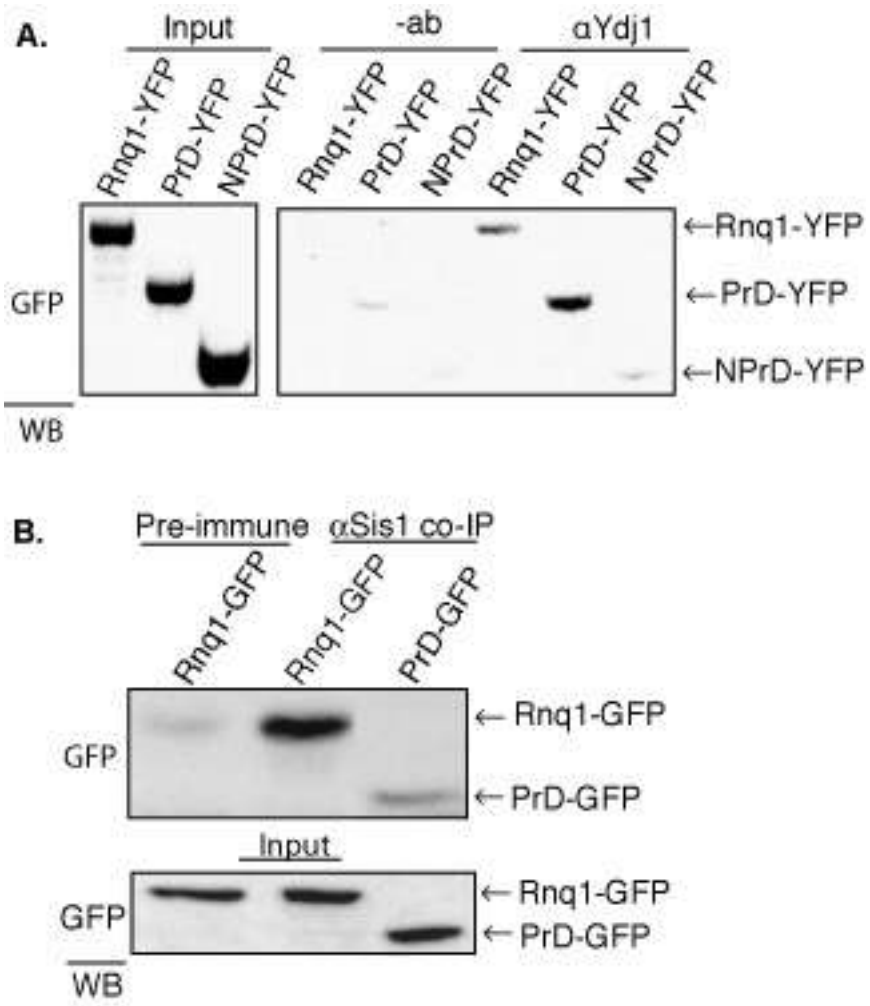

Figure 4.4 Ydj1 specifically binds the PrD of Rnq1. (A) Ydj1 co-immunoprecipitated Rnq1-YFP, PrD-YFP, yet not NPrD-YFP from [*RNQ*$^{+}$] lysates (right panel). Protein levels are shown in the left panel. Binding was assessed by western immunoblotting for GFP. **(B)** Sis1 interaction with the PrD is reduced compared to full length Rnq1. Rnq1-GFP and PrD-GFP were expressed in yeast from a [*RNQ*$^{+}$] background and endogenous Sis1 co-immunoprecipitated from lysates with αSis1 antisera or a pre-immune control. Binding between Sis1 and Rnq1-GFP or PrD-GFP was assessed by western immunoblotting for GFP.

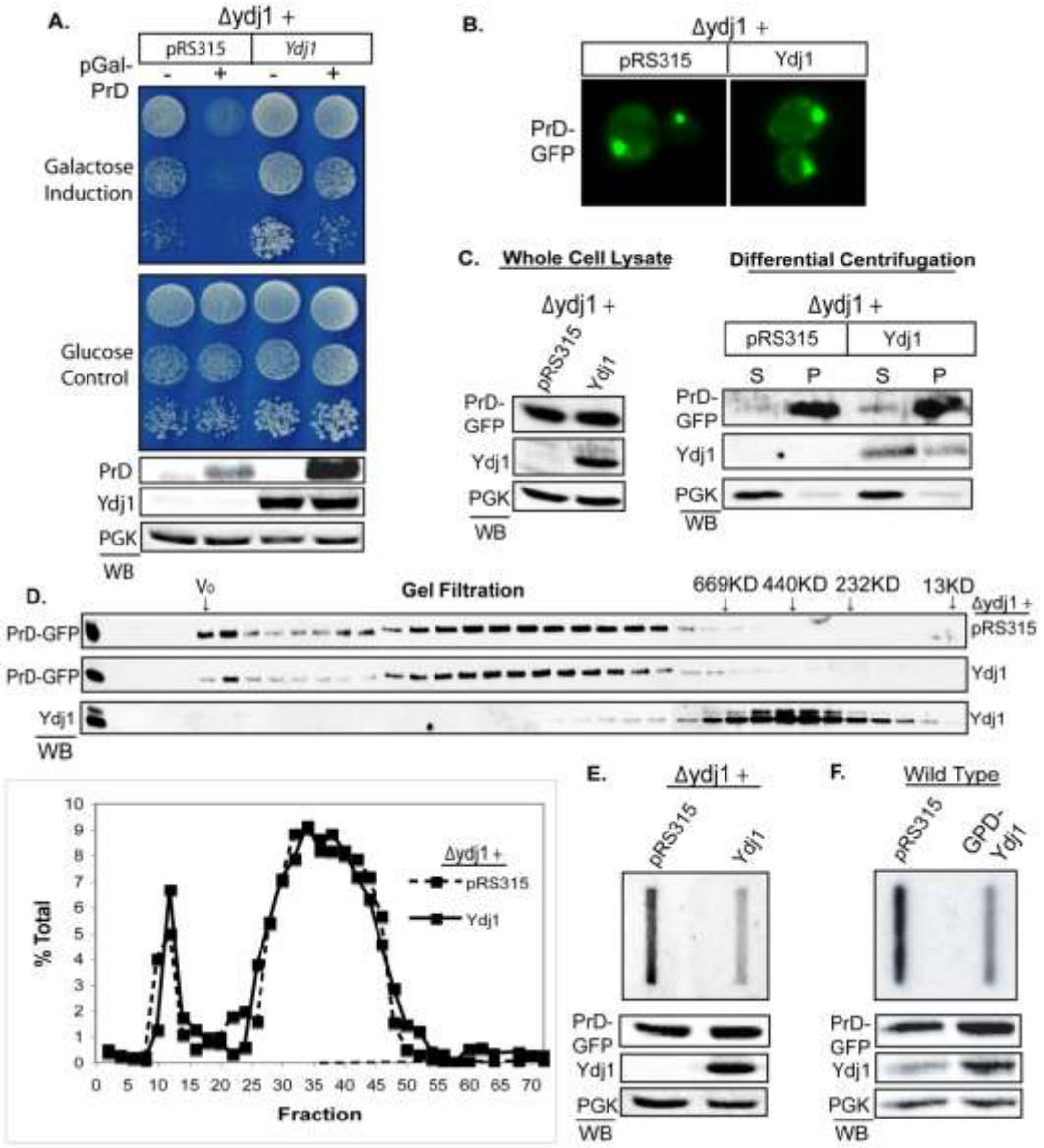

Figure 4.5 Deletion of YDJ1 sensitizes yeast to overexpression of the PrD. **(A)** Cells in a Δ*ydj1* strain ([*RNQ*$^{+}$] background) were transformed with an empty pRS315 plasmid or a pRS315 plasmid expressing Ydj1 from the *YDJ1* promoter. These strains were further transformed with plasmids harboring galactose-inducible PrD or empty plasmid (pRS416). These cells were serially diluted onto selective media containing galactose or glucose. Western blots below show protein expression levels. **(B)** Fluorescence microscopy of representative cells expressing PrD-GFP in the presence or absence of Ydj1. **(C)** Differential centrifugation as performed in Figure 1 of cell lysates from strains expressing PrD-GFP in the presence or absence of Ydj1 [right panel: supernatant (S) and pellet (P)]. Left panel shows protein levels from whole cell lysates. **(D)** Gel filtration analysis of PrD-GFP in the presence or absence of Ydj1 as in Figure 1. Fractions from a *YDJ1*-rescued strain were also assessed for Ydj1 distribution. Below is quantification of PrD-GFP levels in every other fraction normalized to total PrD-GFP. **(E)** The assembly of SDS-resistant PrD-GFP was determined by filter trap analysis. PrD-GFP was induced in the presence or

overexpression was highly toxic to yeast in a *Δydj1* background (Fig. 4.5A). Cell viability was rescued by Ydj1 expression from a low copy plasmid from its own promoter. Even though PrD expression from the *GAL1* promoter was toxic, PrD protein levels were much lower in the *Δydj1* strain compared to the *YDJ1*-rescued strain (Fig 4.5A; lower panel). This was not surprising because *YDJ1* is required for efficient nucleosomal remodeling that is required for activation of the *GAL1* promoter (36).

In contrast to what is observed with [*RNQ*$^{+}$] assembly when Sis1 is depleted (4,27), the PrD still formed intracellular aggregates and did not accumulate as a soluble species when Ydj1 was deleted (Fig. 4.5B-D) In fact, the only difference we observed was a close to 2-fold increase in the levels of SDS-resistant PrD-GFP in the *Δydj1* strain compared to wild type background (Fig. 4.5E). Therefore, Ydj1 appears to enable yeast to tolerate PrD expression by limiting the pool of amyloid-like PrD assemblies. Consistent with this hypothesis, overexpression of Ydj1 decreased the level SDS-resistant PrD-GFP (Fig. 4.5F). Thus, PrD toxicity appears to differ from Rnq1 toxicity in that the accumulation of SDS-resistant forms of PrD, and not a low molecular weight, detergent-soluble species correlates with cell death.

The mechanism via which Ydj1 modulates the accumulation of SDS-resistant PrD and suppresses PrD toxicity is unclear. Ydj1 may cap the exposed ends of elongating PrD amyloid or interact with Hsp104 (37) to maintain the level of this species within a tolerable range. Alternatively, Ydj1 may coat PrD particles to prevent non-specific protein:protein interactions that titrate essential cellular factors. We favor the former model because while Ydj1 co-

Figure 4.5 cont . . .absence of Ydj1 and cells were lysed under denaturing conditions (2% SDS, 62.5mM Tris-HCl pH6.8, 1mM EDTA, 5% glycerol, 2% β-mercaptoethanol). Lysates were applied to a cellulose acetate filter and retained PrD-GFP was assessed by western immunoblotting for GFP. **(F)** Levels of SDS-resistant PrD-GFP were also determined in the presence of overexpressed Ydj1. Wild type yeast harboring an empty vector (pRS315) or *YDJ1* under the control of a constitutively active promoter (GPD) expressing PrD-GFP were lysed as described in **(E)** and lysates analyzed by filter trap. Panels below show protein levels from cell lysates used in filter trap assay.

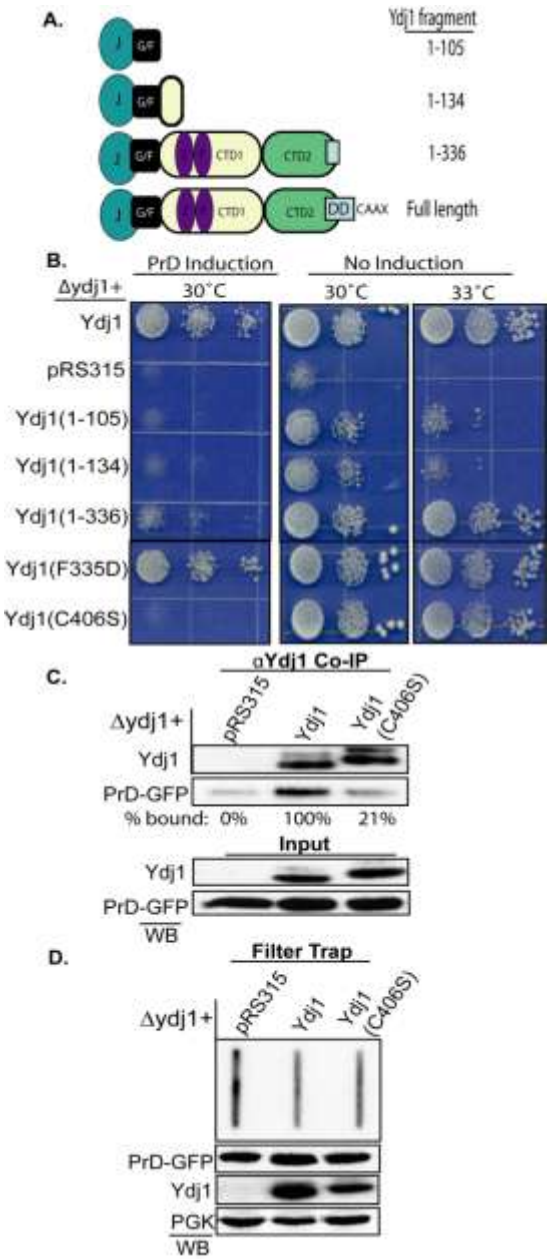

Figure 4.6 The Ydj1 CAAX box is required to suppress PrD toxicity. (A) Domain structure of Ydj1 and truncations used in this study. **(B)** Truncations and mutants were expressed in a pRS315 (low copy) plasmid under control of the *YDJ1* promoter in a *Δydj1* background. These cells, harboring a plasmid expressing the PrD on a galactose-inducible promoter, were serially diluted onto media containing galactose and grown at 30°C. These cells were also serially diluted onto media containing glucose and grown at 30°C or 33°C. **(C)** Binding between Ydj1 or Ydj1(C406S) with PrD-GFP was assessed by co-immunoprecipitation with αYdj1 antisera. PrD-GFP levels in the *Δydj1* strain (pRS315) represent background binding to the Protein G beads. Percentages below represent bound PrD-GFP levels as a percentage of wild type Ydj1 normalized to background. **(D)** SDS-resistant PrD-GFP was compared in a *Δydj1*, Ydj1, or Ydj1(C406S) background by filter trap. Panels below show protein levels from cell lysates.

immunoprecipitates with PrD-GFP we did not observe a large pool of Ydj1 co-migrating with PrD-GFP on gel filtration columns. Instead, Ydj1 eluted in a broad peak higher than the predicted molecular weight for a Ydj1 homodimer (~90kD). This may occur because Ydj1 forms complexes with an array of different cellular proteins. In addition, Ydj1 is farnesylated and this post-translational modification may lead it to behave like a protein with a higher molecular weight in gel filtration analysis. Nevertheless, only a small pool of Ydj1 binds and co-migrates with PrD prions and this does not seem sufficient to serve a coating function.

Mutation of the CAAX box prevents Ydj1 from suppressing PrD toxicity. The ability of Ydj1 to specifically recognize the Gln/Asn-rich PrD was surprising because numerous studies suggest Type I Hsp40s prefer peptides enriched in hydrophobic amino acids (13,38). Thus, we investigated the structural features in Ydj1 that enable it to bind and modulate PrD toxicity. First, we demonstrated that Sis1 could not suppress the toxicity observed when PrD was overexpressed and the *Δydj1* strain (data not shown). Then we sought to define the minimal length of Ydj1 required to suppress PrD toxicity (Fig. 4.6A). The *Δydj1* strain normally exhibits a slow growth phenotype (20) and the Ydj1 J-domain and G/F-rich region can restore normal growth in a *Δydj1* strain (39). Yet, this same Ydj1 fragment could not suppress PrD toxicity (Fig. 4.6B). While the Ydj1 J-domain was not sufficient to suppress PrD toxicity, an active J-domain was still necessary because mutation in the conserved HPD tripeptide motif (H34Q) that severely disrupts interaction between Ydj1 and Hsp70 (40) rendered yeast unable to tolerate PrD toxicity (Fig. 4.7A). Binding between PrD-GFP and Ydj1(H34Q) was only slightly reduced (74% of wild type) and the levels of SDS-resistant PrD-GFP were increased with Ydj1(H34Q) compared to wild type (Fig 2.7B & C). Altogether, these observations suggest functional features of Ydj1 that support normal growth are less complex than those required to suppress PrD toxicity.

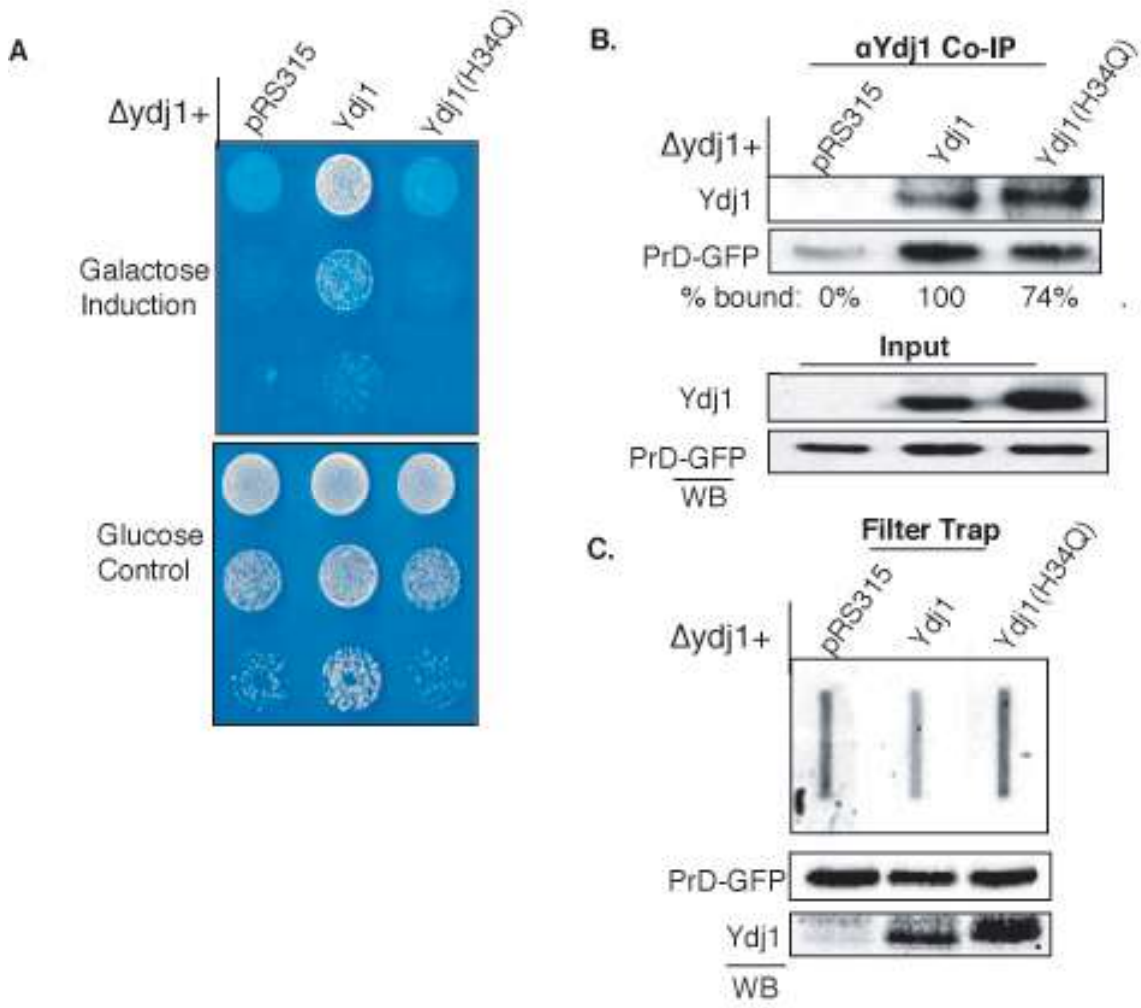

Figure 4.7 A functional J-domain is required for Ydj1 to suppress PrD toxicity. (A) Cells in a *Δydj1*, Ydj1 (wild type), or Ydj1(H34Q) background harboring PrD on a galactose-inducible promoter were serially diluted onto media containing galactose or glucose. **(B)** Binding between PrD-GFP and Ydj1(wild type) and Ydj1(H34Q) was assessed by co-immunoprecipitation with αYdj1 antisera. Percentages below represent bound PrD-GFP levels as a percentage of wild type *YDJ1* normalized to background (*Δydj1*). **(C)** SDS-insoluble PrD-GFP levels was compared between *Δydj1*, Ydj1(wild type), Ydj1 (H34Q) by filter trap. The panel below shows protein expression levels from lysates used in the filter trap assay.

Ydj1(1-336) contains the J-domain, G/F-rich region, ZFLR, and a polypeptide-binding pocket, yet the Ydj1 dimerization domain is severed (41) and a CAAX motif required for farnesylation is missing (22). Ydj1 fragments with similar domain structures bind non-native polypeptides and suppress protein aggregation (42). Expression of Ydj1(1-336) in the *Δydj1* strain restored normal growth, but barely protected against PrD toxicity (Fig. 4.6B). To determine whether dimerization and/or farnesylation are required for complete suppression of PrD toxicity, specific point mutants in the extreme Ydj1 C-terminus were examined. Ydj1(F335D), which contains point mutation in the dimerization domain that monomerizes Ydj1 (data not shown)(41), suppressed PrD toxicity as well as wild type suggesting the Ydj1 monomer is sufficient in this activity. However, mutation of the CAAX box (C406S) eliminated Ydj1's ability to suppress PrD toxicity (Fig. 4.6B).

These data were surprising because farnesylation is thought to be required for membrane localization of Ydj1 yet PrD prions appear cytosolic. Thus, we investigated whether farnesylation is required for Ydj1 to bind the amyloid-like form of the PrD. Indeed, we observed an 80% reduction in complex formation between Ydj1(C406S) and the PrD (Fig. 4.6C). However, the pool of SDS-insoluble PrD-GFP was not increased with Ydj1(C406S) compared to wild type (Fig. 4.6D). The residual binding between Ydj1(C406S) and the PrD may be sufficient to control the accumulation of SDS-insoluble aggregates: though farnesylation of Ydj1 was clearly required for tolerance of PrD overexpression.

To demonstrate that defects in Ydj1 (C406S) function were indeed due to the lack farnesylation, the PrD was expressed in a *Δram1* strain, in which a non-essential farnesyltransferase subunit was deleted. In this strain background Ydj1 is not farnesylated (44) and overexpression of the PrD is toxic (Fig. 4.8). In addition, interactions between Ydj1 and the PrD in the *Δram1* strain were reduced. Thus, defects in the ability of Ydj1(C406S) to suppress PrD toxicity are indeed due to loss of farnesylation. These data provide the first evidence for a

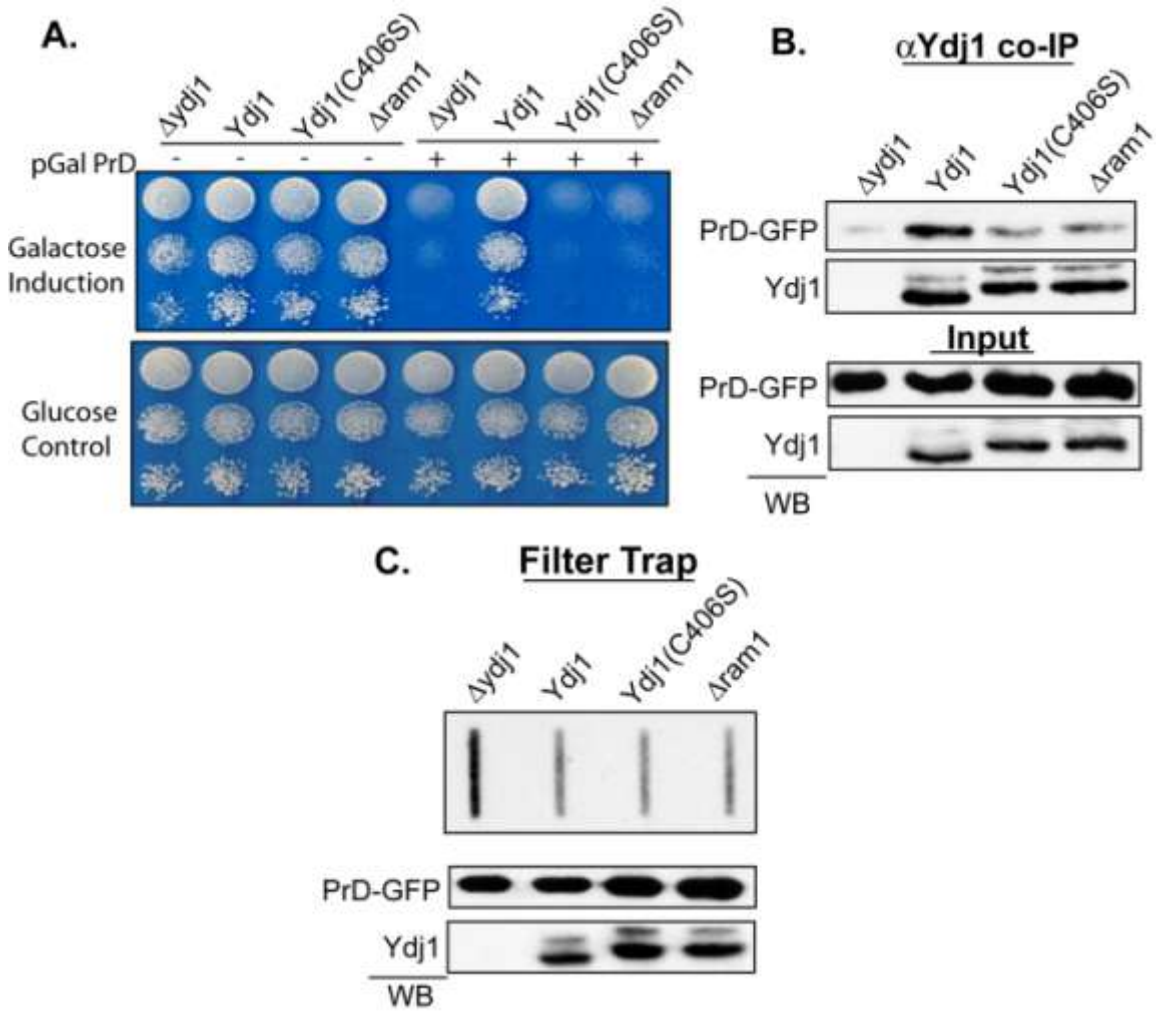

Figure 4.8 Deletion of the farnesyltransferase subunit RAM1 disrupts binding to PrD-GFP. **(A)** Cells deleted for *YDJ1* were transformed with a pRS315 empty vector (*Δydj1*), wild type Ydj1 or Ydj1 (C406S). A *Δram1* strain was also transformed with a pRS315 empty vector. These strains harboring an empty pRS416 vector (-) or pGAL PrD (+) were serially diluted onto selective media containing glucose or galactose and grown for 3 days at 30°C. The PrD was toxic in the *Δydj1*, Ydj1(C406S) and *Δram1* background. **(B)** Ydj1 was co-immunoprecipitated from cell lysates expressing PrD-GFP from a copper promoter as described in the main text. Bound PrD-GFP was assessed by western immunoblotting for GFP. Note that Ydj1(C406S) and endogenous Ydj1 in a *Δram1* strain display reduced mobility by SDS-PAGE demonstrating that Ydj1 is not farnesylated in the *Δram1* background. Binding between PrD-GFP and Ydj1(C406S) as well as endogenous Ydj1 in the *Δram1* strain was reduced. **(C)** The assembly of SDS-resistant PrD-GFP was determined by filter trap as described in the main text. The level of SDS-resistant PrD-GFP is elevated in a *Δydj1* compared to the wild type Ydj1 background. However, no increase is observed in the Ydj1(C406S) or *Δram1* background. These observations demonstrate that farnesylation of Ydj1 is required for efficient binding to PrD-GFP.

role of a farnesyl moiety on a Type I Hsp40 in binding to an amyloid-like substrate and in suppression of prion toxicity.

The ZFLR is required to bind the PrD and suppress toxicity.

Since Ydj1(C406S) could still control levels of amyloid-like PrD prions, we explored the role for the Type I Hsp40 ZFLR (17,31) in complex formation between Ydj1 and the PrD (Fig. 4.9A). Point mutations in Ydj1's individual zinc-binding domains (ZBDs) were tested for their effect on suppression of PrD toxicity. Mutation of ZBD1 (C143S or C201S) had no effect on Ydj1's modulation of PrD toxicity (Fig. 4.9B). However, mutation of ZBDII (C162S or C185S) dramatically disrupted the ability of Ydj1 to suppress PrD toxicity. Thus, ZBDII of Ydj1 is required for yeast to tolerate overexpression of the PrD. Defects in cytoprotection by Ydj1 ZBDII mutants correlated with a substantial 90% decrease binding between PrD-GFP and Ydj1(C162S) (Fig. 4.9C). Furthermore, the pool of SDS-insoluble PrD-GFP was increased in the presence of Ydj1(C162S) to levels observed in the *Δydj1* strain (Fig. 4.9D). We found these data interesting because we knew that ZBDII is required for Ydj1's protein folding function, but action of the ZFLR appeared dispensable for binding globular proteins (15,16,43). Thus, the data presented identify a critical role for the Type I Hsp40 ZFLR in binding and suppressing the toxicity of proteins that form amyloid-like aggregates.

Ydj1 contains a hydrophobic depression in C-terminal Domain I (CTDI) that is required for folding model proteins, is conserved in Type II Hsp40s, and has been co-crystallized in a complex with a hydrophobic peptide (31). Since Ydj1-bound peptides in the PrD that contained hydrophobic peptides (Fig. 4.3), the role of CTDI in suppression of prion toxicity was investigated. To address whether the peptide-binding pocket of Ydj1 participates in PrD binding, several solvent-exposed hydrophobic residues in this groove were mutated (Fig. 4.9E). Point mutations in this pocket disrupt binding and refolding of luciferase *in vitro* (44). However, Ydj1 peptide-binding pocket mutants were capable of suppressing PrD toxicity (Fig. 4.9F). PrD expression was slightly toxic in strains that harbored Ydj1(L135S). Yet, Ydj1(L135S) bound

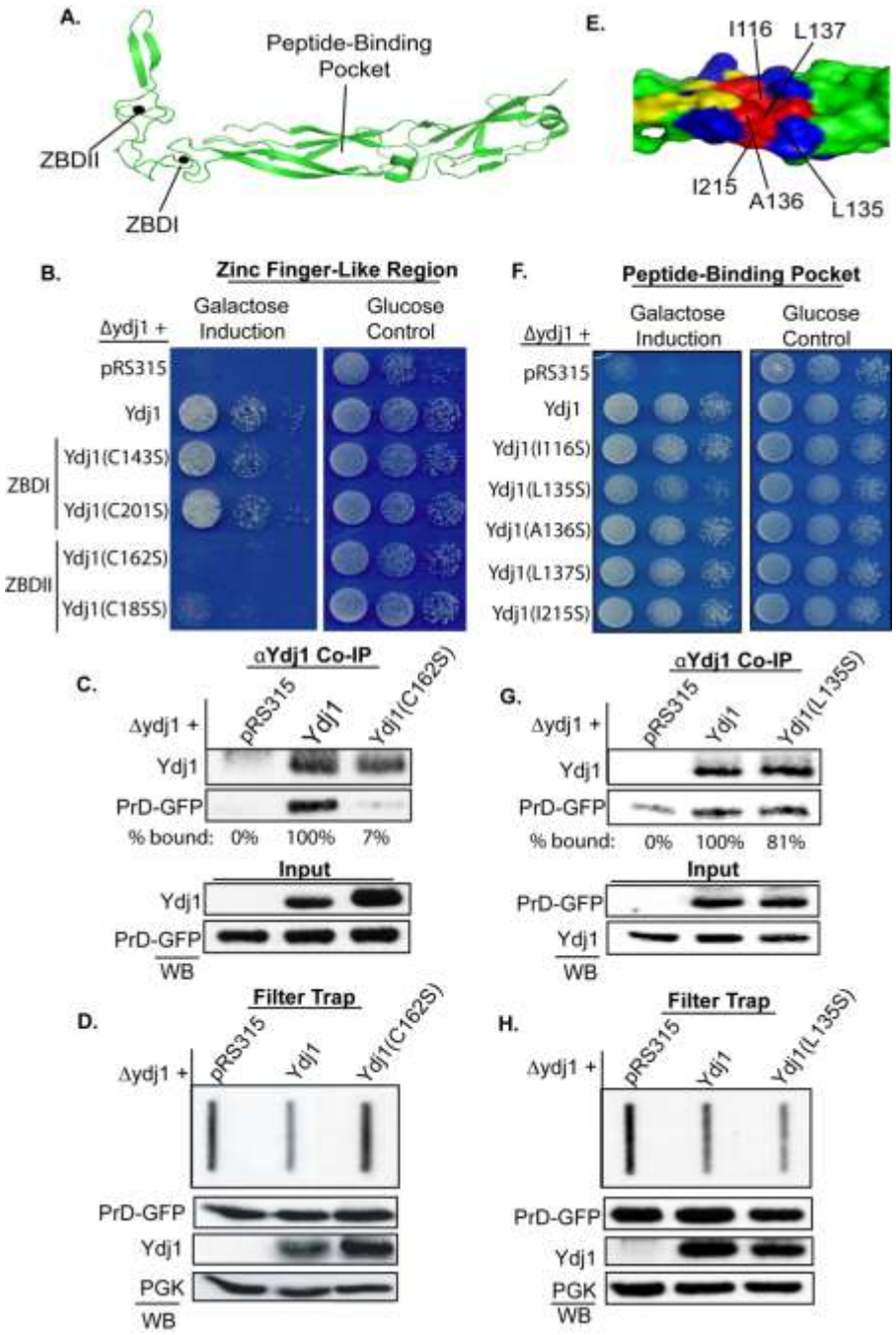

Figure 4.9 Mutation in the Ydj1 ZFLR disrupts binding to the PrD. (A) Ribbon diagram of the x-ray crystal structure from Ydj1(110-337). Zinc binding domains in the Ydj1 ZFLR are noted as well as the peptide-binding pocket. **(B)** Cells from a *Δydj1* background were transformed with pRS315 (low copy) plasmids expressing wild type Ydj1 or the indicated ZFLR mutant from the *YDJ1* promoter. These cells, also harboring a plasmid expressing PrD from a galactose-inducible promoter, were serially diluted onto selective media containing galactose or glucose. (**C)** Binding between PrD-GFP and the indicated form of Ydj1 was assessed by co-immunoprecipitation with αYdj1 antisera. Percentages below represent bound PrD-GFP levels as a percentage of wild type Ydj1 normalized to background (pRS315). **(D)** SDS-resistant PrD-GFP

PrD-GFP almost as well as wild type Ydj1 and no increase in SDS-insoluble PrD-GFP was observed in this mutant background (Fig. 4.9G & H). Thus, when peptide binding by CTDI is compromised through mutation, actions of the ZFLR and farnesyl moiety on Ydj1 appear sufficient for modulation of PrD toxicity.

At, this point we want to note that the role of the Ydj1's ZFLR and farnesyl moiety in binding to amyloid-like prion protein conformers is not limited to the PrD of Rnq1. Ydj1 binding to the prion form of the yeast prion Sup35 was also severely disrupted by mutation of ZBDII in the ZFLR and reduced by mutation of the CAAX box (Fig. 4.10). Thus, conserved domains that are found in Type I Hsp40s enable Ydj1 to bind proteins that assume amyloid-like states.

Structural requirements for Ydj1 binding to HD53Q.

The above observations suggest the Ydj1 ZFLR participates in recognition of β-rich, amyloid-like substrates and that it may or may not require assistance of CTDI. To determine the generality of the data obtained in study of the PrD, we examined structural requirements for Ydj1 binding to a purified huntingtin fragment that contains exon 1 and a 53Q expansion (HD53Q) (45). While wild type Ydj1 suppressed HD53Q aggregation in a dose-dependent manner, Ydj1(C162S) was almost entirely defective (Fig. 4.11). Interestingly, Ydj1(I215S), which contains a point mutation in the peptide-binding pocket, was also inactive in suppressing HD53Q aggregation. I215 is located at the base of the Ydj1 polypeptide-binding pocket and may be required to stabilize this groove, though Ydj1(I215S) could still suppress PrD toxicity suggesting

Figure 4.9 cont. . . . was compared between a *Δydj1*, Ydj1, Ydj1(C162S) background by filter trap. (**E)** PyMOL model of the Ydj1 peptide-binding pocket (hydrophobic:*red*, basic:*blue*, acidic:*yellow*). Specific residues examined in this study are identified. **(F)** Strains from a *Δydj1* background were transformed as described above with plasmids expressing wild type Ydj1 or the indicated polypeptide-binding mutant. These cells, also expressing galactose-inducible PrD, were serially diluted onto media containing galactose or glucose. **(G)** Binding between PrD-GFP and the indicated form of Ydj1 was assessed by co-immunoprecipitation with αYdj1 antisera as above. **(H)** SDS-resistant PrD-GFP was compared between a *Δydj1*, Ydj1, and Ydj1(L135S) background by filter trap. For filter trap assays, panels below show protein expression levels from cell lysates.

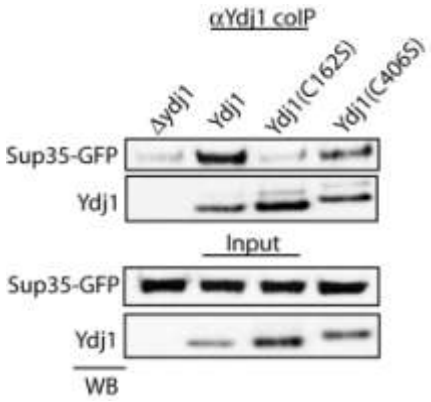

Figure 4.10 Binding between Ydj1 and Sup35 requires the Ydj1 ZFLR and farnesylation. Yeast cells in a *Δydj1* background were transformed with plasmids expressing wild type Ydj1, Ydj1(C162S), or Ydj1(C406S) from the *YDJ1* promoter. These cells were also transformed with a plasmid expressing Sup35-GFP from a CUP1 promoter. Sup35-GFP was induced as described for PrD-GFP. Ydj1 was co-immunoprecipitated from cell lysates generated under non-denaturing conditions (described in Experimental Procedures) and bound Sup35-GFP analyzed by western immunoblotting for GFP. Binding to Ydj1(C162S) was substantially reduced to near background levels. Binding to Ydj1(C406S) was also reduced, though residual binding between Ydj1(C406S) and Sup35-GFP was consistently observed.

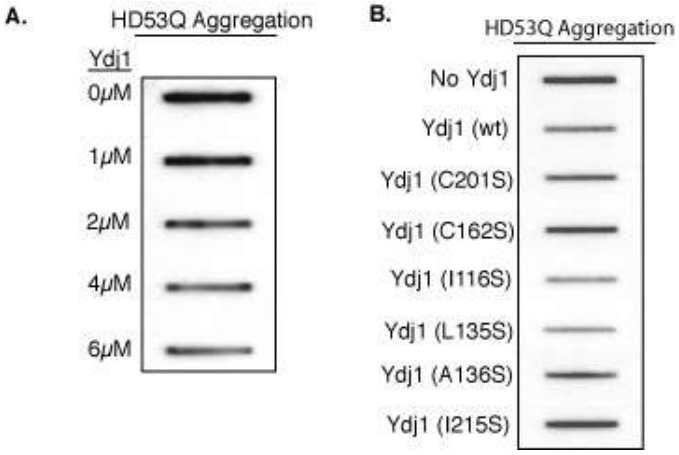

Figure 4.11 The Ydj1 ZLFR is required to suppress HD53Q aggregation. **(A)** Myc-HD53Q (1μM) was incubated with a titration of purified Ydj1 and aggregation assessed by filter trap and western immunoblotting for myc as previously described (46) with the following modifications. First, 1μM GST-myc-HD53Q was incubated in Buffer B (50 mM Tris·HCl (pH 7.0), 150 mM NaCl, 1 mM DTT, 1 mM phenylmethylsulfonyl fluoride, 50 mM KCl, 5 mM $MgCl_2$) with 6μM Ydj1 (wild type or the indicated mutant) and PreScission Protease to start the reaction (47). Reactions were incubated for 150 minutes then stopped with 4x native gel sample buffer (0.24M Tris-HCl pH 6.8, 40% glycerol, 1% Bromphenol Blue). Aggregated myc-HD53Q was analyzed by filter trap and western-immunoblotting with c-Myc antisera (Sigma). **(B)** Myc-HD53Q (1μM) was incubated with the indicated version of Ydj1 (6μM) and aggregation assessed as described above.

it is not grossly misfolded. HD53Q includes a 17-residue peptide from exon 1 of human huntingtin that contains several hydrophobic motifs. Thus, we propose that Ydj1 utilizes a bipartite mechanism to suppress HD53Q aggregation in which b-strands in the ZFLR interact with the polyQ expansion and solvent-exposed residues in the hydrophobic pocket interact with the exon 1 peptide. However, it was difficult to test this hypothesis because Ydj1(C162S) and Ydj1(I215S) were almost entirely inactive. Never the less, function of both the ZFLR and CTDI are required for Ydj1 to suppress HD53Q aggregation.

The Ydj1 ZFLR and peptide-binding pocket regulate luciferase refolding *in vivo*.

Data presented thus far suggest that Type I Hsp40s contain at least three domains that are required for interaction of Ydj1 with non-native substrates, yet the requirements of each are substrate-dependent. To test this model we compared the structural requirements for Ydj1's action in suppression of PrD biogenesis to those for *in vivo* and *in vitro* folding of the globular protein luciferase. Luciferase was expressed from the *GAL1* promoter in a *Δydj1* strain harboring Ydj1 mutants discussed above. Minimal luciferase activity was observed in the *Δydj1* strain, though very little luciferase was expressed from the *GAL1* promoter (Fig. 4.12A & B). Wild type Ydj1 restored luciferase expression and activity. However, mutation of either ZBDI or ZBDII severely reduced luciferase activity even though luciferase expression levels were recovered to near wild type. Ydj1(C162S) still bound luciferase (data not shown) suggesting this defect reflects an inability of Ydj1 to maintain luciferase in a conformation that subsequently is bound by Hsp70 (15). Ydj1(L135S) and Ydj1(I215S) only supported luciferase activity at around ~50% of wild type levels. Interestingly, Ydj1(C406S) supported luciferase expression and activity to near wild type levels. Thus, farnesylation of Ydj1 is dispensable for *in vivo* folding of luciferase

Defects exhibited by Ydj1 mutants with *in vivo* assays of luciferase refolding were recapitulated when activity of the purified forms of these proteins were monitored with *in vitro* luciferase refolding assays (Fig. 4.12C). The ability of Ydj1 to promote expression and folding of

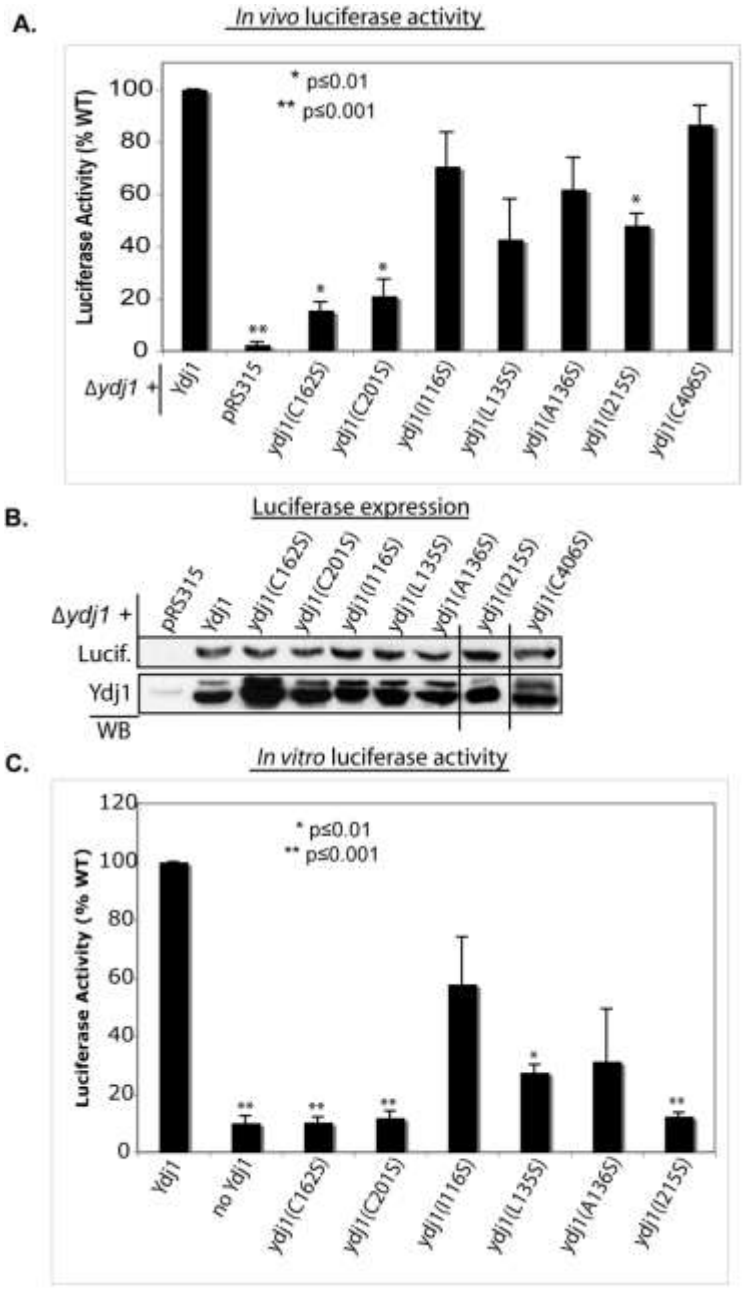

Figure 4.12 Mutations in the Ydj1 ZFLR and peptide-binding pocket disrupt luciferase refolding *in vivo*. (A) Firefly luciferase was expressed in a *Δydj1* strain harboring the indicated form of Ydj1 expressed from a pRS315 plasmid under control of the *YDJ1* promoter. Luciferase activity was measured in intact cells with a luminometer. Luciferase activity is represented as percent of control (wild type Ydj1). **(B)** Expression of firefly luciferase in yeast in the presence of the indicated form of Ydj1. Cell lysates were analyzed by SDS-PAGE and assessed by western immunobloting for luciferase and Ydj1. **(C)** Luciferase activity was also assessed *in vitro*. Purified firefly luciferase (50nM) was incubated with Hsp70 (0.5μM) and the indicated form of Ydj1 (1μM). Error bars represent SEM from three independent trials. (*p≤0.01; **p≤0.001).

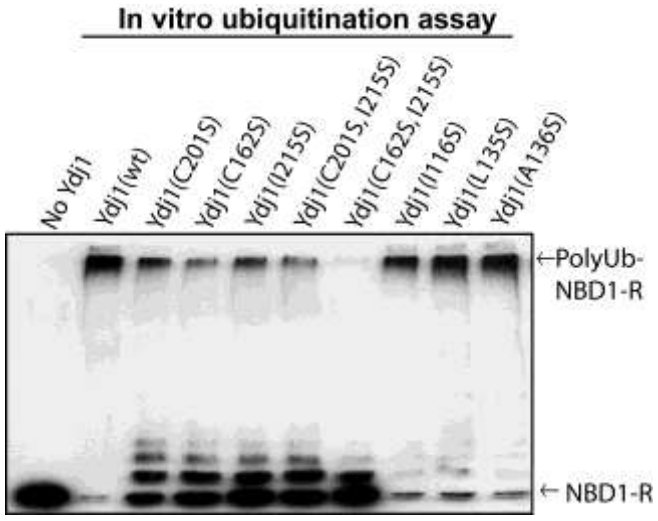

Figure 4.13 Chaperone-dependent polyubiquitination requires the Ydj1 ZFLR and peptide-binding pocket. The role of Ydj1 during *in vitro* polyubiquitination of a fragment from the CFTR ion channel (NBD-R) was assessed. Gst-NBD1-R (1μM) was incubated with E1 (0.1μM), the E2 UbcH5a (4μM), the E3 ubiquitin ligase CHIP (3μM), Hsc70 (2μM), plus or minus the indicated form of Ydj1 (4μM). Polyubiquitinated gst-NBD1-R was retained at the gel front while unmodified gst-NBD-R resolved at its predicted molecular weight.

luciferase requires the ZFLR and CTDI, yet this process occurs when the CAAX box is not farnesylated.

The Ydj1 ZFLR and peptide-binding pocket cooperate in chaperone-dependent polyubiquitination.

Crystal structures demonstrate that the ZFLR and CTDI are in close proximity to each other (31) and these domains appear to cooperate in the process of suppressing HD53Q aggregation. To further study this issue we examined the contribution of the Ydj1 ZFLR and peptide-binding pocket in chaperone-dependent polyubiquitination reactions (31)**.** Purified Ydj1 was incubated with Hsp70, the E2 UbcH5a and the E3 ubiquitin ligase CHIP to assess polyubiquitination of a model Gst fusion (Gst-NBD1-R, which contains nucleotide binding domain 1 and the regulatory domain from CFTR) (48). In the absence of Ydj1 little ubiquitination of Gst-NBD1-R was observed. Yet, upon addition of Ydj1, the majority of gst-NBD1-R was polyubiquitinated and retained at the top of the SDS-PAGE gel (Fig. 4.13A; lanes 1 and 2). This mobility shift was not observed in the absence of ATP, ubiquitin, E1 or any of the other components of the Hsp70/CHIP

E3 complex (48). The ZFLR mutants Ydj1(C201S) and Ydj1(C162S) both exhibited a reduced ability to support polyubiquitination of gst-NBD1-R (Fig. 4.13B; lanes 3 and 4). A similar defect in polyubiquitination was observed when Ydj1(I215S) was used in the reaction (Fig. 4.13B; lane 5), but mutation of other residues in the peptide-binding pocket had no effect (Fig 4.13B lanes 8-10). Yet, the most dramatic reduction in Ydj1 activity was observed when ZBDII and the polypeptide-binding pocket were altered simultaneously (Fig. 4.13B; lanes 6 and 7). Thus, the Ydj1 ZFLR and peptide-binding pocket cooperate in order to modulate the conformation of non-native proteins and this synergism is required to maintain substrates of the Hsp70/CHIP E3 ligase in a ubiquitination-competent state.

4.4 Discussion

Identification of distinct binding sites in the prion Rnq1 for the Type I Hsp40 Ydj1 and Type II Hsp40 Sis1 explains why these chaperones play different roles in prion propagation. In addition, these data support the concept that selective recognition of substrates by Type I and Type II Hsp40s serve to specify cytosolic Hsp70 functions (13,49). Sis1 binding to the non-prion domain serves to increase the efficiency of [RNQ^{+}] assembly and mediate chaperone-dependent shearing of large prions into smaller seeds (4,27). However, if Sis1 is unable to bind Rnq1, then the ability of Ydj1 to recognize Gln/Asn-rich regions in the Rnq1 PrD enables it to regulate the [RNQ^{+}] prion pool size.

Sis1 suppresses Rnq1 toxicity by increasing the efficiency of [RNQ^{+}] assembly, which prevents the accumulation of an SDS-sensitive, toxic off-pathway species (4). Interestingly, the assembly of the PrD into amyloid-like, SDS-resistant particles appears more efficient than the assembly of Rnq1 into a similar species. The PrD is a poor substrate of Sis1, and Ydj1 action is required for yeast to tolerate PrD overexpression. The toxic conformer of the PrD is unknown, yet the cell death that occurs when Ydj1 is inactive correlates with a several-fold increase in the accumulation of SDS-resistant forms of PrD. Thus, the toxic species of Rnq1 and its PrD appear different and the cell's ability to suppress their accumulation is dependent upon distinct Hsp40s. These data help explain why Type I and Type II Hsp40s have differential effects in suppressing conformational disease (50).

Our studies identify the ZFLR, CTDI, and farnesyl moiety as domains in Type I Hsp40s that are required for modulating the conformation of non-native proteins. Interestingly, the requirement of these domains in Ydj1 action is substrate specific. Mutation of the ZFLR and farnesyl moiety, but not CTDI, interfered with Ydj1's ability to bind the amyloid-like form of the PrD and Sup35. In contrast, Ydj1 required action of both the CTDI and the ZFLR, but not the farnesyl moiety to fold luciferase. Furthermore, apparent synergy between the ZFLR and CTDI enabled Ydj1 to facilitate polyubiquitination of misfolded proteins by the quality control E3

ubiquitin ligase CHIP. Thus, Ydj1 contains at least three regions that facilitate substrate binding and different combinations are utilized to recognize different protein conformers. Through the use of multiple domains to mediate interaction with non-native substrates, Ydj1 can cooperate with Hsp70 to facilitate the biogenesis or degradation of a broad range of substrates. Mutation of hydrophobic residues in the peptide-binding site from Type I or Type II Hsp40s causes defects in cell viability and chaperone function (44,51). However, the Ydj1 peptide-binding pocket is not sufficient to perform all it's chaperone duties and depending on the nature of the substrate, it can be dispensable, or its action is assisted by the ZFLR and/or the C-terminal farnesyl moiety. Structural data show that the tip of the ZFLR (adjacent to ZBDII) contains a pair of anti-parallel ß-strands whose orientation and folding appears to be stabilized by ZBDII (31). Interestingly, the Ydj1 CTDI is also constructed from anti-parallel ß-strands and the co-crystal structure of a Ydj1:peptide complex suggests that substrate binding involves formation of an additional β-strand with the two-stranded, anti-parallel ß-sheet in the peptide-binding pocket. There are a number of Gln and Asn side-chains exposed on the surface of the anti-parallel ß-strands at the tip of the ZFLR. Thus, it is conceivable that the ß-strands at the tip of the ZFLR form a ß-strand with exposed surfaces of amyloid-like proteins or regions of protein folding intermediates. Simultaneous binding of substrates to the ZFLR and CTDI may then hold the substrate in a conformation that can be recognized by Hsp70.

Models for Type I Hsp40 structure built from small x-ray scattering data and x-ray crystal structures of Ydj1 fragments demonstrate that Type I Hsp40s function as homodimers (14). The ZFLRs in Ydj1 homodimers are located in a central domain that controls the shape and functional specificity of Ydj1 (13,14). The requirement for the Type I Hsp40 ZFLR in substrate binding further explains the functional differences observed between Type I and Type II Hsp40s (13). Defects in Ydj1 function caused by mutation of the ZFLR could be due to alteration of Ydj1's quaternary structure. However, monomeric forms of Ydj1 retain the ability to suppress to PrD toxicity, so this is unlikely. Thus, the ZFLR appears to control the quaternary structure of Type I

Hsp40s and can also directly participates in substrate binding. Additional, structural studies are now required to define the mechanism for ZFLR action in these processes

It has been thought for some time that lipid modification of the C-terminal CAAX box of Type I Hsp40s only serves to localize these chaperones to intracellular membranes that include the ER (21,22). However, large pools of Ydj1 are cytosolic and it is now clear that farnesylation of Ydj1 enhances its ability to bind cytosolic substrates such the prion Rnq1. In addition, farnesylation of Ydj1 was recently demonstrated to be required for proper folding of kinase Ste11 (52). Interestingly, farnesyl dependent binding of Ydj1 to Ste11 occurs independent of the ZFLR and peptide-binding pocket (52). These data are consistent the model we put forth which suggests that Type I Hsp40s contain multiple domains that are capable of participating in the binding of non-native polypeptides.

The action of a lipid moiety in polypeptide binding by Ydj1 is a novel and somewhat surprising finding. Importantly, a number of human Hsp40s are farnesylated or geranylgeranlyated, so this mechanism for substrate binding appears to be conserved (12). The simplest mechanism for farnesyl action in Hsp40 chaperone function is interaction between the farnesyl chain and hydrophobic surfaces of protein folding intermediates. However, the farnesyl moiety of Ydj1 could also influence the conformation of Ydj1 and thereby regulate it's substrate specificity (53).

A point that should be emphasized is that farnesylation of Ydj1 is critical for biogenesis of some, but not all Ydj1 functions. Farnesylation of Ydj1 is not required for normal growth of yeast, but is required for cells to survive heat-stress (22). Ydj1 cooperates with Hsp70 and Hsp104 to break up large aggregates (54). In the context of PrD toxicity, it is possible that farnesylation enables Ydj1 to bind large PrD assemblies and assist Hsp104 in disaggregation. This activity would help control the PrD pool size and perhaps suppress PrD toxicity. However, while efficient binding between Ydj1 and the PrD required farnesylation, the residual Ydj1 interaction appeared sufficient to control the pool size of SDS-resistant PrD aggregates. In this

situation, the cellular threshold to tolerate SDS-resistant PrD accumulation may be reduced because Ydj1(C406S) is unable to properly fold other cellular proteins required for stress protection. For example, Ydj1 is required for the maturation of numerous kinases implicated in stress response (55) and farnesylation of Ydj1 is required for proper folding of at least one kinase (52). Thus, it is conceivable that reduced stress kinase activity could sensitize yeast that harbor the non-farnesylated form of Ydj1 to PrD toxicity when the pool size of SDS-resistant PrD is not dramatically elevated.

4.5 Materials and Methods

Yeast strains and plasmids- All experiments were conducted in the yeast strain *BY4741* (*MATa Δhis3, Δleu2, Δmet15, Δura3)* in a wild type, *Δydj1 (ydj1::KAN1*), or *Δram1 (ram1:KAN1)* background. Yeast strains were cured of prion seeds by three sequential passages on YPD media containing 3mM Guanidine-HCl. Ydj1 wild type and mutant constructs were expressed from the endogenous *YDJ1* promoter in a pRS315 plasmid backbone (15). The *YDJ1* open reading frame was also subcloned into a pRS315 backbone behind a glyceraldehyde phosphate dehydrogenase (GPD) promoter. The prion domain of Rnq1 (PrD:aa153-405) was generated by PCR amplification of nucleotides 459-1215 from *RNQ1* and subcloned in a pRS416 backbone behind the *GAL1* promoter or into a pRS316 backbone behind the *CUP1* promoter with an EGFP tag at the C-terminus. Sup35 was amplified from genomic DNA and inserted downstream of the *CUP1* promoter and upstream of an EGFP tag in a pRS416 background. Point mutants were generated using a Stratagene Quikchange mutagenesis kit. Yeast strains were generated by transformation using the lithium acetate method and selected on synthetic minimal media supplemented with amino acids required for survival.

Cell Viability Assay- Freshly transformed cells harboring pRS416-*RNQ1* or PrD with the indicated version of *YDJ1* were serially diluted on minimal selection media containing 2% galactose or 2% glucose. Plates were incubated at 30°C for 3-4 days and photographed.

Fluorescence microscopy- Cells transformed with Rnq1-GFP or PrD-GFP under the control of the *CUP1* promoter were induced with 50μM $CuSO_4$ for two hours then mounted on a glass slide and visualized with a Nikon Eclipse E600 fluorescence microscope.

Differential Centrifugation- Yeast cells were grown to mid-log phase and Rnq1-GFP or PrD-GFP induced for 4 hours with 50μM $CuSO_4$. Cells were lysed in Buffer A (50mM Hepes pH 7.4, 150mM NaCl, 0.1% Triton X-100, 1mM PMSF, 1X Protease inhibitor cocktail[Roche]) with glass beads in 30 second intervals for 8 cycles. Crude lysates were cleared of cell debris at

3000rpm for 3 min. About 100µg protein extract was subjected to high-speed centrifugation (100,00 x g) in a Beckman Type 70Ti rotor for 30 minutes. Supernatant and pellet fractions were resolved with input (10%) by SDS-PAGE and assessed by western immunoblotting.

Gel Filtration- Yeast cells were grown and lysed in Buffer A as described above. About 5mg protein extract was applied to a Sephacryl S-500HR gel filtration column (GE Healthcare). The column was calibrated with molecular weight markers from Amersham. Every other fraction was loaded on an acrylamide gel and analyzed by SDS-PAGE.

Rnq1 Peptide Array- A Rnq1 25-mer peptide array from Jenri Peptide Technologies was screened with purified Ydj1 according to manufacturer's instructions and as previously described (4).

Co-immunoprecipitation- Rnq1-YFP, PrD-YFP, and NPrD-YFP were expressed in [RNQ^+] cells from a galactose-inducible promoter and cell lysates were generated in buffer A and co-immunoprecipitations performed with αYdj1 antisera as described in main text. To determine binding with Sis1, Rnq1-GFP and PrD-GFP were expressed from a *CUP1* promoter in [RNQ^+] cells and cell lysates generated in buffer A. 1uL polyclonal αSis1 antisera was used to co-immunoprecipitate Sis1 and non-specific pre-immune antisera was used as a negative control to detect background binding. Rnq1-GFP or PrD-GFP were induced in wild type or *Δydj1* cells expressing the indicated form of Ydj1 as described above. Cell lysates were prepared in Buffer A as described above. Ydj1 was co-immunoprecipitated from about 100µg protein extract using αYdj1 polyclonal antisera and protein G-agarose beads (Roche) with standard techniques. Bound protein was analyzed by SDS-PAGE with 10% original lysate representing input.

Filter Trap Assay- PrD-GFP was induced and cells were lysed in Buffer A as described above. Approximately 20µg protein extract was added to sample buffer (2% SDS, 62.5mM Tris-HCl pH6.8, 1mM EDTA, 5% glycerol, 2% β-mercaptoethanol) then loaded onto a cellulose acetate membrane assembled in a slot blot apparatus. The membrane was washed in 0.1% SDS and

retained PrD-GFP assessed by immunobloting for GFP (Roche). Lysates were also analyzed by SDS-PAGE to determine protein expression levels. Western immunoblotting for 3-phosphoglycerate kinase (PGK) (Molecular Probes) was used as a load control.

Luciferase Reporter Assay- Yeast cells harboring firefly luciferase on a galactose-inducible promoter and the indicated version of *YDJ1* were grown to mid-log phase with 2% raffinose and luciferase induced with 2% galactose. Luciferase activity was measured as previously described (56) with a TD 20/20 luminometer. For *in vitro* luciferase refolding assays, firefly luciferase was purified and refolding measured as previously described (15). A two-sampled t-test (assuming unequal variances) was used to generate p-values comparing luciferase activity between wild type and mutant Ydj1.

Reconstitution of Chaperone-Dependent Polyubiquitination- Recombinant chaperones were purified and experimental conditions were conducted as previously described (48) substituting recombinant Ydj1 or the mutant as the Hsp40.

Immunofluorescence - Thioflavin T staining was performed as previously described (4) by expressing PrD-RFP in yeast overnight from a *CUP1* promoter.

Analysis of SDS-resistant aggregates - SDS-resistant aggregates were assessed by semi-denaturing gel electrophoresis (SDD-AGE) performed as previously described (4). SDS-resistant aggregates were also assessed by filter trap performed as described above

Huntingtin Aggregation Assay - Aggregation of GST-myc-HD53Q was performed as previously described (46) with the following modifications. First, 1μM GST-myc-HD53Q- was incubated in Buffer B (50 mM Tris·HCl (pH 7.0), 150 mM NaCl, 1 mM DTT, 1 mM phenylmethylsulfonyl fluoride, 50 mM KCl, 5 mM $MgCl_2$) with 6μM Ydj1 (wild type or the indicated mutant) and PreScission Protease to start the reaction (47). Reactions were incubated for 150 minutes then stopped with 4x native gel sample buffer (0.24M Tris-HCl pH 6.8, 40%

glycerol, 1% Bromphenol Blue). Aggregated myc-HD53Q was analyzed by filter trap and western-immunoblotting with c-Myc antisera (Sigma).

4.6 References

1. Sipe, J. D., and Cohen, A. S. (2000) *J Struct Biol* **130**, 88-98

2. Chiti, F., and Dobson, C. M. (2006) *Annu Rev Biochem* **75**, 333-366

3. Fiala, J. C. (2007) *Acta Neuropathol* **114**, 551-571

4. Douglas, P. M., Treusch, S., Ren, H. Y., Halfmann, R., Duennwald, M. L., Lindquist, S., and Cyr, D. M. (2008) *Proc Natl Acad Sci U S A*

5. Haass, C., and Selkoe, D. J. (2007) *Nat Rev Mol Cell Biol* **8**, 101-112

6. Magrane, J., Smith, R. C., Walsh, K., and Querfurth, H. W. (2004) *J Neurosci* **24**, 1700-1706

7. Behrends, C., Langer, C. A., Boteva, R., Bottcher, U. M., Stemp, M. J., Schaffar, G., Rao, B. V., Giese, A., Kretzschmar, H., Siegers, K., and Hartl, F. U. (2006) *Mol Cell* **23**, 887-897

8. Cyr, D. M. (2008) *Cell* **133**, 945-947

9. Mayer, M. P., and Bukau, B. (2005) *Cell Mol Life Sci* **62**, 670-684

10. Muchowski, P. J., and Wacker, J. L. (2005) *Nat Rev Neurosci* **6**, 11-22

11. Chai, Y., Koppenhafer, S. L., Bonini, N. M., and Paulson, H. L. (1999) *J Neurosci* **19**, 10338-10347

12. Qiu, X. B., Shao, Y. M., Miao, S., and Wang, L. (2006) *Cell Mol Life Sci* **63**, 2560-2570

13. Fan, C. Y., Lee, S., Ren, H. Y., and Cyr, D. M. (2004) *Mol Biol Cell* **15**, 761-773

14. Ramos, C. H., Oliveira, C. L., Yang-Fan, C., Torriani, I. L., and Cyr, D. M. (2008) *J Mol Biol*

15. Fan, C. Y., Ren, H. Y., Lee, P., Caplan, A. J., and Cyr, D. M. (2005) *J Biol Chem* **280**, 695-702

16. Linke, K., Wolfram, T., Bussemer, J., and Jakob, U. (2003) *J Biol Chem* **278**, 44457-44466

17. Szabo, A., Korszun, R., Hartl, F. U., and Flanagan, J. (1996) *Embo J* **15**, 408-417

18. Langer, T., Lu, C., Echols, H., Flanagan, J., Hayer, M. K., and Hartl, F. U. (1992) *Nature* **356**, 683-689

19. Cyr, D. M. (1995) *FEBS Lett* **359**, 129-132

20. Caplan, A. J., and Douglas, M. G. (1991) *J Cell Biol* **114**, 609-621

21. Meacham, G. C., Lu, Z., King, S., Sorscher, E., Tousson, A., and Cyr, D. M. (1999) *Embo J* **18**, 1492-1505

22. Caplan, A. J., Tsai, J., Casey, P. J., and Douglas, M. G. (1992) *J Biol Chem* **267**, 18890-18895

23. Sondheimer, N., and Lindquist, S. (2000) *Mol Cell* **5**, 163-172

24. Derkatch, I. L., Bradley, M. E., Hong, J. Y., and Liebman, S. W. (2001) *Cell* **106**, 171-182

25. Kurahashi, H., Ishiwata, M., Shibata, S., and Nakamura, Y. (2008) *Mol Cell Biol* **28**, 3313-3323

26. Vitrenko, Y. A., Pavon, M. E., Stone, S. I., and Liebman, S. W. (2007) *Curr Genet* **51**, 309-319

27. Aron, R., Higurashi, T., Sahi, C., and Craig, E. A. (2007) *Embo J* **26**, 3794-3803

28. Bradley, M. E., Edskes, H. K., Hong, J. Y., Wickner, R. B., and Liebman, S. W. (2002) *Proc Natl Acad Sci U S A* **99 Suppl 4**, 16392-16399

29. Lopez, N., Aron, R., and Craig, E. A. (2003) *Mol Biol Cell* **14**, 1172-1181

30. Cohen, E., Bieschke, J., Perciavalle, R. M., Kelly, J. W., and Dillin, A. (2006) *Science* **313**, 1604-1610

31. Li, J., Qian, X., and Sha, B. (2003) *Structure* **11**, 1475-1483

32. Gokhale, K. C., Newnam, G. P., Sherman, M. Y., and Chernoff, Y. O. (2005) *J Biol Chem* **280**, 22809-22818

33. Muchowski, P. J., Schaffar, G., Sittler, A., Wanker, E. E., Hayer-Hartl, M. K., and Hartl, F. U. (2000) *Proc Natl Acad Sci U S A* **97**, 7841-7846

34. Patel, B. K., and Liebman, S. W. (2007) *J Mol Biol* **365**, 773-782

35. Wickner, R. B., Dyda, F., and Tycko, R. (2008) *Proc Natl Acad Sci U S A* **105**, 2403-2408

36. Floer, M., Bryant, G. O., and Ptashne, M. (2008) *Proc Natl Acad Sci U S A* **105**, 2975-2980

37. Chernoff, Y. O., Lindquist, S. L., Ono, B., Inge-Vechtomov, S. G., and Liebman, S. W. (1995) *Science* **268**, 880-884

38. Rudiger, S., Schneider-Mergener, J., and Bukau, B. (2001) *Embo J* **20**, 1042-1050

39. Sahi, C., and Craig, E. A. (2007) *Proc Natl Acad Sci U S A* **104**, 7163-7168

40. Tsai, J., and Douglas, M. G. (1996) *J Biol Chem* **271**, 9347-9354

41. Wu, Y., Li, J., Jin, Z., Fu, Z., and Sha, B. (2005) *J Mol Biol* **346**, 1005-1011

42. Lu, Z., and Cyr, D. M. (1998) *J Biol Chem* **273**, 5970-5978

43. Banecki, B., Liberek, K., Wall, D., Wawrzynow, A., Georgopoulos, C., Bertoli, E., Tanfani, F., and Zylicz, M. (1996) *J Biol Chem* **271**, 14840-14848

44. Li, J., and Sha, B. (2005) *Biochem J* **386**, 453-460

45. Scherzinger, E., Lurz, R., Turmaine, M., Mangiarini, L., Hollenbach, B., Hasenbank, R., Bates, G. P., Davies, S. W., Lehrach, H., and Wanker, E. E. (1997) *Cell* **90**, 549-558

46. Rosser, M. F., Washburn, E., Muchowski, P. J., Patterson, C., and Cyr, D. M. (2007) *J Biol Chem* **282**, 22267-22277

47. Wacker, J. L., Zareie, M. H., Fong, H., Sarikaya, M., and Muchowski, P. J. (2004) *Nat Struct Mol Biol* **11**, 1215-1222

48. Younger, J. M., Ren, H. Y., Chen, L., Fan, C. Y., Fields, A., Patterson, C., and Cyr, D. M. (2004) *J Cell Biol* **167**, 1075-1085

49. Lu, Z., and Cyr, D. M. (1998) *J Biol Chem* **273**, 27824-27830

50. Bonini, N. M. (2002) *Proc Natl Acad Sci U S A* **99 Suppl 4**, 16407-16411

51. Lee, S., Fan, C. Y., Younger, J. M., Ren, H., and Cyr, D. M. (2002) *J Biol Chem* **277**, 21675-21682

52. Flom, G. A., Lemieszek, M., Fortunato, E. A., and Johnson, J. L. (2008) *Mol Biol Cell*

53. Pylypenko, O., Schonichen, A., Ludwig, D., Ungermann, C., Goody, R. S., Rak, A., and Geyer, M. (2008) *J Mol Biol* **377**, 1334-1345

54. Glover, J. R., and Lindquist, S. (1998) *Cell* **94**, 73-82

55. Chapple, J. P., and Cheetham, M. E. (2003) *J Biol Chem* **278**, 19087-19094

56. Tkach, J. M., and Glover, J. R. (2008) *Traffic* **9**, 39-56

Chapter Five

A microtubule-dependent quality control pathway protects misfolded, cytosolic proteins from aggregation

5.1 Abstract

Protein misfolding is a constant cellular burden as unfolded polypeptides must be held in soluble state for refolding or degradation by protein quality control factors. Failure to efficiently process misfolded proteins can result in aggregation which threatens protein homeostasis. Molecular chaperones and E3 ubiquitin ligases cooperate to triage misfolded proteins for refolding or degradation. We find that perturbation of specific steps in the degradation of a multi-domain, misfolded protein in the cytosol has distinct outcomes on the propensity of this protein to aggregate in the cell. Removing the E3 ubiquitin ligases Ubr1 or San1 causes soluble forms of this misfolded protein to accumulate at a perinuclear compartment. Conversely, interfering with the Type I Hsp40 Ydj1 or perturbing the microtubule cytoskeleton selectively partitioned this misfolded protein in insoluble aggregates and impaired degradation. Polyubiquitination of this misfolded protein was unaffected suggesting that polyubiquitinated proteins are particularly sensitive to protein aggregation. Elevating levels of the Type II Hsp40 Sis1 rescued protein degradation during microtubule dysfunction. As a result, disrupting specific stages in degradation of a misfolded protein shifts the folding equilibrium toward aggregation however back-up pathways protect cells from the accumulation of protein aggregates.

5.2 Introduction

Cells are continuously challenged by the formation of misfolded protein species. Unfolded polypeptides expose hydrophobic amino acids that are normally buried in the core of the native protein. As a consequence, unfolded polypeptides have a strong propensity to aggregate in the cell (1). Protein misfolding and aggregation induce global deficiencies in protein homeostasis and underlie a variety of human diseases especially pathologies associated with aging (2-4). Sophisticated protein quality control (PQC) pathways function at each stage of a protein's life cycle to prevent aberrant protein aggregation and partition non-native polypeptides for refolding or degradation (5). Misfolded proteins that are beyond repair are targeted for degradation by the ubiquitin-proteasome system (UPS) (6). The cooperative action of molecular chaperones and E3 ubiquitin ligases recognize non-native protein conformers and recruit E2 ligases to polyubiquitinate the misfolded protein (7). Ubiquitin receptors bind polyubiquitin chains and physically tether polyubiquitinated proteins to the proteasome to facilitate degradation (8). At each step in this pathway, misfolded proteins must be held in a soluble state competent for degradation by the proteasome. How protein quality control factors function in a concerted action to deliver misfolded proteins to the proteasome is a major unanswered question in the field.

The Hsc/Hsp70 molecular chaperone family (herein generally referred as Hsp70s) plays a major role in recognizing non-native polypeptides and suppressing protein aggregation (5,9). Hsp70 polypeptide binding is regulated by cycles of ATP binding and hydrolysis (10). ATP hydrolysis is rate-limiting, but a family of Hsp70 co-chaperones known collectively as Hsp40s (or J-proteins) stimulate Hsp70 ATPase activity via a conserved J-domain (11-14). ATP hydrolysis by the Hsp70 causes a conformational change that increases Hsp70 substrate affinity. Hsp40 molecular chaperones have evolved specialized protein domains that tether Hsp70 function to a wide variety of basic cellular activities including protein degradation (15,16). For example, the yeast Hsp40 Ydj1 possesses multiple substrate binding domains that recognize diverse non-native proteins and suppress protein aggregation (17-19). This activity is crucial for holding non-native polypeptides in a refolding

competent state (20,21) or a conformation favorable for polyubiquitination by E3 and E2 ubiquitin ligases (22-24). Sis1 is another Hsp40 in the yeast cytosol that can bind non-native polypeptides. While Ydj1 and Sis1 share some overlapping activities (25), these Hsp40s also couple Hsp70 to very distinct functions in the cell (21,26). The conventional model is that Hsp70/Hsp40s bind non-native polypeptides and recruit additional PQC factors including E3 ubiquitin ligases to triage non-native polypeptides for refolding or degradation.

In addition to the Hsp70/Hsp40 chaperone machine, E3 ubiquitin ligases supply another layer of selectivity in PQC. For example, the mammalian E3 ligase CHIP (carboxyl terminus of the Hsc70-interacting protein) promotes degradation of misfolded proteins in the cytosol and ER membrane (22,27-29). However, CHIP also possesses co-chaperone activity and contributes to Hsc70-dependent refolding of non-native polypeptides (30-32). As a result, specialized chaperone/E3 ligase complexes can selectively partition misfolded proteins between refolding and degradation pathways. Budding yeast lack a CHIP ortholog, yet the E3 ubiquitin ligases Ubr1, San1, and Doa10 have been shown to mediate degradation of misfolded cytosolic proteins (23,33-37). Ubr1 has been studied predominantly for its role in N-End-rule degradation (38,39). However, Ubr1 can also suppress protein aggregation (23) and deletion of *UBR1* sensitizes yeast to a variety of stress-inducing agents suggesting this E3 ligase has broad influence in protein homeostasis (23,35). San1 is predominantly nuclear and participates in degradation of misfolded proteins in the nucleus (40). Nonetheless, San1 is required for efficient degradation of misfolded, cytosolic proteins in conjunction with Ubr1 or with the ER membrane E3 ligase Doa10 (34-36). How misfolded proteins are selectively targeted by these distinct E3 ligase pathways for protein degradation is currently unknown.

Under conditions of proteasome dysfunction, misfolded proteins are selectively targeted via the microtubule cytoskeleton to specialized protein quality control compartments in the cell (41). For example, Kaganovich *et al* demonstrated that polyubiquitinated proteins are held in a soluble state at a perinuclear site called the JUNQ compartment. Alternatively, insoluble, or amyloidogenic proteins are trafficked to a perivaculouar compartment called the IPOD (42,43). Thus, if misfolded proteins

escape the PQC pathways described above, then back-up pathways redirect these proteins to specific intracellular locations (44). Whether compartments such as the JUNQ and IPOD function in basal PQC is still unclear. Polyubiquitination is an important targeting signal for selectively trafficking misfolded proteins to the JUNQ. As such, molecular chaperones and E3 ligases function at a critical intersection by which misfolded proteins are targeted to the proteasome for degradation or diverted to quality control compartments via the microtubule cytoskeleton. As a misfolded protein is funneled through multiple quality control factors, it is still unclear how PQC complexes suppress aberrant aggregation at each step *en route* to the proteasome and how interfering with distinct components influences the fate of a misfolded protein.

In this study, we demonstrate that perturbation of individual steps in the degradation of a misfolded, cytosolic protein differentially affects aggregation of this protein. For example, loss of the E3 ubiquitin ligases Ubr1 or San drives soluble forms of this misfolded protein to accumulate in a juxta-nuclear compartment. In contrast, loss of the Type I Hsp40 Ydj1 partitions this misfolded protein into an insoluble state and abrogates degradation. Surprisingly, disrupting the microtubule cytoskeleton similarly drove this misfolded protein to form insoluble aggregates and resulted in a lag in degradation. Interfering with Ydj1 or the microtubule cytoskeleton did not affect ubiquitination of this misfolded protein suggesting that PQC factors are required for holding polyubiquitinated proteins in a soluble state before delivery to the proteasome. Interestingly, microtubule depolymerization also induced aggregation of von Hippel Lindau protein however degradation of this misfolded protein was accelerated. Thus, misfolded proteins are differentially susceptible to perturbations in cellular PQC factors and back-up pathways are present to remove aggregated proteins.

5.3 Results

Ydj1 holds a misfolded, cytosolic protein in a soluble state.

To analyze how protein quality control factors protect misfolded proteins from aggregation we examined the degradation pathway of a labile, multi-domain protein. This protein (herein referred to as slGFP for short-lived GFP) consists of two GFP moieties that are flanked at the N-terminus by a 126 amino acid domain enriched in hydrophobic residues (Figure 5.1A) (45). Importantly, slGFP is modular and contains natively folded domains as well as an unstructured region with several putative chaperone-binding sites (Figure 5.2)(26,46). Cycloheximide-chase analysis demonstrated that slGFP was unstable with approximately a 15 minute half-life (Figure 5.1B). Treatment with the proteasome inhibitor MG-132 blocked turnover of this protein indicating that slGFP is degraded via the ubiquitin-proteasome system. Thus, slGFP is a model misfolded protein that is targeted for degradation and perturbing individual steps in the pathway will reveal how specific PQC factors protect slGFP from aggregation.

Several sequences in the N-terminus of slGFP matched putative binding sites for the Type I Hsp40 Ydj1 (47). Ydj1 participates in degradation of numerous misfolded proteins in the cytosol and ER membrane (24,34,35,37,48,49), thus we predicted that Ydj1 would be involved in the degradation of slGFP. Indeed, slGFP degradation was delayed in a Δ*ydj1* strain to a half-life of over 60min (Figure 5.1C). A delay in turnover was also observed in the presence of a temperature sensitive allele of *YDJ1* (Figure 5.2B) suggesting that Ydj1 is required for slGFP degradation.

Ydj1 functions as a chaperone to hold non-native polypeptides in a soluble state and prevents aggregation (19,20). Accordingly, we investigated whether deleting *YDJ1* impacted slGFP solubility. High-speed centrifugation analysis of yeast cell extracts demonstrated that slGFP was shifted to a triton-insoluble state in a Δ*ydj1* strain (Figure 5.1D). Ydj1 has been shown to cooperate with Hsp70 and E3 ubiquitin ligases to promote polyubiquitination of multiple non-native polypeptides (18,24,35,48).

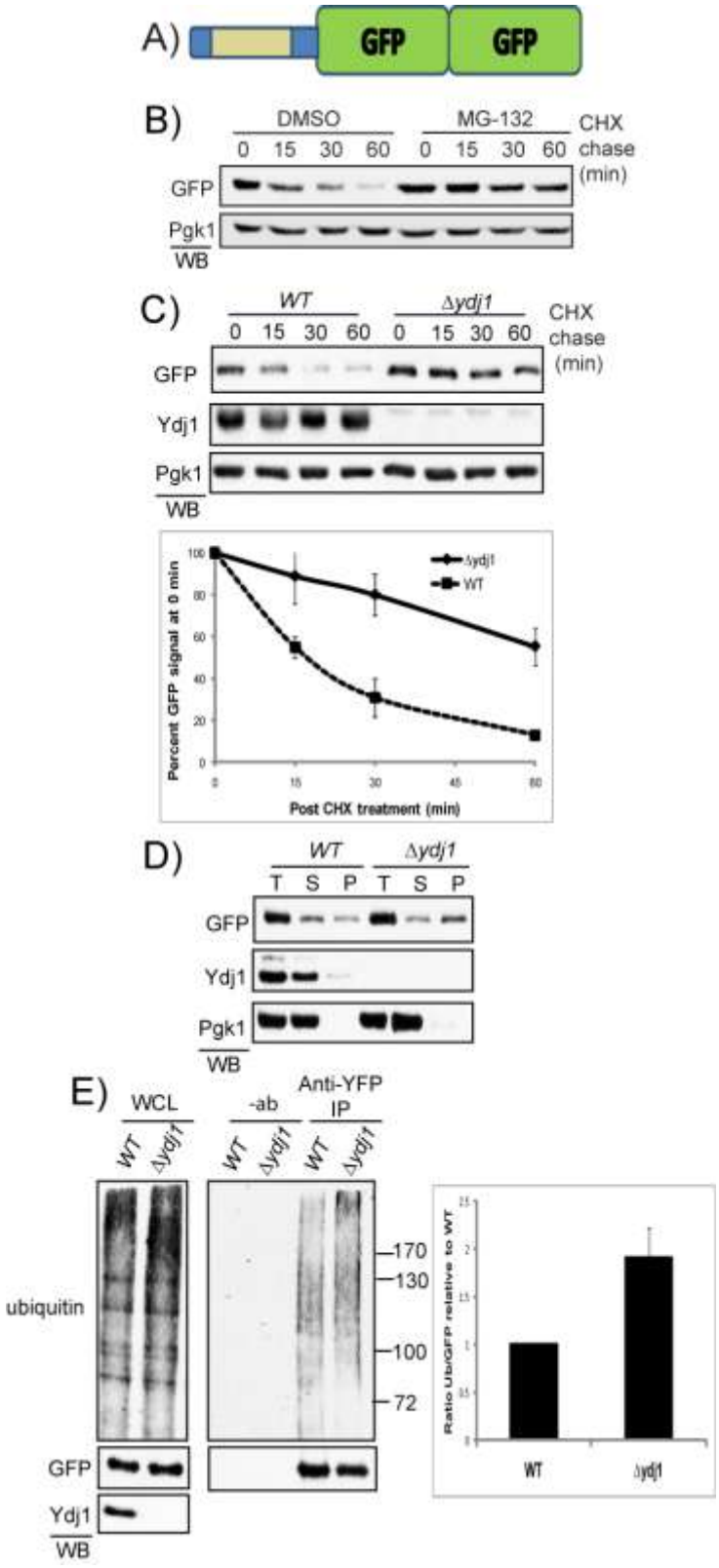

Figure 5.1 **Ydj1 holds a misfolded, cytosolic protein in a soluble state.** A) Domain structure of short-lived reporter protein (slGFP) with N-terminal domain and two GFP moieties. B)

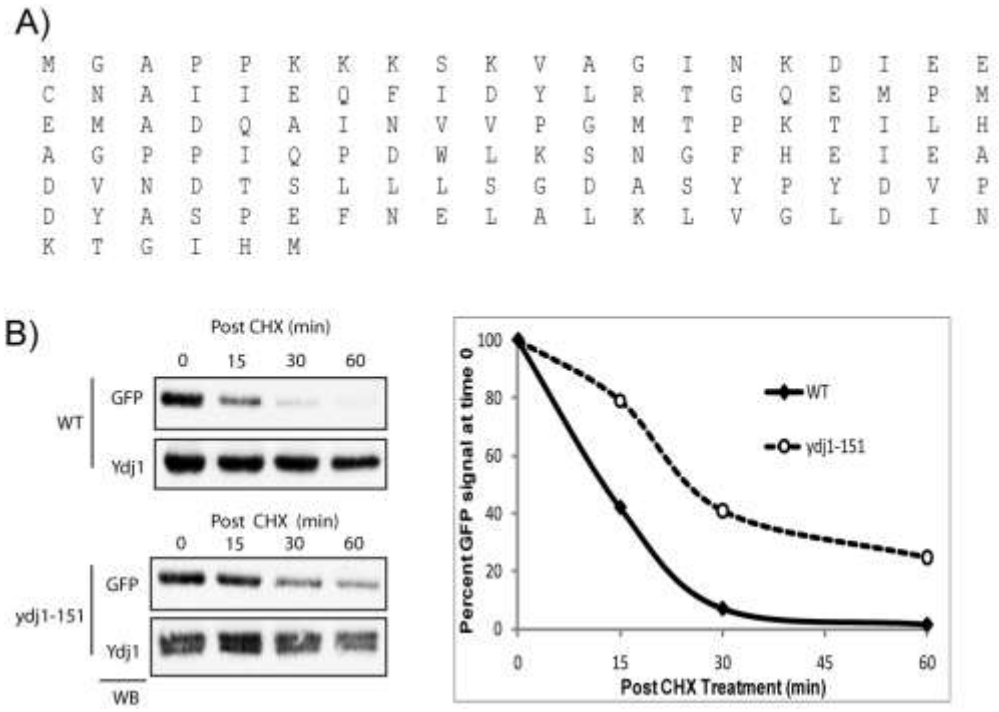

Figure 5.2 Ydj1-151 delays slGFP degradation. A) Amino acid sequence of N-terminal domain from slGFP B) Turnover of slGFP in wildtype or ydj1-151 strain at 37°C. Quantification of GFP signal is shown on the right.

Figure 5.1 . . . ***cont*** Cycloheximide-chase (CHX) analysis of slGFP turnover in Δpdr5 cells treated with DMSO or the proteasome inhibitor MG-132 (100μM). C) Turnover of slGFP in wildtype (WT) or a Δ*ydj1* strain was assessed by cycloheximide chase analysis. Quantification of three independent experiments is shown below in which GFP signal is represented as a percentage of signal at start of chase (0min). D) Differential, high speed centrifugation to examine solubility of slGFP reporter in WT or a Δ*ydj1* strain (T-total, S-supernatant, P-pellet). D) Ubiquitination of slGFP in WT or a Δ*ydj1* strain. SlGFP was immunoprecipitated from WT or Δ*ydj1* lysates (αYFP IP). Quantification of three independent experiments is shown on the right as a ratio of ubiquitin signal to level of immunoprecipitated GFP and normalized to WT. Error bars represent ±1SEM.Total input levels are shown on the left (Whole cell lysates).

We expected that slGFP ubiquitination would be reduced in a Δ*ydj1* background. To test this hypothesis, slGFP was immunoprecipitated from wildtype or Δ*ydj1* lysates and analyzed by western blotting for ubiquitin. However, there was a slight increase in the pool of ubiquitinated slGFP in a Δ*ydj1* strain background compared to wildtype (Figure 5.1E). Thus, Ydj1functions to hold polyubiquitinated forms of slGFP in a soluble state and without this Hsp40, polyubiquitinated forms of slGFP are unable to be degraded by the proteasome.

The slGFP reporter is degraded by the Ubr1/San1 E3 ligases

If polyubiquitinated forms of slGFP aggregate when this misfolded protein cannot reach the proteasome, we were interested if interfering with ubiquitination of slGFP would have a similar effect. Several E3 ubiquitin ligases including Ubr1, San1, and Doa10 are implicated in degradation of misfolded, cytosolic proteins (23,33-37). SlGFP was stabilized in Δ*ubr1* and Δ*san1* strain backgrounds yet not in a Δ*doa10* strain background (Figure 5.3A). Consistent with these observations, slGFP ubiquitination was decreased in a Δ*ubr1* or a Δ*san1* background (Figure 5.4A). Thus, slGFP is degraded in a Ubr1/San1-dependent manner.

Steady state levels of slGFP accumulate in the absence of Δ*ubr1* or a Δ*san1* (Figure 5.3 and Figure 5.4B). As a consequence, we expected that excess levels would drive slGFP to aggregate in an insoluble state. However, slGFP remained predominantly soluble in either a Δ*ubr1* or Δ*san1* strain background (Figure 5.3C). To determine if slGFP accumulated in a specific intracellular location or was globally diffuse, the localization of slGFP in these strains was investigated under fluorescence microscopy. In a wildtype background, slGFP is diffuse throughout the cytosol in a majority of cells(>90%). In Δ*ubr1* or Δ*san1* strains, the percentage of cells displaying a single slGFP aggregate significantly increased (Figure 5.3). Interestingly, these aggregates were often localized proximal to the nucleus and did not colocalize with Rnq1-mRFP (Figure 5.4) or the spindle-pole body marker Spc72 (data not shown) suggesting these aggregates do not represent IPODs or aggresomes. If

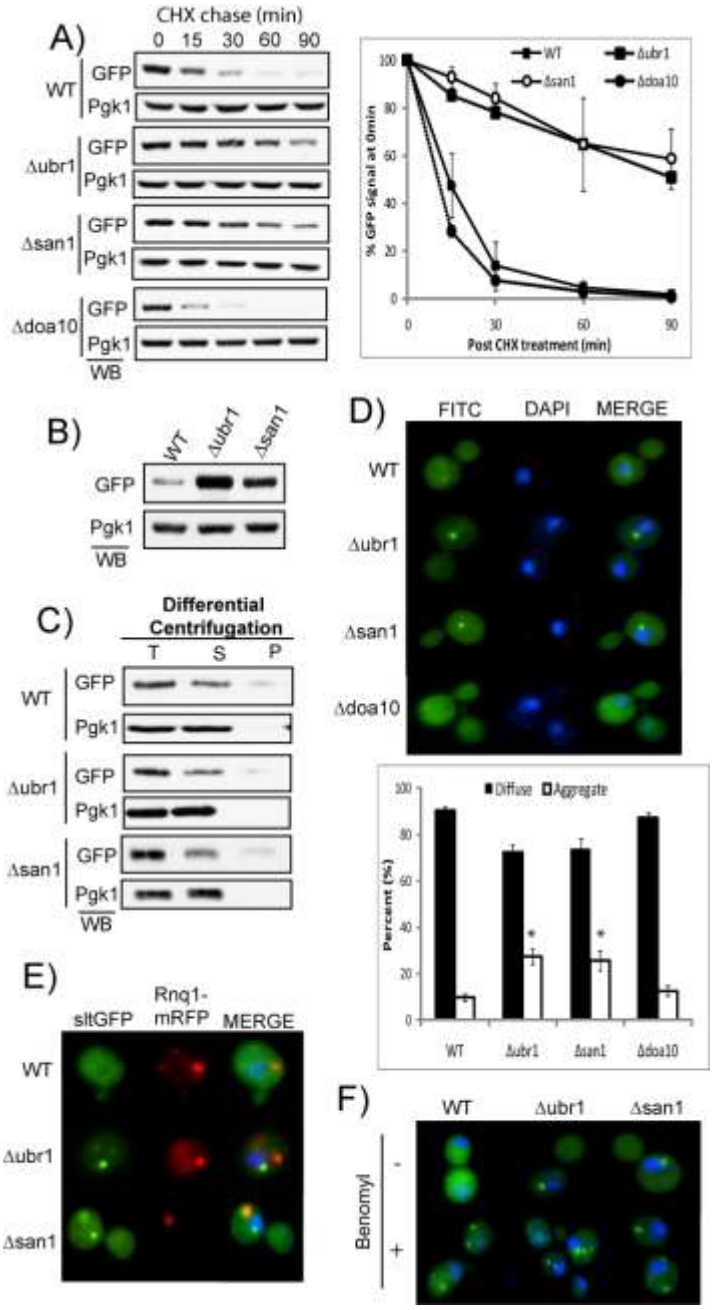

Figure 5.3 Ubr1 and San1 E3 ligases participate in degradation of slGFP reporter. A) Turnover of slGFP reporter in WT, Δ*ubr1*, Δ*san1* or Δ*doa10* strain was assessed by cycloheximide chase analysis. Quantification of three independent experiments is shown on the right. B) Steady state levels of slGFP from WT, Δ*ubr1*, or Δ*san1* strains. C) Detergent solubility of slGFP in WT, Δ*ubr1*, or Δ*san1* strains was assessed after high speed centrifugation (T-total, S-supernatant, P-pellet). D) Localization of slGFP reporter was analyzed in WT, Δ*ubr1*, Δ*san1* or Δ*doa10* strains by fluorescence microscopy. Quantification of slGFP aggregates in different strain backgrounds is shown on the right (*$p<0.05$ n=500 cells in three independent experiments). Error bars represent ±1 SEM. E) Colocalization of slGFP aggregates in WT, Δ*ubr1*, or Δ*san1* strains with Rnq1-mRFP under fluorescence micrscopy (DAPI is overlaid in blue). F) Localization of slGFP in WT, Δ*ubr1*, or Δ*san1* strains treated with DMSO or benomyl for 30 minutes.

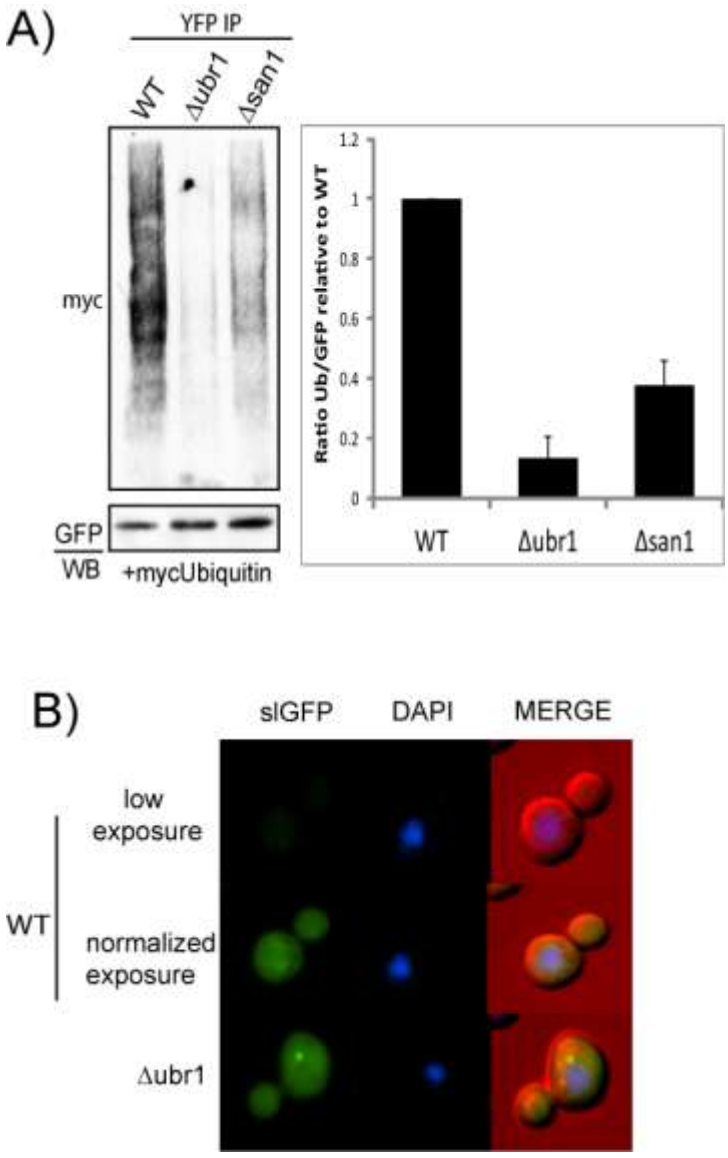

Figure 5.4 Ubiquitination and accumulation of slGFP in Δ*ubr1* and Δ*san1* backgrounds. A) Ubiquitination of the slGFP reporter in WT, Δ*ubr1*, or Δ*san1* strains expressing myc-ubiquitin. SlGFP was immunoprecipitated from cell extracts with anti-YFP antisera and immunoprecipitated material assessed by western immunobloting for myc and GFP. B) Localization of slGFP under fluorescence microscopy. Upper panel shows WT cell expressing slGFP under same exposure as Δ*ubr1* strain shown on bottom. Middle panel shows WT cell under longer exposure to normalize intensity of signal to Δ*ubr1* strain. Merge images show DIC, DAPI, and GFP signal together.

these perinuclear aggregates represent intracellular PQC compartments, the formation of this structure should be dependent upon the microtubule cytoskeleton. To test this prediction, cells were treated with the microtubule depolymerizing drug benomyl. In Δ*ubr1* or Δ*san1* cells treated with benomyl, slGFP was not longer localized in juxtanuclear foci yet formed multiple aggregates that were dispersed throughout the cytosol (Figure 5.3F). Interestingly, benomyl also induced slGFP aggregation in a wildtype strain suggesting that an intact microtubule cytoskeleton is normally required for suppressing aggregation of a misfolded protein.

Microtubules are required for holding slGFP in a soluble state

While microtubules are required for trafficking misfolded proteins to specialized compartments under stress (ex. proteasome inhibition)(44), a basal role for microtubules in PQC has not been investigated. Timecourse analysis revealed that small slGFP aggregates were visible after only 15 minutes post-benomyl treatment and several large, cytosolic aggregates were observed by 45 minutes (Figure 5.5A). The kinetics of slGFP aggregation are consistent with previous reports demonstrating that benomyl induces microtubule depolymerization as early as 15 minutes (50). Upon microtubule depolymerization, slGFP relocalized in two distinct pools, small aggregates dispersed throughout the cytosol and a large, single aggregate that co-localized with Rnq1-mRFP foci (Figure 5.5B-arrow) suggesting pools of the slGFP reporter might become insoluble. High speed centrifugation analysis demonstrated that a substantial fraction of the slGFP reporter redistributed from a triton-soluble to a triton-insoluble state after microtubule depolymerization (Figure 5.5C). Benomyl-induced slGFP aggregation was independent of the [*RNQ+*] prion (Figure 5.6A&B) suggesting co-colocalization with Rnq1 was coincidental with slGFP becoming insoluble after benomyl treatment and not a result of slGFP being templated by an amyloidogenic prion. Importantly, benomyl did not result in aggregation of monomeric GFP (Figure 5.5D) and did not induce a heat shock response suggesting that microtubule dysfunction does not cause general misfolding of cellular proteins (Figure 5.5E). Thus, perturbing the microtubule cytoskeleton interferes with quality control of a misfolded, cytosolic protein.

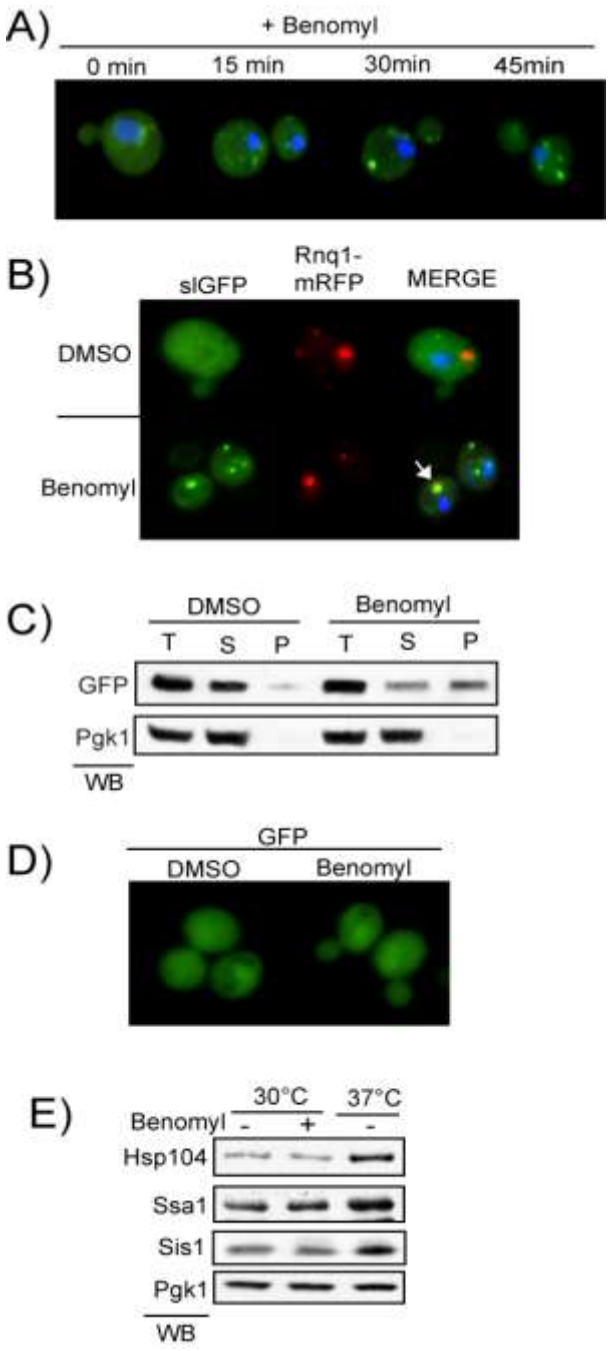

Figure 5.5. Benomyl treatment causes slGFP to form insoluble aggregates. A) Fluorescence microscopy of slGFP in cells treated with MG-132 after the indicated time (upper panel). Colocalization of slGFP and Rnq1mRFP in cells treated with DMSO or MG-132 (lower panel). Merge images show slGFP and Rnq1-mRFP with DAPI overlay (blue). B) Localization of the slGFP reporter in cells treated with treated with MG-132 alone or in combination with benomyl for 30 minutes. C) Timecourse of slGFP aggregation after benomyl treatment (DAPI is overlaid in blue). F) Colocalization of slGFP aggregates with Rnq1-mRFP after benomyl treatment. Arrow indicates slGFP aggregate that colocalizes with Rnq1-mRFP inclusion H) Detergent-solubility of slGFP reporter after high speed centrifugation from cells treated with DMSO or benomyl (T-total, S-supernant, P-pellet) G) Localization of GFP in cells treated with DMSO or benomyl.

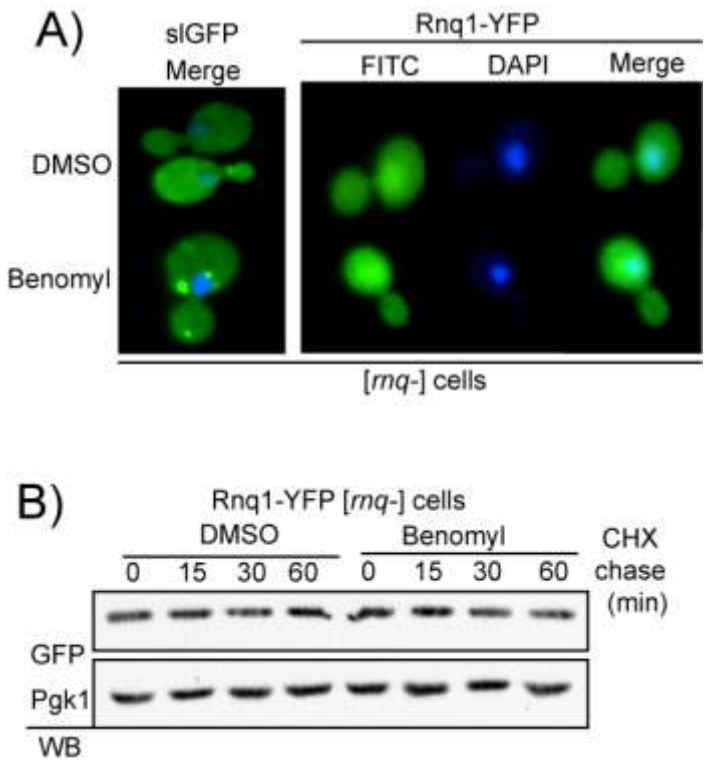

Figure 5.6 Benomyl-induced slGFP aggregation is [*RNQ*+] independent. A) SlGFP localization in [*rnq*-] cells treated with DMSO or 40μM benomyl for 30 minutes (left panel). DAPI is shown with blue overlay. Rnq1-YFP expressed from the *GAL1* promoter for 1 hour in [*rnq*-] cells treated as described for slGFP. B) Turnover of Rnq1-YFP in [*rnq*-] cells pretreated with DMSO or benomyl demonstrating that Rnq1YFP is stable in this background.

Disrupting microtubule dynamics selectively impacts degradation of misfolded proteins

If depolymerizing the microtubule cytoskeleton induces slGFP aggregation, what is the consequence on degradation of this misfolded protein? Cells expressing slGFP were treated with benomyl for 10 minutes and slGFP degradation analyzed by cycloheximide-chase analysis. Benomyl treatment extended the slGFP half-life from 15 minutes to approximately 50 minutes (Fig 5.7A). To alter microtubule dynamics by an alternative method, we expressed a dominant-lethal form of the α-tubulin subunit Tub1(E255A) in yeast. This mutant incorporates into polymerizing microtubules and results in static microtubules (51). Like benomyl, expression of Tub1(E255A) also caused a lag in slGFP degradation suggesting that a dynamic microtubule cytoskeleton is required for the efficient degradation of a misfolded protein (Figure 5.7B).

We were interested in whether the microtubule cytoskeleton broadly influences solubility and degradation of short-lived proteins or do specific misfolded proteins rely on this pathway. To test this question, the turnover and localization of several unstable proteins was assessed after benomyl treatment. Recently, Heck *et al* showed that a truncated form of the glycolytic enzyme Gnd1(tGnd1) is a short-lived substrate for the E3 ubiquitin ligases San1 and Ubr1 (35). Disrupting the microtubule cytoskeleton induced aggregation of 3HA-tGnd1GFP with similar kinetics to slGFP (Figure 5.8A). Moreover, benomyl treatment extended the half-life of 3HA-tGnd1GFP from 15 min to 25 min (Fig. 5.8B). Therefore, interfering with the microtubule cytoskeleton disrupts quality control of multiple misfolded proteins in the cell.

The misfolded proteins examined thus far are rapidly degraded (half-life<30min) suggesting that PQC machinery bypasses repair and targets slGFP and tGnd directly for degradation. Other misfolded proteins can exist in a conformation that is accessible to both folding and degradation factors. For example, folding of von Hippel Lindau (VHL) protein requires chaperone-dependent assembly with partner proteins to form a stable ternary complex (52-54). In the absence of these partner proteins, VHL folding is inefficient and VHL is targeted for degradation by a distinct network of PQC factors. As a result, VHL is different from from the other misfolded proteins analyzed in that

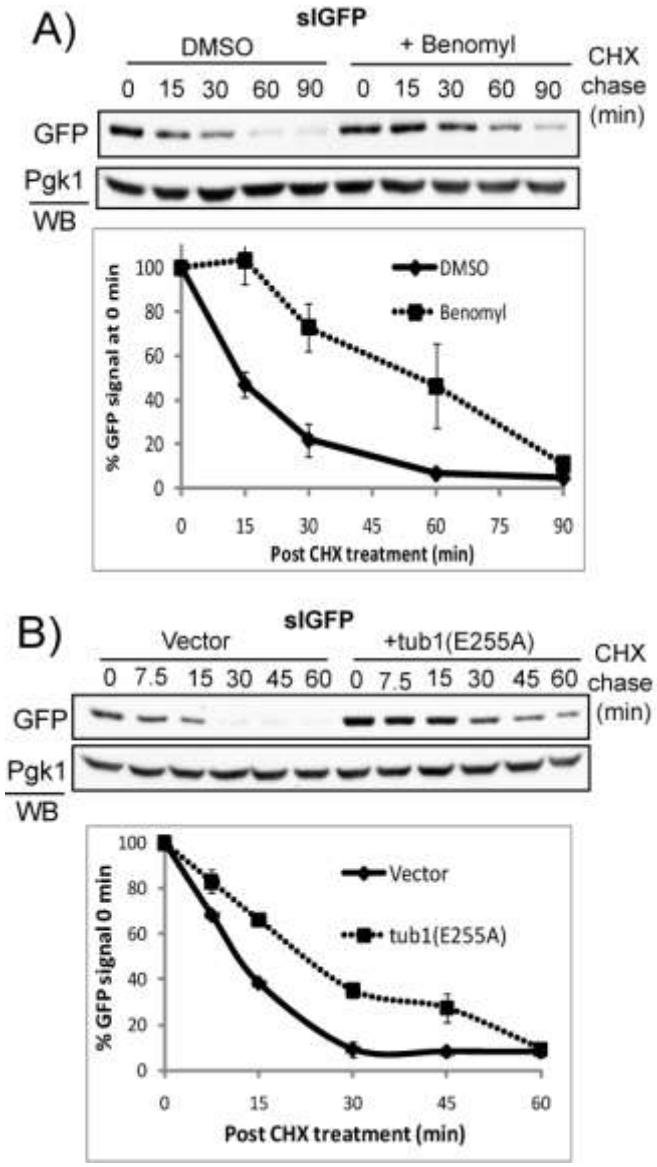

Figure 5.7. Disrupting microtubule dynamics inhibits slGFP degradation. A) Cycloheximide-chase analysis of slGFP turnover in cells pretreated with DMSO or benomyl for 10 minutes. Quantification of three independent experiments is shown on the right. B) Cycloheximide-chase analysis of slGFP after expression of tub1(E355A) for 2 hours. Quantification of three independent experiments is shown on the right.

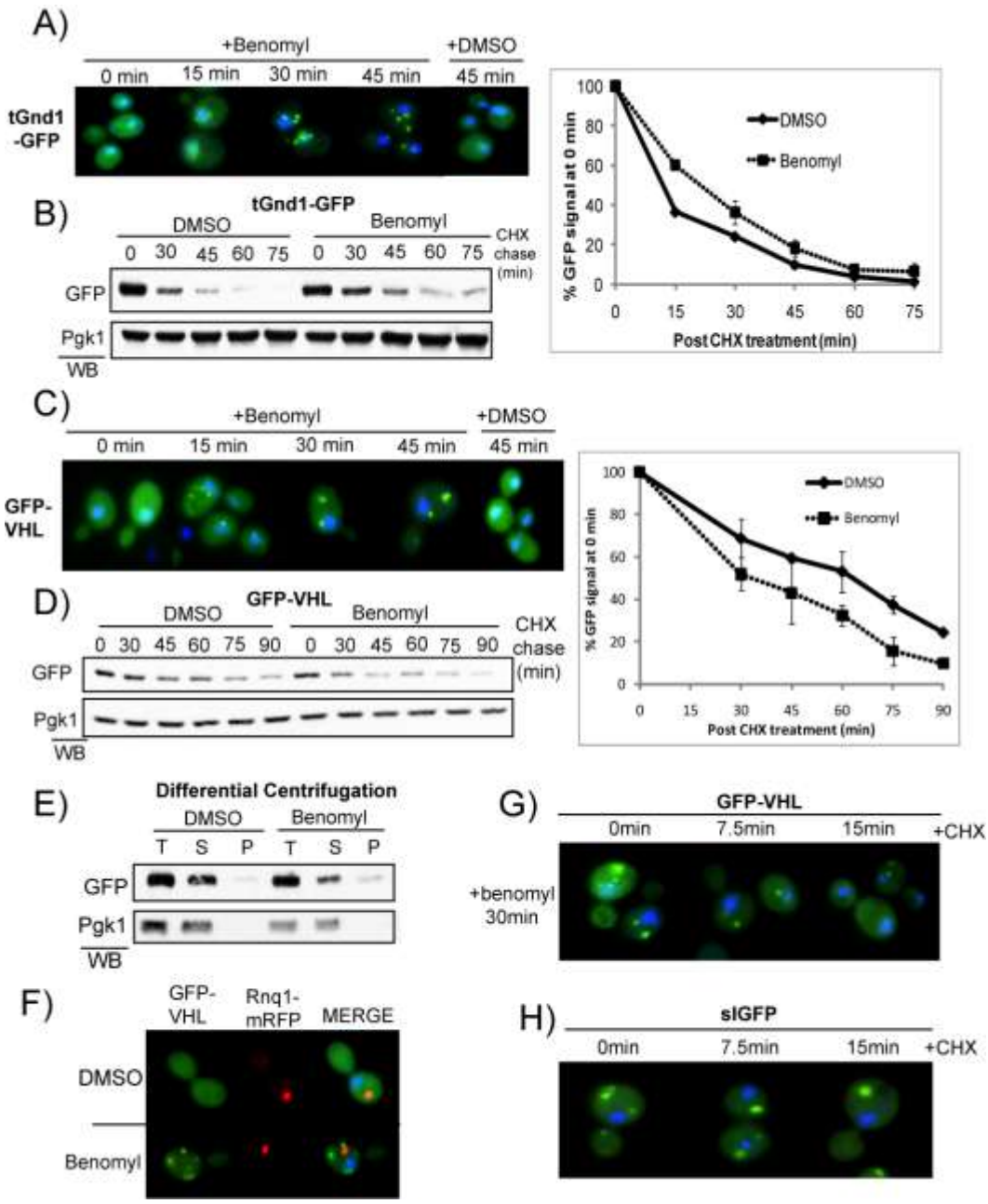

Figure 5.8 Benomyl selective impacts solubility and degradation of misfolded proteins. A) Timecourse of 3HA-tGnd1GFP aggregation after benomyl treatment under fluorescence microscopy (DAPI overlay in blue). B) Cycloheximide-chase analysis of 3HA-tGnd1GFP in cells pretreated with DMSO or benomyl as described above. Quantification of three independent experiments is shown on the right. Error bars on quantification represent ±1SEM. C) Timecourse of GFP-VHL aggregation after benomyl treatment under fluorescence microscopy (DAPI overlay in blue). D) Cycloheximide-chase analysis of GFP-VHL after treatment with DMSO or benomyl. Quantification of three independent experiments is shown below. E) Solubility of GFP-VHL after high speed centrifugation in cells treated with DMSO or benomyl. F) GFP-VHL aggregates do not colocalize with Rnq1-mRFP foci after benomyl treatment. G) Cells expressing GFP-VHL were treated with benomyl for 30 minutes then treated with cycloheximide and cells visualized at the indicated times. On the right, cells expressing slGFP were treated as described for GFP.

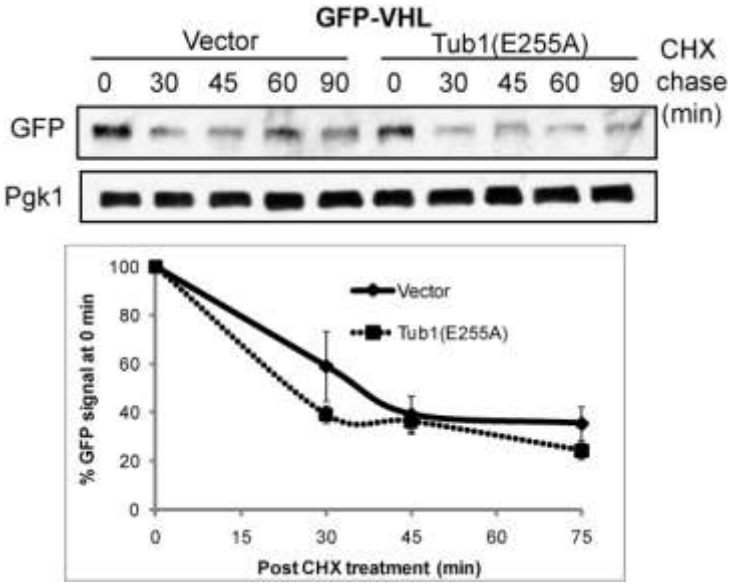

Figure 5.9 Expression of dominant-lethal Tub1 does not affect GFP-VHL turnover. A) Cells transformed with an empty vector or pGAL-Tub1(E255A) were treated with 2% galactose for 2 hoursto induce GFP-VHL and dominant-lethal Tub1. Turnover of GFP-VHL was assessed by cycloheximide chase analysis. Quantification of three independent experiments is shown below. Error bars represent ±1 SEM.

the half-life of VHL is longer than slGFP and tGnd1 and degradation of VHL is independent of *YDJ1* (55). Depolymerizing microtubules rapidly induced aggregation of GFP-VHL (Figure 5.8C). However, in striking contrast to slGFP or tGnd1, benomyl treatment accelerated degradation of GFP-VHL from a half-life of approximately 60 minutes to 30 minutes (Figure 5.8D). Similar results were observed when GFP-VHL was co-expressed with tub1(E255A) (Figure 5.9). Consequently, interfering with the microtubule cytoskeleton induces aggregation of a wide-variety of misfolded proteins yet selectively impairs degradation of a subset of unstable proteins.

We were surprised that benomyl induced GFP-VHL aggregation yet concurrently accelerated degradation because protein aggregates are considered poor substrates for the proteasome (56). One possibility is that under conditions of microtubule dysfunction, GFP-VHL self-assembled into aggregates that are biochemically distinct from the aggregates formed by slGFP. Indeed, GFP-VHL remained predominantly triton-soluble after benomyl treatment (Figure 5.8E) and GFP-VHL aggregates did not co-localize with Rnq1-mRFP foci (Figure 5.8F). To be degraded, GFP-VHL aggregates would need to be dissolved to release unfolded, monomeric GFP-VHL so it can be degraded by the proteasome. To test this hypothesis, the fate of benomyl-induced GFP-VHL aggregates was monitored after cycloheximide treatment. After only 7.5min post-cycloheximide treatment GFP-VHL aggregates were smaller and less prominent (Figure 5.8G). By 15 minutes, which is less than one GFP-VHL half-life, GFP-VHL was predominantly diffuse in most cells. In contrast, microtubule depolymerization generated slGFP aggregates that persisted beyond 15 minutes after cycloheximide treatment (approximately one half-life of the slGFP in DMSO treated cells) (Figure 5H). As a result, interfering with the microtubule cytoskeleton does not impact all misfolded proteins the same way. Misfolded proteins are partitioned through distinct degradation pathways and reach divergent intermediate states that are differentially susceptible to perturbations of the microtubule cytoskeleton.

The short-lived proteins examined thus far are misfolded and targeted for degradation by chaperone-dependent PQC pathways (35,55). However, many short-lived proteins are degraded in

conjunction with regulated cell signaling pathways and not as a consequence of misfolding. Will disrupting the microtubule cytoskeleton affect solubility and degradation of a regulated, short-lived protein? The transcription factor Cup9 is degraded in response to dipeptide levels in the cell by the N-end rule E3 ubiquitin ligase Ubr1 (57), thus representing a short-lived protein that is not misfolded but degraded in a regulated manner. To examine how benomyl affects the turnover and localization of Cup9, we used a yeast strain in which a GFP moiety was integrated into the *CUP9* locus and expressed as a C-terminal tag (58). Benomyl treatment had no effect on the turnover of Cup9-GFP and did not alter the predominantly nuclear localization of Cup9-GFP (Figure 5.10A & B). Thus, the microtubule cytoskeleton does not influence solubility or degradation of all unstable proteins yet seems to impact quality control of select misfolded proteins.

Microtubule dysfunction impairs slGFP recogtion by the ubiquitin receptors Rad23 and Rpn10

As described above, the fate of slGFP is exquisitely sensitive to perturbations in various PQC stages. Disrupting the microtubule cytoskeleton drove slGFP to form insoluble aggregates however it is unclear at what stage in the life cycle of slGFP this defect is occurring. Polyubiquitination is a central step in targeting a misfolded protein to the proteasome for degradation (6). To determine if disrupting the microtubule cytoskeleton impairs slGFP polyubiquitination, cells expressing slGFP were treated with benomyl for 30 minutes and slGFP was immunoprecipiated from cell lysates. Ubiquitinated slGFP levels were increased after microtubule depolymerization (Figure 5.11A) suggesting that slGFP is still recognized by PQC machinery responsible for polyubiquitination however a downstream step in slGFP degradation is impaired.

Several E3 ubiquitin ligases including Ubr1 and San1 bind non-native polypeptides (23,59) and function in PQC triage decisions (60). To determine if microtubule dysfunction disrupted interaction between Ubr1 and slGFP, Flag-Ubr1 was co-expressed with slGFP in yeast cells that were treated with DMSO or benomyl for 30 minutes. Flag-Ubr1 was isolated from yeast cell extracts via FLAG affinity resin and eluted with FLAG peptide. As shown in Figure 5.11B, slGFP is isolated

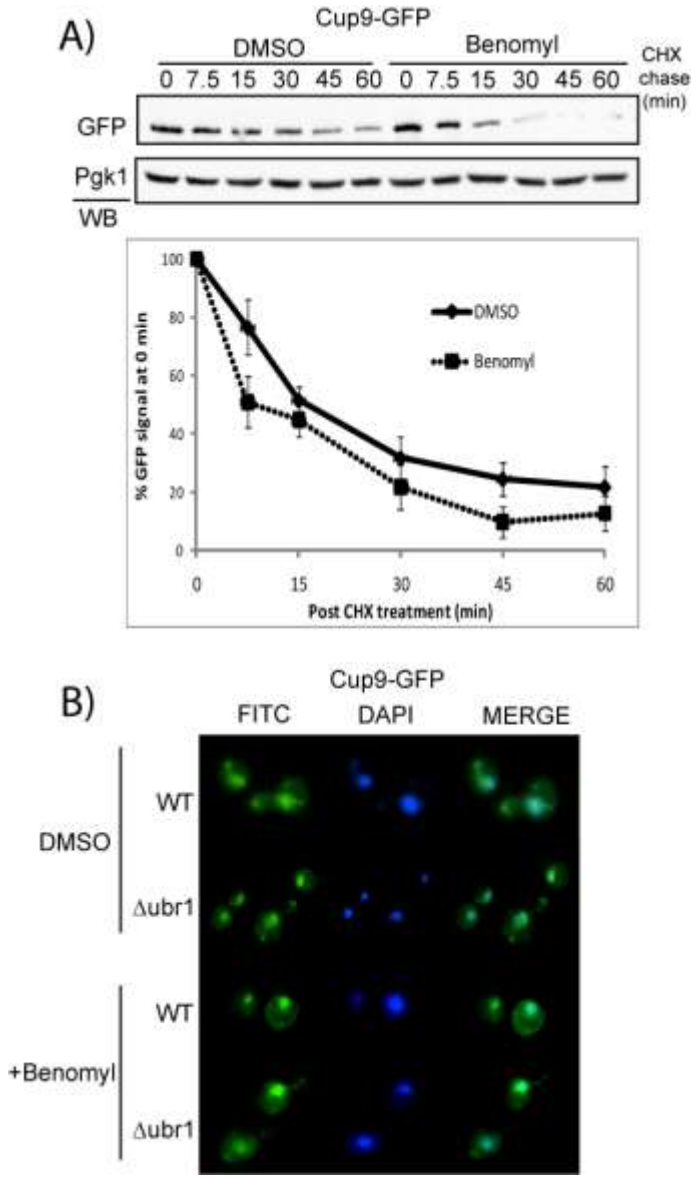

Figure 5.10. Degradation and localization of CupGFP is unaffected by benomyl. A) Turnover Cup9GFP expressed from endogenous *CUP9* locus pretreated with DMSO or 40μM benomyl for 10 minutes. Quantitation of three independent experiments is shown below where error bars represent 1 SEM. B) Localization of Cup9GFP in wildtype and Δ*ubr1* treated with DMSO or 40μM benomyl for 30 minutes.

from cell extracts specifically when co-expressed with Flag-Ubr1 (lane 4) Under conditions of microtubule depolymerization we observe a slight decrease in the level of slGFP that is isolated with Flag-Ubr1 (lane 8). However we consistently observe a slight decrease in the total level of slGFP in benomyl-treated samples that express Flag-Ubr1 and lysed under non-denaturing conditions (lane 8-whole cell lysate). The ratio between slGFP in DMSO or benomyl treated samples is the same in the pull-down and whole cell lysate samples. This decrease might represent a pool of slGFP that is forming insoluble aggregates that are lost during extraction or reduced expression of slGFP in cells co-expressing FLAG-Ubr1. Interestingly, we consistently observed that Sis1, a Type II Hsp40 in yeast reproducibly eluted with Flag-Ubr1 while we could not detect Ydj1. This interaction was independent of the slGFP reporter (lanes 3 and 4) and was unaffected by benomyl (lanes 3 and 7). Thus, Ubr1 forms a complex with slGFP that is independent of the microtubule cytoskeleton. We were unable to detect an interaction between the slGFP reporter and tagged versions of San1. San1 has polypeptide binding activity yet is also intrinsically disordered making this interaction particularly difficult to test (59). Regardless, polyubiquitinated forms of slGFP accumulate when the microtubule cytoskeleton is disrupted.

Degradation of slGFP is hindered when this misfolded protein is partitioned into an insoluble state. Thus, even though slGFP is polyubiquitinated, slGFP aggregates might not be delivered to the proteasome. We investigated this hypothesis by identifying the ubiquitin receptors that participate in slGFP degradation. SlGFP was strongly stabilized a Δ*rpn10* strain and partially stabilized in a Δ*rad23* strain background (Figure 5.11C). No effect was observed in Δ*ddi1* and Δ*dsk2* strains, two other ubiquitin receptors implicated in protein turnover (data not shown). Does deletion of *RPN10* or *RAD23* affect solubility of the slGFP reporter? SlGFP was predominantly triton-soluble in Δ*rpn10* and Δ*rad23* strains (Figure 5.11D). Furthermore, slGFP was diffuse in Δ*rpn10* and Δ*rad23* strains under fluorescence microscopy (Figure 5.11E). Thus perturbing these post-ubiquitin steps in slGFP degradation does not drive this misfolded protein into an insoluble state.

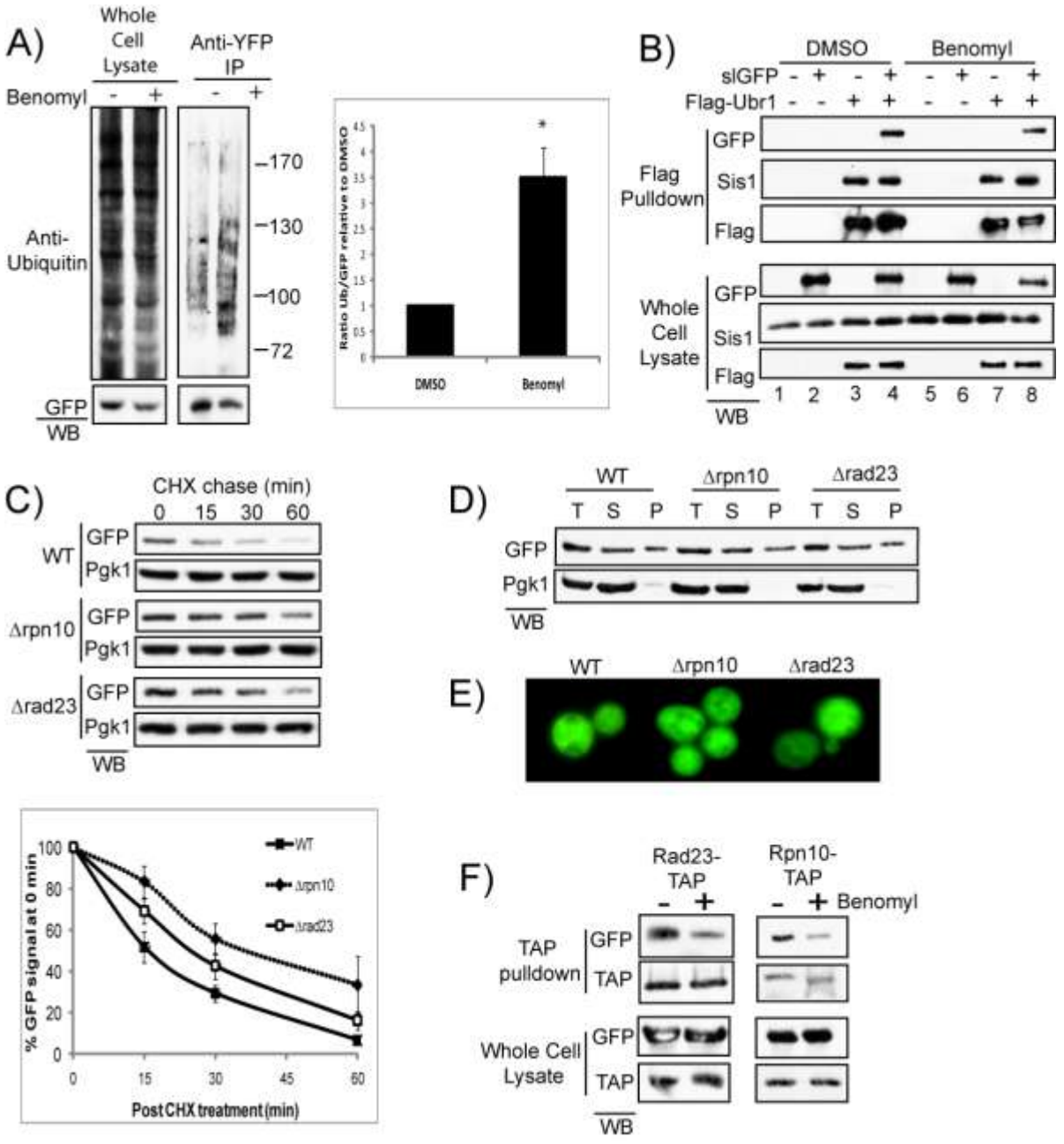

Figure 5.11 Benomyl disrupts interaction between slGFP and the ubiquitin receptors Rad23 and Rpn10. A) Ubiquitination of slGFP in cells treated with DMSO or benomyl. SlGFP was immunoprecipitated from cell lysates with anti-YFP antisera. Immunoprecipitated material was assessed by western blotting for ubiquitin and GFP. Input levels are shown on the left from whole cell lysates. Quantification of three independent experiments is shown on the right as a ratio of ubiquitin signal to level of immunoprecipitated GFP and normalized to WT. Error bars represent ±1SEM (*p<0.05). B) Interaction between slGFP reporter and Flag-Ubr1 in cells treated with DMSO or benomyl. Cell lysates were incubated with Flag resin and bound proteins were eluted with Flag peptide and analyzed by western immunbloting to for the indicated proteins. Input protein levels are shown on the right. C) Turnover of slGFP was analyzed in *WT*, Δ*rad23* or Δ*rpn10* strains by cycloheximide chase analysis. Quantification of three independent experiments is shown on the right.

Rpn10 and Rad23 display both overlapping as well as specific roles in protein degradation (61,62). Rpn10 resides predominantly as a subunit in the regulatory particle of the proteasome (63) while Rad23 association with the proteasome occurs through its ubiquitin-like domain (64). We were interested if benomyl treatment abrogated interaction between slGFP and either Rpn10 or Rad23. TAP-tagged versions of Rpn10 and Rad23 were expressed from their endogenous promoters to facilitate isolation of a complex with slGFP. SlGFP was isolated with both Rad23-TAP and Rpn10-TAP. Importantly, depolymerizing microtubules resulted in a large decrease in the quantity of slGFP in complex with either Rad23-TAP or Rpn10-TAP (Figure 5.11F). We were unable to perform the reciprocal pulldown through the slGFP due to background binding between the TAP tag and antisera employed to immunoprecipitate slGFP. These data suggest that depolymerization of microtubules prevents the slGFP from being recognized by ubiquitin receptors responsible for its degradation.

Microtubule depolymerization interferes with chaperone binding to slGFP

Disrupting microtubule dynamics drives slGFP off-course from its pathway to the proteasome and results in the formation of insoluble aggregates. Molecular chaperones normally prevent non-native polypeptides from self-associating into insoluble aggregates. As a result, we were curious how diverting slGFP into this insoluble state influence interaction with molecular chaperones. We observed that the Type I Hsp40 Ydj1 is required to hold slGFP after polyubiquitination. SlGFP co-immunoprecipitated with Ydj1 from yeast cell extracts (Figure 8A lane 3). However there was a substantial decrease in the level of slGFP that co-immunoprecpitated with Ydj1 in samples treated with benomyl as early as 15 minutes (Figure 5.12A lane 4 and Figure 5.13A). The Ydj1:slGFP complex was independent of Hsp70 because slGFP co-immunoprecipitated with a mutant form of Ydj1 that is unable to interact with Hsp70 suggesting this interaction is specific (Figure 5.13B)

Figure 5.11 . . . *cont.* D) Triton-solubility of the slGFP reporter after high-speed centrifugation in the indicated strain background (T-total, S-supernatant, P-pellet). E) Fluorescence microscopy of slGFP in the indicated strain background. F) TAP-pulldown of slGFP in yeast strain expressing Rpn10-TAP or Rad23-TAP treated with DMSO or benomyl.

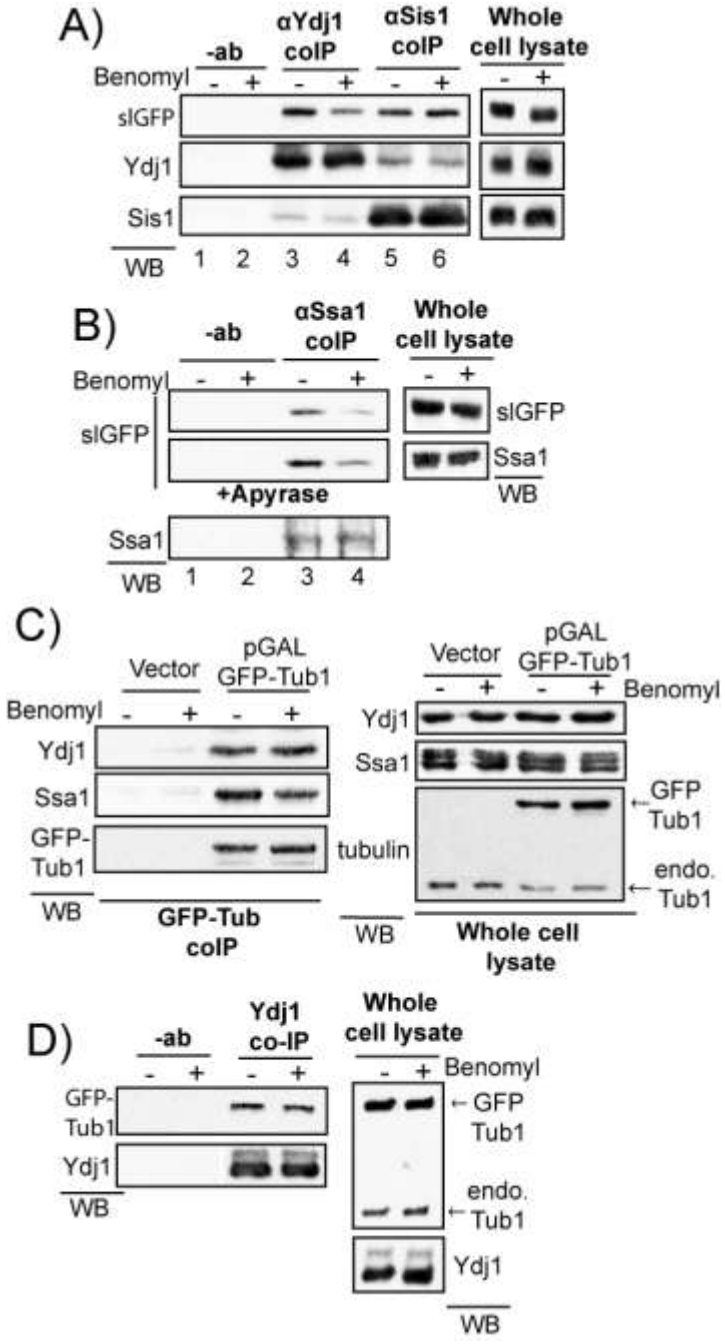

Figure 5.12 Benomyl treatment selectively disrupts chaperone interactions with slGFP. A) Ydj1 and Sis1 were co-immunoprecipitated from cells treated with DMSO or benomyl. Whole cell lysates are shown on the right. B) Co-immunoprecipitation of Ssa1 from cells treated with DMSO or benomyl. Lysates were divided in half and one set treated with Apyrase (lower panel). Then lysates were incubated with anti-Ssa1 antisera or no antibody (-ab). Whole cell lysates are shown on the right. C) Cells transformed with an empty vector or GFP-Tub1 and treated with DMSO or benomyl. Cell lysates were incubated with anti-YFP antisera and assessed for chaperone levels. D) Cells expressing GFP-Tub1 were treated with DMSO and benomyl and Ydj1 co-immunoprecipitated with anti-Ydj1 antisera.

(65). SlGFP also co-immunoprecpitated with Sis1 however this interaction was unaffected by microtubule depolymerization. Interaction between Sis1 and slGFP was independent of either Ubr1 or San1 demonstrating that this complex was not indirectly occurring through the E3 ligase (Figure 5.13C). Of note, we observed a small amount of Ydj1 that co-immunoprecipitated with the Sis1 anti-sera. This might be due to cross-reactivity with the conserved Ydj1 J-domain or a consequence of shared binding partners such as Ssa1. Regardless, this does not appear to influence the level of slGFP reporter that co-immunoprecipitated with Sis1 because this interaction was consistently insensitive to benomyl treatment. Furthermore, benomyl treatment did not affect the solubility of these chaperones indicating that reduced binding was not a consequence of Ydj1 or Ssa1 forming triton-insoluble aggregates (Figure 5.13D). If binding between slGFP and an Hsp40 is reduced upon microtubule depolymerization, we expected that interaction between slGFP and an Hsp70 would also be decreased. SlGFP co-immunoprecipitated with Ssa1 (Figure 5.12), an Hsp70 isoform that is associated with degradation of several misfolded proteins (34,37,66,67). This interaction was enhanced when cell lysates were treated with Apyrase to deplete ATP, consistent with the ATP-bound form of Hsp70 having lower substrate affinity (Figure 5.12). Benomyl treatment reduced the level of slGFP that co-immunoprecipitated with Ssa1 in the presence or absence of Apyrase (Figure 5.12 lower panel). Therefore, slGFP is a poor substrate for Ydj1and Ssa1when microtubule dynamics are disrupted.

Both Ydj1 and Ssa1 are previously implicated in the recovery of the microtubule cytoskeleton after depolymerization with benomyl (68). Benomyl treatment might release free tubulin monomers that bind Ydj1 or Ssa1 and titrate these molecular chaperones from other cellular substrates including slGFP. To test this hypothesis, we examined how benomyl affected interaction between Ydj1, Ssa1 and tubulin. We were unable to detect an interaction between Ydj1 or Ssa1 with endogenous tubulin which migrated at the same molecular weight as the IgG heavy chain. To overcome this obstacle, we expressed GFP-Tub1 in yeast cells. This GFP-fusion protein was expressed to approximately 3-fold

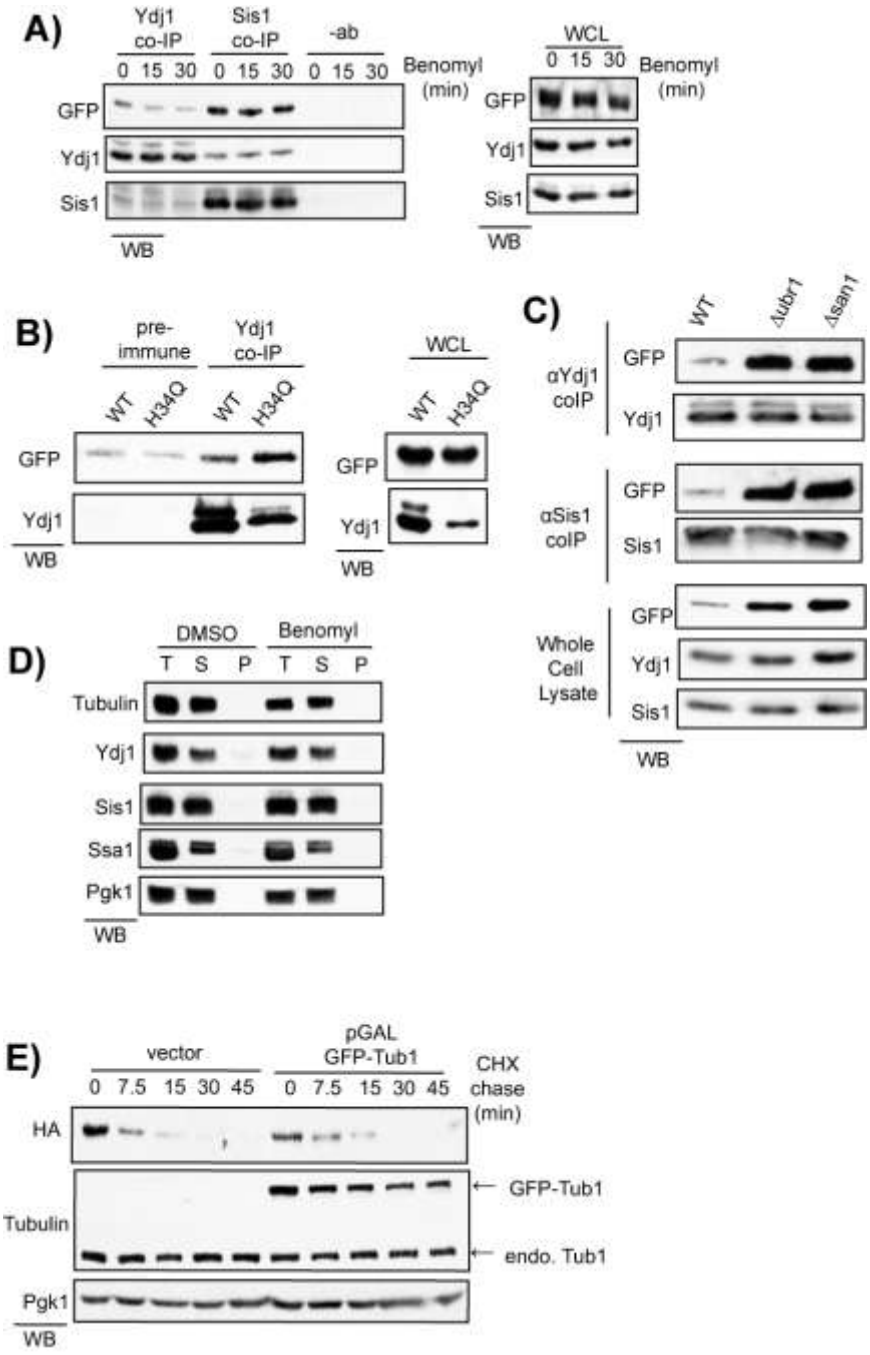

Figure 5.13. Chaperone interaction with slGFP after benomyl treatment. A) Levels of slGFP reporter that co-immunoprecipitated with Ydj1 and Sis1during benomyl timecourse (left panel). Total protein levels from whole cell lysates are shown on the right. B) Levels of slGFP that co-immunoprecipitated with wildtype Ydj1 or ydj1(H34Q) (left panel). In this experiment, rabbit preimmune antisera shows background levels of slGFP in the co-IP. Total levels from whole cell lysates are shown on the right. C) Levels of slGFP that co-immunoprecipitated with Ydj1 or Sis1 antisera in *WT*, Δ*ubr1*, or Δ*san1* strain background. D) Solubility of tubulin, Pgk1, Ssa1, Ydj1, and Sis1 after treatment with DMSO or 40μM benomyl for 30 minutes (T-total, S-supernatant, P-pellet).. E) Turnover of slGFP reporter in cells expressing GFP-Tub1 for 2 hours. SlGFP reporter was detected using an HA epitope in N-terminus.

above enodogenous tubulin yet still incorporates into endogenous microtubules (51) and did not affect turnover of the slGFP reporter (Figure 5.13E). Both Ydj1 and Ssa1 co-immunoprecipitated with GFP-Tub1 however benomyl had no effect on this interaction (5.12C). Furthermore, benomyl had no effect on the level of GFP-Tub1 that co-immunoprecpitated with Ydj1 (Figure 5.12D) suggesting that benomyl treatment was not altering the interaction between Ydj1 and tubulin.

Elevating Sis1 levels rescues slGFP degradation in the absence of a functional cytoskeleton

If perturbing the microtubule cytoskeleton interferes with chaperone recognition, we were curious if elevating levels of Ydj1 or Sis1 could partition slGFP back into a soluble state competent for degradation. Overexpressing Ydj1 from a strong, constitutive promoter had no effect on the degradation of slGFP. However, elevating Sis1 levels accelerated slGFP turnover (Figure 5.14A). Both Ydj1 and Sis1 could be expressed approximately 5-fold over endogenous levels (Figure 5.14B). Thus, these two Hsp40 co-chaperones exert distinct functions on the same misfolded protein.

If increasing Sis1 levels accelerates slGFP degradation, we were interested if Sis1 overexpession could rescue slGFP degradation after microtubule depolymerization. Indeed, while benomyl treatment delays slGFP turnover, overexpression of Sis1 still accelerated slGFP degradation to about the same kinetics as in the absence of benomyl (Figure 5.14C). Notably, Sis1 overexpression did not impact slGFP solubility (Figure 5.14D) or the presence of slGFP aggregates (Figure 5.14E). As a result, Sis1 was likely not acting as a holdase to maintain slGFP in a soluble state. Instead, Sis1 might function directly on slGFP aggregates to promote degradation. To test this hypothesis, we examined the fate of benomyl-induced slGFP aggregates in the presence of excess Sis1. Cells were treated with benomyl for 30min then protein synthesis inhibited with cycloheximide. Large, slGFP aggregates were typically stable over a 20min period however we observed a reduction in the number of cells with large, single aggregates at 20min when Sis1 levels were elevated (Figure 5.14F). Consequently, Sis1 appears to participate in the removal of slGFP aggregates after microtubule depolymerization thus acting as an auxiliary mechanism for the disposal of misfolded polypeptides that have assembled into aggregates.

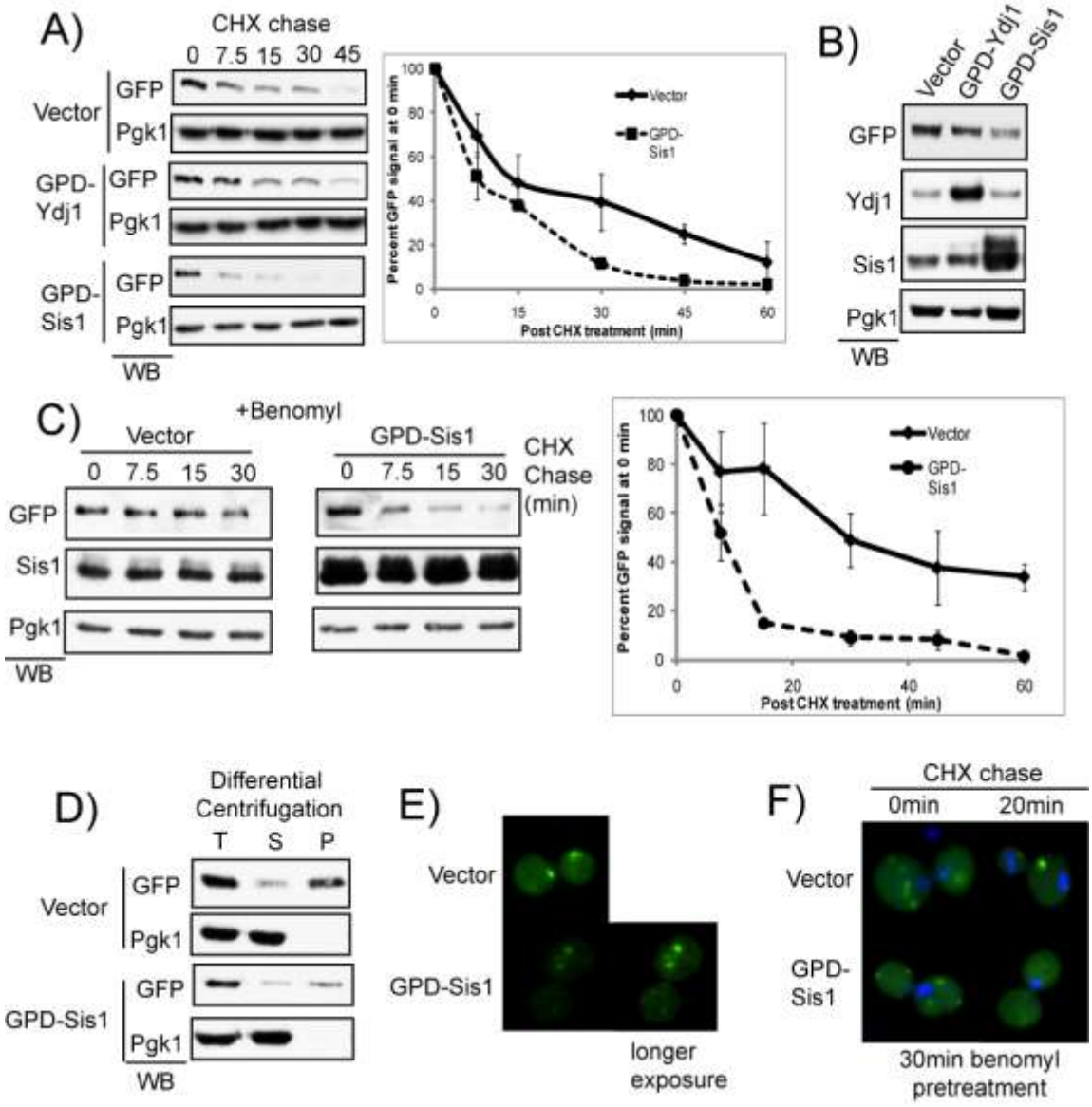

Figure 5.14. Elevation of Sis1 levels accelerates slGFP turnover. A) Turnover of slGFP in cells transformed with an empty vector, a plasmid overexpressing Ydj1 (GPD-Ydj1) or Sis1 (GPD-Sis1). Quantification of three independent experiments examining turnover of slGFP with overexpressed Sis1. B) Whole cell lysates from cells overexpressing Ydj1 or Sis1. C) Turnover of slGFP in cells pretreated with benomyl transformed with an empty vector or a plasmid overexpressing Sis1. Quantification of three independent experiments is shown on the right. D) Solubility of slGFP in cells pretreated benomyl with overexpressed Sis1 (T-total, S-supernatant, P-pellet). E) Localization of slGFP in cells pretreated with benomyl and overexpressed Sis1 (a longer exposure normalized to the intensity in an empty vector sample is shown on the right). F) Localization of slGFP in cells pretreated with benomyl then treated with cycloheximide after the indicated time.

5.4 Discussion

Misfolded proteins are strongly predisposed to spontaneous self-assembly into protein aggregates that threaten cellular homeostasis (1). While PQC pathways exert enormous resources to prevent protein aggregation, we find that interfering with specific stages in the degradation of a misfolded protein drives this protein to aggregate in the cytosol (Figure 5.15). Disrupting PQC stages that function after polyubiquitination appear to predispose this misfolded protein to form insoluble aggregates that are poorly recognized by ubiquitin receptors and molecular chaperones. Polyubiquitin chains might inherently drive protein aggregation and thus abundant molecular chaperone such as Ydj1 are required to maintain polyubiquitinated proteins in a soluble state. Interestingly, elevating Sis1 levels restores degradation demonstrating that multiple chaperone pathways exist in the cell to remove non-native polypeptides in monomeric as well as assembled states.

The cell likely favors holding misfolded proteins in a soluble state. Indeed, PQC networks are robust enough to tolerate the accumulation of misfolded proteins as we observed when either Ubr1 or San1 were absent. Under these conditions, pools of slGFP were sequestered in a single, juxtanuclear aggregate yet maintained in a soluble state. This aggregate resembles the JUNQ compartment however Kaganovich *et al* demonstrated that recruitment to this location required ubiquitination. Redundant E3 pathways might be sufficient to ubiquitinate low levels of the slGFP reporter that self-assemble with un-ubiquinated pools and recruit this complex to the JUNQ compartment. Alternatively, these aggregates may represent a distinct subcellular compartment. Regardless, sequestration of misfolded proteins via the microtubule cytoskeleton into subcellular inclusions appears to be a widely employed mechanism to protect cells from protein misfolding and aberrant aggregation (44).

Surprisingly, there is a basal requirement for an intact microtubule cytoskeleton to prevent misfolded proteins from self-assembling into aggregates. The precise role of the microtubule cytoskeleton in PQC is unclear. Microtubules might facilitate trafficking of polyubiquitinated protein species to the proteasome. In this model, microtubule motors would be predicted to connect

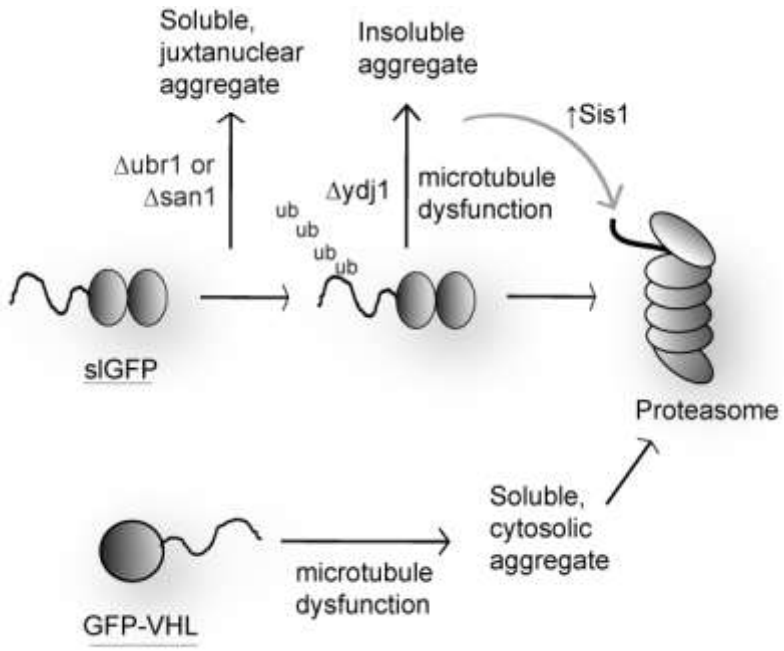

Figure 5.15 Model for PQC pathways that participate in degradation of misfolded cytosolic proteins and consequence of interference with specific components.

polyubiquitinated proteins to the microtubule cytoskeleton and ferry these proteins selectively to the proteasome which is predominantly located at the ER membrane and nucleus (42,69). We did not observe a requirement for the minus-end motors Dyn1 or Kar3 in degradation of slGFP (data not shown). However there are numerous other microtubule binding proteins that could act as conduits between the microtubule cytoskeleton and PQC machinery. Disruption of this pathway would cause polyubiquitinated proteins to accumulate in the cytosol. Polyubiquitinated proteins are normally shuttled to the JUNQ however this pathway likewise requires the microtubule cytoskeleton (42). As a result, misfolded proteins such as slGFP are caught in an intermediate state and accumulate in aggregates that are poorly recognized by ubiquitin receptors and not delivered to the proteasome. Disrupting the microtubule cytoskeleton reduced binding between slGFP and the molecular chaperones Ydj1 and Ssa1. While reduced binding might reflect slGFP aggregating and burying polypeptide binding sites, the microtubule cytoskeleton might act as a scaffold for interactions between molecular chaperones and misfolded proteins. Scaffolding of PQC components might favor a stable complex that holds a misfolded protein in a soluble state long enough for recognition by ubiquitin receptors and delivery to the proteasome.

The results described herein further demonstrate that aggregation *per se* does not render a misfolded protein insensitive to proteasomal degradation. For example, VHL forms aggregates upon microtubule dysfunction yet degradation is accelerated. Presumably there are back-up pathways that facilitate solubilization of aggregated proteins (ex. Hsp104) (70). Why are VHL aggregates detergent-soluble when slGFP aggregates are detergent-insoluble? Intrinsic properties within these two misfolded proteins might predispose one or the other to assemble into distinct aggregates. Alternatively, unique binding partners might hold VHL in a soluble state. Still, why is VHL degradation accelerated after benomyl treatment? Folding of VHL requires the TriC chaperonin complex (53). TriC also participates in folding of tubulin (71,72). Accordingly, microtubule depolymerization might disrupt TriC activity generating larger pools of unfolded VHL in the cell.

TriC is not required for VHL degradation (55) so pathways that target unfolded VHL for degradation are still intact to degrade this excess pool.

Misfolded proteins are funneled through distinct PQC complexes that alter the fate of that protein and the predisposition to form insoluble aggregates. For example, slGFP degradation requires Ydj1, a co-chaperone that is dispensable for VHL degradation (55). Similar to benomyl treatment, deletion of *YDJ1* did not inhibit slGFP ubiquitination however this misfolded protein was partitioned into an insoluble state suggesting both Ydj1 and the microtubule cytoskeleton are required to hold polyubiquitinated forms of slGFP in a soluble state. While Ydj1 has been previously linked to ubiquitination of several unstable proteins (22,35,48) Ydj1 also acts with Ssa1 downstream of ubiquitination to hold another cytosolic, misfolded protein in a soluble state (67). Thus, Ydj1's function in protein degradation is substrate-specific. Sis1 contributes a distinct role to PQC. Elevating Sis1 levels might partition slGFP into an alternative degradation pathway that is independent of the microtubule cytoskeleton. Sis1 has also been implicated with Hsp104 in the shearing of prion fibrils (73,74). Accordingly, Sis1 might recruit Hsp104 to slGFP aggregates and promote unfolding of assembled domains to enhance degradation efficiency. Importantly, overlapping PQC networks maintain protein homeostasis by diverting misfolded proteins through various intracellular pathways that ultimately remove aberrant protein species from the cytosol.

5.5 Materials and Methods

Yeast strains, growth conditions, and reagents

Strains were generated using the lithium acetate transformation method. Freshly transformed colonies were used to inoculate synthetic drop-out media lacking specific amino acids to maintain cultures under selection and incubated at 30°C throughout the experiment unless otherwise noted. Cells transformed with pESC-GFP-VHL were grown overnight prior to the experiment in 2% galactose as previously described (55). Cells transformed with pGAL-GFP-Tub or pGAL-tub1(E255A) were grown overnight under selection in 2% raffinose prior to the addition of galactose. Benomyl (Sigma) was dissolved in DMSO as a 40mM stock immediately prior to experiment. Cells were treated at a final concentration of 40μM in all experiments for the indicated times. Guanidine hydrochloride (Fisher) was dissolved in sterile H_2O at stock concentration of 6M.

Cycloheximide-chase analysis

Yeast cultures expressing the indicated proteins were induced or treated with chemicals as described in the text. To inhibit protein translation, cultures were treated with 200μg/mL cycloheximide (SIGMA) and aliquots removed at indicated time points. Cells were lysed by alkaline pretreatment (75). Briefly, cells were resuspended jn 0.1M NaOH and incubated for 5min at room temperature, washed in sterile, H_2O, and boiled for 15min in denaturing lysis buffer (60mM Tris-HCl pH6.8, 2%SDS, 2mM DTT). Cell lysates were precleared at 3,000rpm for 3min and the supernatant normalized using BioRad protein determination. Normalized lysates in sample buffer (60mM Tris-HCl pH 6.8, 2% SDS, 10% glycerol, 2mM EDTA, 5% β-mercaptoethanol, 1mg/mL bromophenol blue) were analyzed by SDS-PAGE and western immunoblotting for the indicated proteins.

Co-immunoprecipitation analysis of protein complexes

Yeast strains expressing the indicated proteins were lysed by glass bead disruption in Buffer A (150mM NaCl, 50mM Hepes pH7.4, 1mM EDTA, 0.1% Triton X, 1mM PMSF, and 1x yeast protease inhibitor cocktail [Roche]). Cell extracts were precleared at 3,000xg for 3min at 4°C. The supernatant was saved and protein concentrations assessed with a BioRad protein determination kit.

Protein concentrations were normalized between samples to approximately 3 mg/mL and 300µg of protein incubated with the indicated antisera for 1 hour at 4°C then incubated with Protein G beads (50% slurry preblocked with BSA from Roche) for 30min at 4°C. Beads were washed 2-3 times with Buffer A then resuspended in sample buffer and analyzed by SDS-PAGE and western immunoblotting.

Detection of ubiquitinated forms of slGFP reporter

Yeast strains expressing the slGFP report were grown under selection in mid-log phase. Cells were washed with cold H_2O (+1mM NaN_3 and 20mM NEM) and lysed by glass bead disruption in Buffer A (+1mM NEM). Cell extracts were precleared at 3,000 rpm for 3min at 4°C, protein concentrations normalized, and GFP immunoprecipitated with anti-YFP antisera and protein G resin (Roche) using standard methods. Protein G resin was washed three times in Buffer A supplemented with 0.1% SDS. Ubiquitinated forms of slGFP were detected after SDS-PAGE and western immunoblotting for ubiquitin (Covance). Ubiquitinated slGFP reporter levels were quantified using ImageJ software (NIH) and normalized as a ratio to the level of slGFP that was immunoprecipitated from the lysate (detected using anti-GFP [Roche]).

Fluorescence microscopy

Yeast strains expressing the indicated proteins and treated as described in the text were fixed in 3.7% formaldehyde and stored in phosphate buffered saline (pH 7.5) supplemented with 1.2M sorbitol. Fixed cells were permeabilized and DNA visualized with DAPI as described in (76). Rnq1-mRFP was expressed from the *GAL1* promoter for 4 hours before cells were processed as described. Cells were visualized with an Olympus IX81 Fluorescence microscope and images processed with Metamorph software. Exposure times and all other settings were standardized across individual experiments unless otherwise noted.

TAP pulldown for slGFP reporter

Yeast strains expressing Rad23-TAP or Rpn10-TAP were transformed with pCUP-slGFP reporter were induced with 100µM $CuSO_4$ for 1 hour and treated with DMSO or 40µM benomyl for 30

minutes. Cells were collected by centrifugation and washed in cold H_2O (+ 1mM NaN_3 and 20mM NEM). Cells were lysed by glass bead disruption in Buffer A(+NEM) and lysates pre-cleared at 3,000rpm for 3min at 4°C. The supernatant was normalized and aliquots were incubated with Rabbit IgG resin (Sigma) for 1 hour at 4°C and washed 2 times with buffer A. The resin was resuspended in sample buffer and analyzed by SDS-PAGE and western immunoblotting for GFP (Roche) and TAP (Genscript).

Differential high speed centrifugation

Yeast strains expressing slGFP were treated with DMSO or 40μM benomyl for 30min. Cells were lysed by glass bead disruption in Buffer A (+1mM DTT) and lysates pre-cleared at 3,000 rpm for 3min at 4°C. The supernatant was saved and 200μg protein spun at 100,000xg for 30min at 4°C. An aliquot was saved prior to the spin to represent the total input. Equivalent volumes from total, supernatant, and pellet fractions were added to 2x sample buffer and analyzed by SDS-PAGE and western immunoblotting for the indicated proteins.

5.6 References

1. Dobson, C. M. (2004) *Semin Cell Dev Biol* **15**, 3-16

2. Gidalevitz, T., Ben-Zvi, A., Ho, K. H., Brignull, H. R., and Morimoto, R. I. (2006) *Science* **311**, 1471-1474

3. Carrell, R. W., and Lomas, D. A. (1997) *Lancet* **350**, 134-138

4. Balch, W. E., Morimoto, R. I., Dillin, A., and Kelly, J. W. (2008) *Science* **319**, 916-919

5. Hartl, F. U., and Hayer-Hartl, M. (2002) *Science* **295**, 1852-1858

6. Hochstrasser, M. (1996) *Annu Rev Genet* **30**, 405-439

7. Cyr, D. M., Hohfeld, J., and Patterson, C. (2002) *Trends Biochem Sci* **27**, 368-375

8. Elsasser, S., and Finley, D. (2005) *Nat Cell Biol* **7**, 742-749

9. Mayer, M. P., and Bukau, B. (2005) *Cell Mol Life Sci* **62**, 670-684

10. Liberek, K., Galitski, T. P., Zylicz, M., and Georgopoulos, C. (1992) *Proc Natl Acad Sci U S A* **89**, 3516-3520

11. Cyr, D. M., Lu, X., and Douglas, M. G. (1992) *J Biol Chem* **267**, 20927-20931

12. Langer, T., Lu, C., Echols, H., Flanagan, J., Hayer, M. K., and Hartl, F. U. (1992) *Nature* **356**, 683-689

13. Szabo, A., Langer, T., Schroder, H., Flanagan, J., Bukau, B., and Hartl, F. U. (1994) *Proc Natl Acad Sci U S A* **91**, 10345-10349

14. Laufen, T., Mayer, M. P., Beisel, C., Klostermeier, D., Mogk, A., Reinstein, J., and Bukau, B. (1999) *Proc Natl Acad Sci U S A* **96**, 5452-5457

15. Walsh, P., Bursac, D., Law, Y. C., Cyr, D., and Lithgow, T. (2004) *EMBO Rep* **5**, 567-571

16. Summers, D. W., Douglas, P. M., Ramos, C. H., and Cyr, D. M. (2009) *Trends Biochem Sci* **34**, 230-233

17. Lian, H. Y., Zhang, H., Zhang, Z. R., Loovers, H. M., Jones, G. W., Rowling, P. J., Itzhaki, L. S., Zhou, J. M., and Perrett, S. (2007) *J Biol Chem*

18. Summers, D. W., Douglas, P. M., Ren, H. Y., and Cyr, D. M. (2009) *J Biol Chem* **284**, 3628-3639

19. Cyr, D. M. (1995) *FEBS Lett* **359**, 129-132

20. Lu, Z., and Cyr, D. M. (1998) *J Biol Chem* **273**, 5970-5978

21. Lu, Z., and Cyr, D. M. (1998) *J Biol Chem* **273**, 27824-27830

22. Younger, J. M., Ren, H. Y., Chen, L., Fan, C. Y., Fields, A., Patterson, C., and Cyr, D. M. (2004) *J Cell Biol* **167**, 1075-1085

23. Nillegoda, N. B., Theodoraki, M. A., Mandal, A. K., Mayo, K. J., Ren, H. Y., Sultana, R., Wu, K., Johnson, J., Cyr, D. M., and Caplan, A. J. (2010) *Mol Biol Cell* **21**, 2102-2116

24. Nakatsukasa, K., Huyer, G., Michaelis, S., and Brodsky, J. L. (2008) *Cell* **132**, 101-112

25. Johnson, J. L., and Craig, E. A. (2001) *J Cell Biol* **152**, 851-856

26. Fan, C. Y., Lee, S., Ren, H. Y., and Cyr, D. M. (2004) *Mol Biol Cell* **15**, 761-773

27. Jiang, J., Ballinger, C. A., Wu, Y., Dai, Q., Cyr, D. M., Hohfeld, J., and Patterson, C. (2001) *J Biol Chem* **276**, 42938-42944

28. Meacham, G. C., Patterson, C., Zhang, W., Younger, J. M., and Cyr, D. M. (2001) *Nat Cell Biol* **3**, 100-105

29. Qian, S. B., McDonough, H., Boellmann, F., Cyr, D. M., and Patterson, C. (2006) *Nature* **440**, 551-555

30. Rosser, M. F., Washburn, E., Muchowski, P. J., Patterson, C., and Cyr, D. M. (2007) *J Biol Chem* **282**, 22267-22277

31. Kampinga, H. H., Kanon, B., Salomons, F. A., Kabakov, A. E., and Patterson, C. (2003) *Mol Cell Biol* **23**, 4948-4958

32. Dai, Q., Zhang, C., Wu, Y., McDonough, H., Whaley, R. A., Godfrey, V., Li, H. H., Madamanchi, N., Xu, W., Neckers, L., Cyr, D., and Patterson, C. (2003) *Embo J* **22**, 5446-5458

33. Eisele, F., and Wolf, D. H. (2008) *FEBS Lett* **582**, 4143-4146

34. Prasad, R., Kawaguchi, S., and Ng, D. T. (2010) *Mol Biol Cell* **21**, 2117-2127

35. Heck, J. W., Cheung, S. K., and Hampton, R. Y. (2010) *Proc Natl Acad Sci U S A* **107**, 1106-1111

36. Lewis, M. J., and Pelham, H. R. (2009) *PLoS One* **4**, e5038

37. Metzger, M. B., Maurer, M. J., Dancy, B. M., and Michaelis, S. (2008) *J Biol Chem* **283**, 32302-32316

38. Bartel, B., Wunning, I., and Varshavsky, A. (1990) *Embo J* **9**, 3179-3189

39. Byrd, C., Turner, G. C., and Varshavsky, A. (1998) *Embo J* **17**, 269-277

40. Gardner, R. G., Nelson, Z. W., and Gottschling, D. E. (2005) *Cell* **120**, 803-815

41. Kopito, R. R. (2000) *Trends Cell Biol* **10**, 524-530

42. Kaganovich, D., Kopito, R., and Frydman, J. (2008) *Nature* **454**, 1088-1095

43. Tyedmers, J., Treusch, S., Dong, J., McCaffery, J. M., Bevis, B., and Lindquist, S. (2010) *Proc Natl Acad Sci U S A* **107**, 8633-8638

44. Tyedmers, J., Mogk, A., and Bukau, B. (2010) *Nat Rev Mol Cell Biol* **11**, 777-788

45. Stade, K., Ford, C. S., Guthrie, C., and Weis, K. (1997) *Cell* **90**, 1041-1050

46. Rudiger, S., Schneider-Mergener, J., and Bukau, B. (2001) *Embo J* **20**, 1042-1050

47. Kota, P., Summers, D. W., Ren, H. Y., Cyr, D. M., and Dokholyan, N. V. (2009) *Proc Natl Acad Sci U S A* **106**, 11073-11078

48. Lee, D. H., Sherman, M. Y., and Goldberg, A. L. (1996) *Mol Cell Biol* **16**, 4773-4781

49. Huyer, G., Piluek, W. F., Fansler, Z., Kreft, S. G., Hochstrasser, M., Brodsky, J. L., and Michaelis, S. (2004) *J Biol Chem* **279**, 38369-38378

50. Frey, S., Pool, M., and Seedorf, M. (2001) *J Biol Chem* **276**, 15905-15912

51. Anders, K. R., and Botstein, D. (2001) *Mol Biol Cell* **12**, 3973-3986

52. Feldman, D. E., Thulasiraman, V., Ferreyra, R. G., and Frydman, J. (1999) *Mol Cell* **4**, 1051-1061

53. Melville, M. W., McClellan, A. J., Meyer, A. S., Darveau, A., and Frydman, J. (2003) *Mol Cell Biol* **23**, 3141-3151

54. Schoenfeld, A. R., Davidowitz, E. J., and Burk, R. D. (2000) *Proc Natl Acad Sci U S A* **97**, 8507-8512

55. McClellan, A. J., Scott, M. D., and Frydman, J. (2005) *Cell* **121**, 739-748

56. Holmberg, C. I., Staniszewski, K. E., Mensah, K. N., Matouschek, A., and Morimoto, R. I. (2004) *Embo J* **23**, 4307-4318

57. Turner, G. C., Du, F., and Varshavsky, A. (2000) *Nature* **405**, 579-583

58. Huh, W. K., Falvo, J. V., Gerke, L. C., Carroll, A. S., Howson, R. W., Weissman, J. S., and O'Shea, E. K. (2003) *Nature* **425**, 686-691

59. Rosenbaum, J. C., Fredrickson, E. K., Oeser, M. L., Garrett-Engele, C. M., Locke, M. N., Richardson, L. A., Nelson, Z. W., Hetrick, E. D., Milac, T. I., Gottschling, D. E., and Gardner, R. G. (2011) *Mol Cell* **41**, 93-106

60. Connell, P., Ballinger, C. A., Jiang, J., Wu, Y., Thompson, L. J., Hohfeld, J., and Patterson, C. (2001) *Nat Cell Biol* **3**, 93-96

61. Verma, R., Oania, R., Graumann, J., and Deshaies, R. J. (2004) *Cell* **118**, 99-110

62. Elsasser, S., Chandler-Militello, D., Muller, B., Hanna, J., and Finley, D. (2004) *J Biol Chem* **279**, 26817-26822

63. Deveraux, Q., Ustrell, V., Pickart, C., and Rechsteiner, M. (1994) *J Biol Chem* **269**, 7059-7061

64. Elsasser, S., Gali, R. R., Schwickart, M., Larsen, C. N., Leggett, D. S., Muller, B., Feng, M. T., Tubing, F., Dittmar, G. A., and Finley, D. (2002) *Nat Cell Biol* **4**, 725-730

65. Tsai, J., and Douglas, M. G. (1996) *J Biol Chem* **271**, 9347-9354

66. Youker, R. T., Walsh, P., Beilharz, T., Lithgow, T., and Brodsky, J. L. (2004) *Mol Biol Cell* **15**, 4787-4797

67. Park, S. H., Bolender, N., Eisele, F., Kostova, Z., Takeuchi, J., Coffino, P., and Wolf, D. H. (2007) *Mol Biol Cell* **18**, 153-165

68. Oka, M., Nakai, M., Endo, T., Lim, C. R., Kimata, Y., and Kohno, K. (1998) *J Biol Chem* **273**, 29727-29737

69. Enenkel, C., Lehmann, A., and Kloetzel, P. M. (1998) *Embo J* **17**, 6144-6154

70. Glover, J. R., and Lindquist, S. (1998) *Cell* **94**, 73-82

71. Lundin, V. F., Leroux, M. R., and Stirling, P. C. (2010) *Trends Biochem Sci* **35**, 288-297

72. Frydman, J., Nimmesgern, E., Erdjument-Bromage, H., Wall, J. S., Tempst, P., and Hartl, F. U. (1992) *Embo J* **11**, 4767-4778

73. Aron, R., Higurashi, T., Sahi, C., and Craig, E. A. (2007) *Embo J* **26**, 3794-3803

74. Tipton, K. A., Verges, K. J., and Weissman, J. S. (2008) *Mol Cell* **32**, 584-591

75. Kushnirov, V. V. (2000) *Yeast* **16**, 857-860

76. Douglas, P. M., Summers, D. W., Ren, H. Y., and Cyr, D. M. (2009) *Mol Biol Cell* **20**, 4162-4173

Chapter Six

Final Conclusions and Future Directions

6.1. Introduction

Protein misfolding is the underlying cause of an extensive group of human diseases known collectively as "conformational disorders" (1). Complex protein quality control networks target non-native polypeptides for refolding, degradation, or in some cases, protective aggregation (2-4). Molecular chaperones encounter enormous diversity in non-native protein conformers. These might include polypeptides enriched in hydrophobic residues as well as beta-rich, amyloid-like fibrils that accumulate in diseases such as Alzheimer's disease and Huntington's disease (5). How protein quality control components such as molecular chaperones discriminate between these various protein conformers and efficiently triage non-native proteins between refolding, degradation, or protective aggregation is a major unanswered question in the field.

The studies described herein contribute two significant points to this question. First, the Type I Hsp40 Ydj1 recognizes diverse non-native polypeptides including amyloid-like conformers by utilizing various combinations of unique chaperone modules. Thus, Ydj1 is an adaptable molecular chaperone that can tether Hsp70 function to a wide variety of non-native polypeptides to suppress protein aggregation or influence triage decisions. Second, the microtubule cytoskeleton is required for maintaining some misfolded proteins in a soluble state competent for degradation. Interfering with the microtubule cytoskeleton not only impairs degradation of specific misfolded proteins but also disrupts trafficking of misfolded proteins to quality control compartments, illustrating a novel and extensive role for the microtubule cytoskeleton in protein quality control. How molecular chaperones and the microtubule cytoskeleton cooperate to suppress aggregation and promote degradation of misfolded proteins is a future area of study.

6.2 The Hsp40 co-chaperone Ydj1 utilizes multiple polypeptide binding sites to regulate protein folding and suppress aggregation.

The Hsp70/Hsp40 molecular chaperone system is an ancient quality control pathway that protects cells from misfolded protein conformers (6). Hsp70s are abundant cellular proteins, yet very limited in diversity and exhibit broad substrate selectivity (7,8). As a result, specification of Hsp70 activity is conferred by the more expanded Hsp40 family that stimulates Hsp70 ATP hydrolysis via action of a conserved J-domain (9,10). Importantly, these J-domain containing proteins have evolved diverse protein:protein interaction domains that couple Hsp70 polypeptide binding to numerous cellular activities including protein refolding and degradation (11).

The yeast Type I Hsp40 Ydj1 is one of the more well-characterized members of the Hsp40 co-chaperone family. Ydj1 is implicated in a plethora of cellular activities including protein translocation across membranes, cell cycle, protein folding, protein degradation, prion propagation and many other functions (12-17). Ydj1 is the most abundant Hsp40 in budding yeast (119,000 mol/cell)(18) however high concentration does not account for such broad influence. Ydj1 interacts with highly disparate non-native clients including polypeptides enriched in hydrophobic residues (19) as well as beta-sheet rich, amyloid-like substrates (20-22). A perplexing question is how might a single molecular chaperone recognize such diverse non-native conformations?

Ydj1 utilizes at least three independent domains to interact with non-native polypeptides. For example, a hydrophobic pocket in the C-terminal domain of Ydj1 binds short, hydrophobic polypeptides (23). Computational analysis of Ydj1-bound peptides from multiple studies identified a consensus binding sequence that is found a wide variety of yeast proteins (24). Thus, Ydj1 scans the cellular environment for exposed hydrophobic sequences that are prevalent in unfolded polypeptides and prevents these proteins from self-associating into aggregates (16,25).

In addition, the zinc finger-like region (ZFLR) of Ydj1 contributes to interaction with a subset of Ydj1 clients including glutamine-enriched prions such as the yeast prion protein Rnq1 (21). Ydj1 actually prefers to bind Rnq1 in its beta-sheet rich, amyloid-like [RNQ^{+}] prion conformation.

The Ydj1 ZFLR is composed of two beta-strands that extend from the Ydj1 C-terminal domain (26) and might interact with a beta-enriched substrate via a donor strand exchange mechanism previously described for bacterial chaperones (27,28). Site-directed mutagenesis of solvent-exposed, hydrophilic residues in these beta-strands is one way to test this hypothesis. Consequently, the Ydj1 ZFLR supplies an additional protein interaction surface to selectively bind non-native proteins enriched in beta-structure.

Ydj1 employs at least one additional feature to bind non-native proteins. Ydj1 is farnesylated at a C-terminal CaaX motif (29) and this lipid modification is required for interaction with the glutamine/asparagine-rich prion domain from Rnq1 (21) as well as the Hsp90 client Ste11 (30). Whether the Ydj1 farnesyl moiety directly binds non-native proteins or contributes indirectly via interaction with a membrane bilayer is an open question. Both scenarios are feasible because the farnesyl moiety could interact with hydrophobic residues in an unfolded polypeptide and stabilize a Ydj1:substrate interaction long enough for efficient transfer to Hsp70. Farnesylation of Ydj1 is required for localizing a small pool of this chaperone to the ER membrane (29). How membrane localization impacts chaperone activity is a relatively unexplored question though some misfolded, cytosolic proteins need to be recruited to the ER membrane for efficient degradation (31). Importantly, farnesylation is required for only a subset of Ydj1:substrate interactions (21) so more information is required on how lipid modification of a molecular chaperone confers specificity in substrate interaction. All studies analyzing Ydj1 activity *in vitro* purified Ydj1 from bacteria and thus utilized a form that is not farnesylated. Ydj1 should be purified from yeast cell extracts and used in future studies to explore how farnesylation impacts direct binding between Ydj1 and non-native substrates. In addition, more rigorous analysis is required to determine how ER-localization contributes to Ydj1 function. For example, how Ydj1 is targeted specifically to the ER membrane is unknown and what additional protein quality control components function with Ydj1 at this surface is also an ongoing question. To address this issue, Ydj1 can be targeted to other subcellular compartments by the addition of various localization signals (ex. nuclear localization signal).

Alternatively Ydj1 can be constitutively tethered to the ER membrane via the addition of C-terminal tail anchored domains that are post-translationally inserted into the ER membrane (32).

Altogether, a model emerges in which Ydj1 scans the yeast cytosol for non-native protein conformers utilizing at least three distinct chaperone modules that cooperatively select a diverse array of non-native polypeptides for interaction. Loss of an individual binding module selectively interferes with a subset of Ydj1:client interactions with varying effects on cell physiology. For example, loss of the ZFLR or farnesyl moiety confers sensitivity to heat stress (29,33) as well as aggregation of amyloid-like proteins (21). Multiple chaperone binding sites not only expands the repertoire of potential clients, specific Ydj1:substrate contacts could orient a Ydj1 client in a distinct conformation in relation to the J-domain influencing interaction with downstream chaperones including Hsp70, Hsp90, E3 ubiquitin ligases, etc and thus facilitate triage between refolding or degradation. We still lack a structural understanding of this process and solving X-ray crystal structures of diverse Ydj1:client complexes will be of significant value in the future.

6.3 The cooperative action of molecular chaperones and the microtubule cytoskeleton protect cells from aggregation of misfolded proteins

The cell devotes enormous resources to the selective recognition of non-native protein conformers and triage of these polypeptides between repair or degradation pathways. This "decision" is not to be taken lightly as the cell needs to prevent aberrant protein aggregation while maintaining a pool of functional proteins to carry out essential cellular processes (34). Protein aggregates are conventionally poor substrates for the proteasome (35) and could interfere with cellular folding equilibrium by titrating chaperones away from essential tasks or directly inducing the misfolding of native proteins (36-38). However, protein aggregation in the form of facilitated compartmentalization is a mechanism by which cells actively sequester non-native polypeptides under conditions of stress (3,39). Furthermore, facilitated assembly of amyloid-like aggregates is protective in some models for neurodegeneration (40-42). Consequently, diverse misfolded proteins are processed by sophisticated protein quality control networks that shuttle these polypeptides between distinct outcomes.

To shed light on this process, I characterized a cytosolic reporter protein that is misfolded and degraded by the ubiquitin proteasome system. When proteasome activity is inhibited, this misfolded protein traffics through two recently described quality control compartments; a juxtanuclear compartment that houses soluble, polyubiquitinated proteins called the JUNQ and a perivacuolar compartment called the IPOD that stores insoluble, amyloidogenic proteins (43). Efficient degradation of this misfolded reporter was dependent upon the Hsp40 co-chaperone Ydj1, the E3 ubiquitin ligases Ubr1 and San1, and surprisingly the microtubule cytoskeleton.

The Hsp40/Hsp70 system functions at the front lines of protein quality control through binding non-native polypeptides. This chaperone machine is a potent suppressor of protein aggregation (20-22,25). While Ydj1 has been previously linked to stimulating polyubiquitination in conjunction with E3 ubiquitin ligases (13,21,44,45), Ydj1 is also required to hold misfolded proteins in a soluble state independent of ubiquitination. Surprisingly, interfering with microtubule dynamics disrupts interaction between Ydj1 and misfolded proteins. This observation reveals a surprising, novel

link between chaperone-dependent suppression of protein aggregation and the microtubule cytoskeleton.

How does the microtubule cytoskeleton contribute to protein quality control? Microtubule dysfunction did not impair ubiquitination of the misfolded proteins examined thus far suggesting microtubules are required for holding polyubiquitinated proteins a soluble state. In a crowded cellular environment, microtubules might stabilize chaperone:substrate complexes long enough for refolding or degradation pathways to process a non-native polypeptide for polyubiquitination and delivery to the proteasome. Alternatively, polyubiquitinated proteins might be trafficked to the proteasome by action of microtubule motors. Disrupting this step would likewise result in the accumulation of polyubiquitinated proteins that would have a high propensity to aggregate and might be poor substrates for molecular chaperones such as Ydj1. Identifying the molecular conduits between the microtubule cytoskeleton and misfolded proteins will greatly enhance our understanding of protein quality control pathways function in the crowded cytosol.

Interestingly, microtubule dysfunction impacts aggregation and degradation of specific misfolded proteins. For example, depolymerization of the microtubule cytoskeleton induces aggregation of von Hippel Lindau (VHL) protein yet degradation of VHL is actually accelerated. VHL misfolded conformers are either less predisposed to assemble as insoluble aggregates or VHL is recognized by specialized chaperone complexes that hold this protein in a soluble state. Consequently, conformational subtleties in misfolded proteins can influence selective recognition by unique chaperone complexes as well as propensity to assemble into degradation-incompetent aggregates.

Finally, protein aggregation is a fundamental threat to cellular homeostasis. However protein quality control pathways are exquisitely adapted to suppress aberrant protein aggregation as well as facilitate specialized assembly of non-native polypeptides into protective, compartmentalized structures (Figure 6.1). The first line of defense appears to rely on preventing protein aggregation. Hence, Hsp70 molecular chaperones are abundant proteins with broad polypeptide preferences to

manage the large scale burden of protein misfolding in the cytoplasm (6,7). Some Hsp40 co-chaperones such as Ydj1 are also very abundant yet possess more select binding specificities and unique protein interaction domains (46). These molecular chaperones are also stress-inducible such that the cell is able to compensate under conditions when bulk protein misfolding (ex. heat stress) (47).

However, a back-up system is also in place when this first protective layer becomes overwhelmed. Cellular pathways sequester misfolded proteins in specialized compartments including the JUNQ and IPOD (43). This form of protective aggregation serves distinct functions. First, quality control compartments such as the JUNQ store polyubiquitinated proteins when proteasome function is inhibited (39,43). As a result, misfolded proteins that pass through chaperone/E3 ligases checkpoints yet are unable to be degraded are maintained in a soluble state. The IPOD is an additional layer of support by acting as a deposition site for misfolded proteins that have adopted an amyloid-like, or insoluble conformation. This compartment might be especially important under conditions of prolonged stress when misfolded proteins accumulate beyond the capacity of the Hsp70/Hsp40 system. In yeast, the IPOD also might facilitate propagation of yeast prions (48) or help retain chronically misfolded proteins in the mother cell during cell division (49). While the JUNQ and IPOD are most prominent under conditions of stress these quality control compartments might contribute to basal protein quality control. Future studies should identify the receptors and motor molecules that selectively deliver misfolded proteins to these compartments. How are misfolded proteins selectively partitioned between these compartments by the cooperative action of molecular chaperones, E3 ligases, and the microtubule cytoskeleton? Answering these questions will elevate our understanding of the sophisticated protein quality control networks that protect the cellular environment.

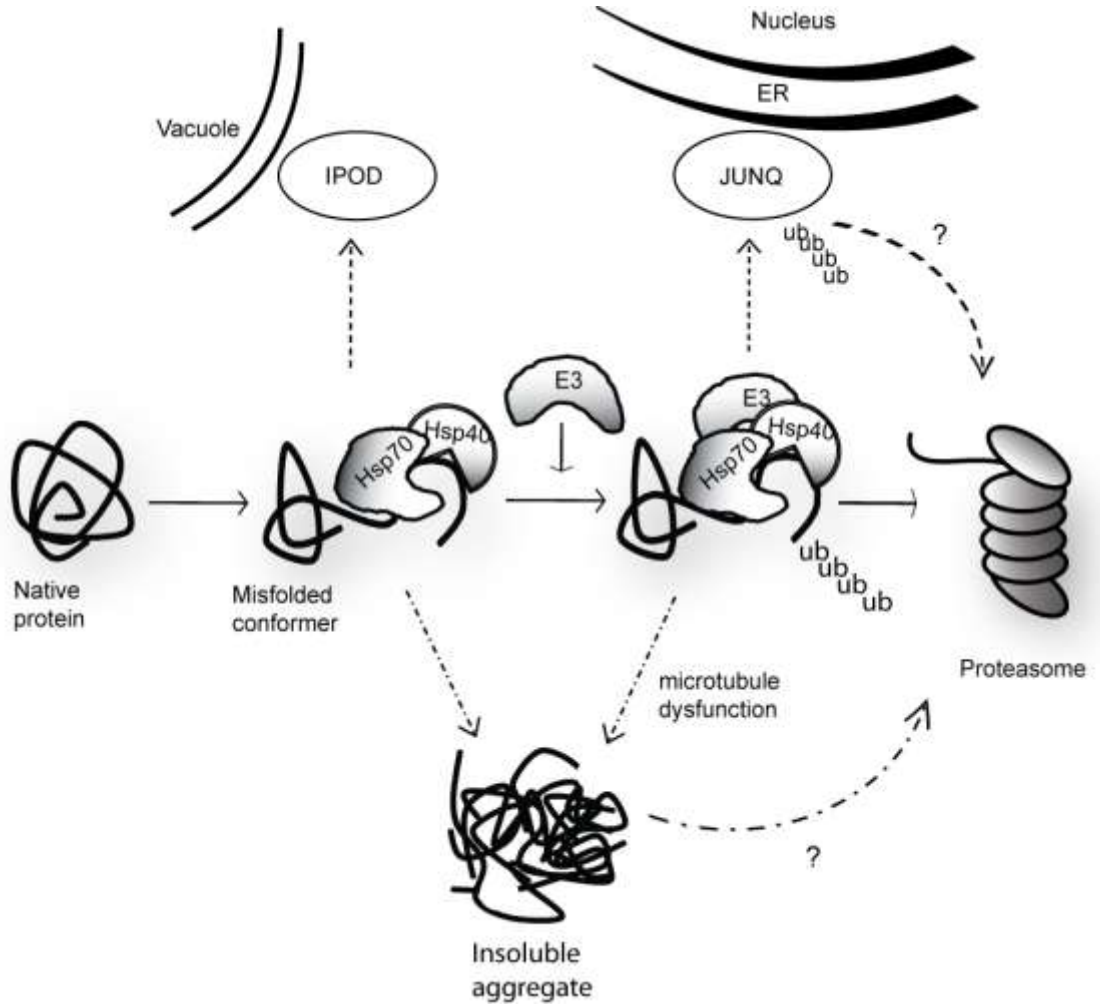

Figure 6.1 Degradation pathway of a cytosolic, misfolded protein by chaperone action and subcellular compartmentalization. When a native protein misfolds in the cytosol, molecular chaperones including Hsp40/70 family members bind unfolded sequences in this protein. If this misfolded protein escapes this quality control step, then this non-native protein could assemble into insoluble aggregates. Alternatively, this protein could be trafficked to the IPOD with other insoluble proteins. If the misfolded protein is held in a soluble state, then additional degradation cofactors such as E3 ligases could be recruited to promote polyubiquitination. Some E3 ligases such as CHIP can act as chaperones to suppress protein aggregation and influence triage between refolding and degradation. If proteasome activity is jeopardized, polyubiquitinated proteins are stored in a soluble state at the JUNQ compartment and subsequently degraded if proteasome activity is restored. If the polyubiquitinated protein escapes from this chaperone complex or if the microtubule cytoskeleton is impaired, this protein might assemble into insoluble aggregates. However, auxiliary pathways that might include the Hsp40 Sis1 and/or the AAA Type ATPase Hsp104 appear to solubilize some aggregates in the cell.

6.4 References

1. Carrell, R. W., and Lomas, D. A. (1997) *Lancet* **350**, 134-138

2. Hartl, F. U., and Hayer-Hartl, M. (2002) *Science* **295**, 1852-1858

3. Tyedmers, J., Mogk, A., and Bukau, B. (2010) *Nat Rev Mol Cell Biol* **11**, 777-788

4. Douglas, P. M., Summers, D. W., and Cyr, D. M. (2009) *Prion* **3**

5. Sipe, J. D., and Cohen, A. S. (2000) *J Struct Biol* **130**, 88-98

6. Mayer, M. P., and Bukau, B. (2005) *Cell Mol Life Sci* **62**, 670-684

7. Schlecht, R., Erbse, A. H., Bukau, B., and Mayer, M. P. (2011) *Nat Struct Mol Biol* **18**, 345-351

8. Rudiger, S., Schneider-Mergener, J., and Bukau, B. (2001) *Embo J* **20**, 1042-1050

9. Szabo, A., Langer, T., Schroder, H., Flanagan, J., Bukau, B., and Hartl, F. U. (1994) *Proc Natl Acad Sci U S A* **91**, 10345-10349

10. Cyr, D. M., Langer, T., and Douglas, M. G. (1994) *Trends Biochem Sci* **19**, 176-181

11. Walsh, P., Bursac, D., Law, Y. C., Cyr, D., and Lithgow, T. (2004) *EMBO Rep* **5**, 567-571

12. Caplan, A. J., Cyr, D. M., and Douglas, M. G. (1992) *Cell* **71**, 1143-1155

13. Lee, D. H., Sherman, M. Y., and Goldberg, A. L. (1996) *Mol Cell Biol* **16**, 4773-4781

14. Cyr, D. M., Lu, X., and Douglas, M. G. (1992) *J Biol Chem* **267**, 20927-20931

15. Kimura, Y., Yahara, I., and Lindquist, S. (1995) *Science* **268**, 1362-1365

16. Lu, Z., and Cyr, D. M. (1998) *J Biol Chem* **273**, 5970-5978

17. Moriyama, H., Edskes, H. K., and Wickner, R. B. (2000) *Mol Cell Biol* **20**, 8916-8922

18. Ghaemmaghami, S., Huh, W. K., Bower, K., Howson, R. W., Belle, A., Dephoure, N., O'Shea, E. K., and Weissman, J. S. (2003) *Nature* **425**, 737-741

19. Fan, C. Y., Lee, S., Ren, H. Y., and Cyr, D. M. (2004) *Mol Biol Cell* **15**, 761-773

20. Muchowski, P. J., Schaffar, G., Sittler, A., Wanker, E. E., Hayer-Hartl, M. K., and Hartl, F. U. (2000) *Proc Natl Acad Sci U S A* **97**, 7841-7846

21. Summers, D. W., Douglas, P. M., Ren, H. Y., and Cyr, D. M. (2009) *J Biol Chem* **284**, 3628-3639

22. Lian, H. Y., Zhang, H., Zhang, Z. R., Loovers, H. M., Jones, G. W., Rowling, P. J., Itzhaki, L. S., Zhou, J. M., and Perrett, S. (2007) *J Biol Chem*

23. Wu, Y., Li, J., Jin, Z., Fu, Z., and Sha, B. (2005) *J Mol Biol* **346**, 1005-1011

24. Kota, P., Summers, D. W., Ren, H. Y., Cyr, D. M., and Dokholyan, N. V. (2009) *Proc Natl Acad Sci U S A* **106**, 11073-11078

25. Cyr, D. M. (1995) *FEBS Lett* **359**, 129-132

26. Li, J., Qian, X., and Sha, B. (2003) *Structure* **11**, 1475-1483

27. Choudhury, D., Thompson, A., Stojanoff, V., Langermann, S., Pinkner, J., Hultgren, S. J., and Knight, S. D. (1999) *Science* **285**, 1061-1066

28. Sauer, F. G., Futterer, K., Pinkner, J. S., Dodson, K. W., Hultgren, S. J., and Waksman, G. (1999) *Science* **285**, 1058-1061

29. Caplan, A. J., Tsai, J., Casey, P. J., and Douglas, M. G. (1992) *J Biol Chem* **267**, 18890-18895

30. Flom, G. A., Lemieszek, M., Fortunato, E. A., and Johnson, J. L. (2008) *Mol Biol Cell* **19**, 5249-5258

31. Metzger, M. B., Maurer, M. J., Dancy, B. M., and Michaelis, S. (2008) *J Biol Chem* **283**, 32302-32316

32. Beilharz, T., Egan, B., Silver, P. A., Hofmann, K., and Lithgow, T. (2003) *J Biol Chem* **278**, 8219-8223

33. Fan, C. Y., Ren, H. Y., Lee, P., Caplan, A. J., and Cyr, D. M. (2005) *J Biol Chem* **280**, 695-702

34. Buchberger, A., Bukau, B., and Sommer, T. (2010) *Mol Cell* **40**, 238-252

35. Holmberg, C. I., Staniszewski, K. E., Mensah, K. N., Matouschek, A., and Morimoto, R. I. (2004) *Embo J* **23**, 4307-4318

36. Gidalevitz, T., Ben-Zvi, A., Ho, K. H., Brignull, H. R., and Morimoto, R. I. (2006) *Science* **311**, 1471-1474

37. Bence, N. F., Sampat, R. M., and Kopito, R. R. (2001) *Science* **292**, 1552-1555

38. Balch, W. E., Morimoto, R. I., Dillin, A., and Kelly, J. W. (2008) *Science* **319**, 916-919

39. Kopito, R. R. (2000) *Trends Cell Biol* **10**, 524-530

40. Cohen, E., Paulsson, J. F., Blinder, P., Burstyn-Cohen, T., Du, D., Estepa, G., Adame, A., Pham, H. M., Holzenberger, M., Kelly, J. W., Masliah, E., and Dillin, A. (2009) *Cell* **139**, 1157-1169

41. Douglas, P. M., Treusch, S., Ren, H. Y., Halfmann, R., Duennwald, M. L., Lindquist, S., and Cyr, D. M. (2008) *Proc Natl Acad Sci U S A* **105**, 7206-7211

42. Cohen, E., Bieschke, J., Perciavalle, R. M., Kelly, J. W., and Dillin, A. (2006) *Science* **313**, 1604-1610

43. Kaganovich, D., Kopito, R., and Frydman, J. (2008) *Nature* **454**, 1088-1095

44. Younger, J. M., Ren, H. Y., Chen, L., Fan, C. Y., Fields, A., Patterson, C., and Cyr, D. M. (2004) *J Cell Biol* **167**, 1075-1085

45. Heck, J. W., Cheung, S. K., and Hampton, R. Y. (2010) *Proc Natl Acad Sci U S A* **107**, 1106-1111

46. Summers, D. W., Douglas, P. M., Ramos, C. H., and Cyr, D. M. (2009) *Trends Biochem Sci* **34**, 230-233

47. Morimoto, R. I. (2008) *Genes Dev* **22**, 1427-1438

48. Tyedmers, J., Treusch, S., Dong, J., McCaffery, J. M., Bevis, B., and Lindquist, S. (2010) *Proc Natl Acad Sci U S A* **107**, 8633-8638

49. Liu, B., Larsson, L., Caballero, A., Hao, X., Oling, D., Grantham, J., and Nystrom, T. (2010) *Cell* **140**, 257-267